AD-A108 367 TEL-AVIV UNIV (ISRAEL) DEPT OF FLUID MECHANICS AND --ETC F/G 20/4
ON THE RELATIONSHIP BETWEEN TRANSITIONAL AND FULLY TURBULENT SH--ETC(U)
MAY 81 I WYGNANSKI AFOSR-77-3275

UNCLASSIFIED AFOSR-TR-81-0764 NL

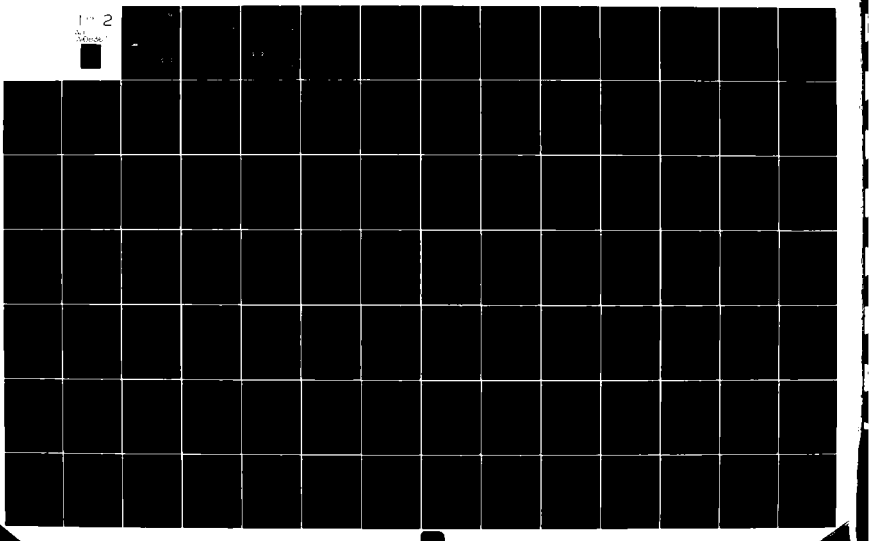

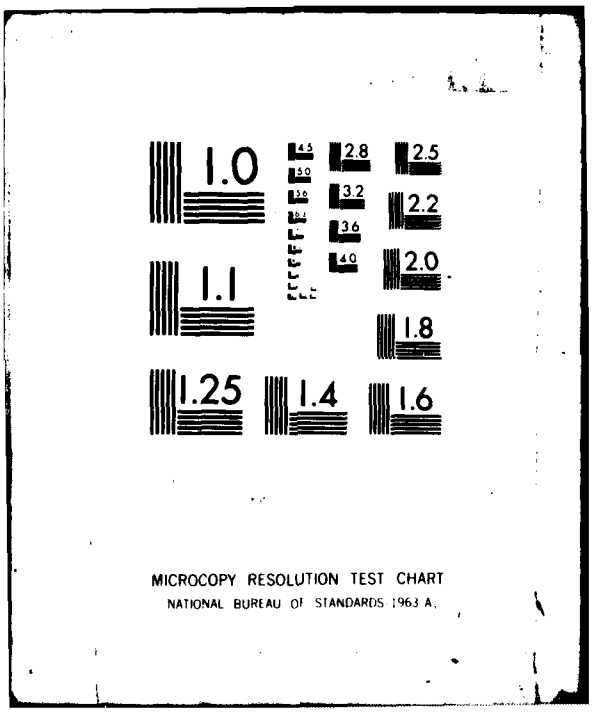
1.0
1.1
1.25
1.4
1.6
1.8
2.0
2.2
2.5
2.8
3.2
3.6
4.0
4.5
5.0
5.6
MICROCOPY RESOLUTION TEST CHART
NATIONAL BUREAU OF STANDARDS 1963 A.

AFOSR-TR- 81-0764

AD A108367

3

LEVEL II

AFOSR- Contract/Grant Number
77-3275

ON THE RELATIONSHIP BETWEEN TRANSITIONAL AND FULLY TURBULENT SHEAR FLOW

(12) 164

I. Wygnanski
School of Engineering
Tel-Aviv University

31 May 1981

Annual Scientific Report, 1 March 1980 - 31 March 1981

Approved for public release; distribution unlimited.

Prepared for

AFOSR Bolling Airforce base, Washington D.C. 20332

and

EUROPEAN OFFICE OF AEROSPACE RESEARCH AND DEVELOPMENT
London, England

XX

UNCLASSIFIED

SECURITY CLASSIFICATION OF THIS PAGE (When Data Entered)

REPORT DOCUMENTATION PAGE		READ INSTRUCTIONS BEFORE COMPLETING FORM
1. REPORT NUMBER AFOSR-TR- 81 -0764	2. GOVT ACCESSION NO. AD-A108367	3. RECIPIENT'S CATALOG NUMBER
4. TITLE (and Subtitle) ON THE RELATIONSHIP BETWEEN TRANSITIONAL AND FULLY TURBULENT SHEAR FLOW		5. TYPE OF REPORT & PERIOD COVERED 1 Mar 80 - 31 Mar 81 ANNUAL 6. PERFORMING ORG. REPORT NUMBER
7. AUTHOR(s) I. WYGNANSKI		8. CONTRACT OR GRANT NUMBER(s) AFOSR-77-3275
9. PERFORMING ORGANIZATION NAME AND ADDRESS DEPT OF FLUID MECHANICS AND HEAT TRANSFER TEL-AVIV UNIVERSITY, RAMAT-AVIV TEL-AVIV 69978 ISRAEL		10. PROGRAM ELEMENT, PROJECT, TASK AREA & WORK UNIT NUMBERS 61102F 2307/A2
11. CONTROLLING OFFICE NAME AND ADDRESS AIR FORCE OFFICE OF SCIENTIFIC RESEARCH/NA BOLLING AIR FORCE BASE, DC 20332		12. REPORT DATE 31 MAY 81 13. NUMBER OF PAGES 170
14. MONITORING AGENCY NAME & ADDRESS(if different from Controlling Office) (12) 169		15. SECURITY CLASS. (of this report) UNCLASSIFIED 15a. DECLASSIFICATION/DOWNGRADING SCHEDULE

16. DISTRIBUTION STATEMENT (of this Report)

Approved for public release; distribution unlimited.

17. DISTRIBUTION STATEMENT (of the abstract entered in Block 20, if different from Report)

18. SUPPLEMENTARY NOTES

19. KEY WORDS (Continue on reverse side if necessary and identify by block number)

PIPE FLOW
TURBULENT SPOT
PULSATING FLOW
TURBULENT FLOW
LAMINAR FLOW

20. ABSTRACT (Continue on reverse side if necessary and identify by block number)

Pulsating flow of air in a straight smooth pipe was investigated experimentally. The period of forcing ranged from 0.5sec to 5 sec which resulted in the change in the non-dimensional frequency parameter $\alpha = R\sqrt{\omega/\nu}$ of 4.5 to 15. The introduction of periodic surging had no effect on the time mean quantities. The present data was compared in detail with the theory of Uchida (1956) in the laminar flow regime. The time dependent components at the forcing frequency were presented by the radial distribution of amplitude and phase. An integral

DD FORM 1 JAN 73 1473 EDITION OF 1 NOV 65 IS OBSOLETE

UNCLASSIFIED 412677

SECURITY CLASSIFICATION OF THIS PAGE (When Data Entered)

momentum equation in a time dependent flow requires a force triangle to be maintained at any instant. The triad of forces are: pressure, inertia and shear. All terms of the force balance equation were measured independently providing a good check of data. The measured turbulent characteristics of the flow, including the RMS values of the velocity fluctuations, Reynolds stress and short-time power spectra are dependent on the phase of the forced oscillations. The radial distribution of the phase angle of velocity is qualitatively different in laminar and turbulent flows. In order to explain this difference the concept of a relaxation time of the turbulent flow was employed. Transitional flow in a boundary layer is also briefly discussed.

GENERAL INTRODUCTION

The project entitled "On the relationship between transitional and fully turbulent shear flow" is concerned with various aspects of this complex process.

Research is carried out simultaneously in a wind tunnel where transition of a laminar boundary layer is extensively investigated, in a pipe, and most recently, a large two dimensional channel facility was added. The ability to compare data obtained in different geometries, Reynolds numbers, and pressure gradients enables us to take advantage of the unique properties of each facility and have an overview of the universal aspects of the problem.

For example: transition in a boundary layer takes place in a form of "spot" bounded on one side only, by a solid surface. The spots, thus grow spatially in all three directions forming complicated three dimensional structures. The pressure gradient over the surface is easily controlled and may be made to vanish on a flat plate at no incidence, yet there is no control over the growth of the Reynolds number and the local thickness of the boundary layer. In a pipe, on the other hand, a transitional turbulent structure "a puff" is limited by the diameter of the pipe and can only grow in the streamwise direction, the Reynolds number is easily controlled by controlling the mass flux but the pressure gradient in a given pipe at a fixed Re depends on the structure of the flow, and is thus a dependent variable. Although the

ensemble-averaged turbulent structure in transitional pipe flow is axisymmetric, there is little evidence that this is a dominant mode of the transition process. The two dimensional channel facility was constructed because it provides a link between the boundary layer and the pipe flow. Although the pressure gradient in a channel is a dependent variable the transitional structure may take a form of a boundary-layer-spot if generated locally by a point-source-disturbance, or a "puff" (or "slug") if generated by a two dimensional disturbance spanning the channel. However, even three dimensional disturbances set in channel-flow can only propagate in two directions thus theoretical and experimental analysis of the proolem is simpler then in the boundary layer.

The resulting turbulent flow in pipes, channels and boundary layers is of course quite similar. The viscous sublayer, the logarithmic law-of-the-wall, the mean turbulent intensities and even the wall-streaks and large coherent structures are all alike. This implies that only those features which are common to all geometries are of paramount importance in the final transition process. The overall research program on transition at the School of Engineering in Tel- Aviv was guided by this view. During the CY 1980-1981 work was done on the internal structure of the boundary layer spot (some of the experiments were carried out at the University of Southern California); on the interaction of spots and on the effects of favorable pressure gradient on spots. In pipe flow, the axisymmetric mode of transition was investigated by making 8 simultaneous measurements at different azimuthal locations, but the bulk of this years scientific report is concerned with the pulsating

pipe flow. The introduction of harmonic pulsations to pipe flow was proposed by us in 1972 but was not executed because of experimental difficulties and a lack of an adequate data acquisition system. The program was reestablished in 1978 after the relationship between puffs and slugs was understood (Rubin, Haritonidis and Wygnanski, 1980). In the attached thesis by L. Shemer, pulsating laminar and turbulent pipe flows are discussed in detail. The response of the system which contains a plenum chamber, a piston pump and a pipe to controlled sinosoidal oscillations was investigated, as was the effect of the finite velocity of sound on the propagation of disturbances in a long pipe. There are marked differences between the structure of turbulence in a pulsating pipe flow and in "steady" fully developed turbulent flow, these differences are associated with the memory of the turbulent structure and point again to the need of considering relaxation time in modeling turbulent flows. A portion of the thesis, concerned with the differences between laminar and turbulent pulsating flows and the modeling of relaxation times using complex variables to denote phase relationships, will be presented at the 1981 Davis conference on turbulent shear flows. The effects of harmonic pulsations on relaminarization of turbulent flow and on transition to turbulence will be considered during the coming year CY 81-82.

ON THE SUBSTRUCTURE IN A TRANSITIONAL SPOT

By I. Wygnanski

Department of Fluid Mechanics and Heat Transfer
School of Engineering
Tel-Aviv University.

1) INTRODUCTION

Photographs of transitional boundary layer spots (Gad el Hak Blackwelder and Riley (1980), Cantwell, Coles and Dimotakis (1978) and Matsui (1980)) reveal that the spot contains numerous eddies. In fact at sufficiently high Reynolds number, the interior of the spot is indistinguishable visually from the fully developed turbulent boundary layer. Longitudinal streaks aligned roughly with the direction of streaming figure prominently in every plan-view photograph of the spot and the boundary layer. Yet, the subtructure within the spot can not occur entirely at random in view of the universality of the shape of the spot, and its linear growth in the spanwise and streamwise directions.

Ensemble avaraged data, conditioned on the pertutbation generating the spot, does not reveal a dominant structure within the spot itself (Wygnanski, Sokolov and Friedman (1976), Cantwell, Coles and Dimotakis (1978)). Consecutive spots may differ slightly from one to another in their shape and their celerity which results in desynchronization of the acquisition process and masks the internal structure deduced from the averaged data. Thus the velocity field reconstructed from ensemble averaged data would lead one to believe that the spot consists of a single large coherent eddy. The apparent eddy, however, does not scale correctly with any characteristic boundary layer length-scale because the spot can becomes as large as the facility in which it is generated.

Although the overall dynamics of the spot is of some practical interest as it may help in predicting skin friction, heat transfer and noise generated in the transition region, it can hardly explain the dynamics of the transition process itself.

It was previously observed (Wygnanski, Haritonidis and Kaplan 1979) that a wave packet trails the spot. The precise relationship between the packet and the spot is not fully understood, particularly at low Reynolds numbers, but on numerous occasions the wave packet broke down generating a new transitional spot which, at least initially, did not manage to catch-up with the parent structure. The breakdown of a wave packet into structures resembling hair-pin eddies suggests that the spot may contain a fairly orderly array of such eddies. Incipient spots in favorable pressure gradient (Wygnanski 1980) contained initially three, then five distinctive eddies arranged in a Λ formation. The number of these eddies increased for a while with downstream distance, but later they merged to become indistinguishable further downstreams as a result of the averaging process.

Thus in order to map the structure of a "typical" spot more sophisticated averaging techniques have to be employed. In the following discussion few attempts are made to pry the information from streamwise velocity measurements made with a normal hot-wire rake which supplies instanteneous velocity information across the entire boundary layer.

Measurements were made in the absance of pressure gradient at a

free stream velocity of 5m/sec and a perturbation located at $Re_{\delta^*} = 780$ based on the local displacement thickness of the laminar boundary layer. The experimental facility, the instrumentation and the data acquisition system were discussed previously (Wygnanski, Haritonidis and Kaplan 1979) and will not be repeated in the present context.

2) ON THE LONGITUDINAL STRUCTURE IN A SPOT

An example of 10 simultaneous, streamwise, velocity perturbation signals , observed during a passage of a spot is shown in fig.1. The abscissa in this figure is time while the ordinate corresponds to velocity. The numbers opposite each trace correspond the dimensionless distance of a given wire from the surface of the plate, expressed in terms of the local laminar boundary layer thickness, δ_L . One may clearly discern large velocity fluctuations which are coherent across most of the laminar boundary layer. A characteristic frequency associated with these fluctuations corresponds to the most amplified "Tollmien-Schlichting frequency appropriate to this case (see also Wygnanski, Haritonidis and Kaplan 1979). Power spectra averaged over 200 events confirm the existance of energetic fluctuations at the Tollmien-Schlichting frequency. The spectral peak, however, is not very strong relative to the background turbulence, and it is not clear at this point, how it may be used in reconstructing the flow field associated with a typical (or a most probable) spot.

After examining numerous velocity records a simple criterion was

devised which classifies the record according to easily distinguishable number of large coherent fluctuations. The velocity records are first low-pass-filtered digitally in order to remove from each record the effects of the small scale turbulent fluctuations. The filtered record is scanned and the times at which the velocity drops to a minimum locally, are recorded and stored in memory as indicated by the vertical lines in figure 2. The local minimum velocity has to pass an arbitrarily determind treshold level relative to the neighboring maxima before being recorded. The treshold criterion eliminates small amplitude fluctuations from the count but introduces an element of subjectivity to the procedure. It was empirically established that the following discussion is insensitive to the choice of the treshold level. For example halfing the treshold level would result in accounting for one additional minimum (6 rather than 5) in the upper velocity trace shown in fig. 2.

Adopting this procedure for each measuring station enables the classification of spots according to the number of large eddies which they contain. Some typical probability density distributions showing the most probable number of eddies on the plane of symmetry of the spot at a given distance from the perturbation are shown in fig. 3. The most important conclusion from these histograms is that the avarage number of large eddies in a spot is small.

For example; measurements made 375mm downstream of the perturbation (975mm from the leading edge of the plate) indicate that the average number of large eddies in a spot is 4.6 and the most probable spot

detected on the plane of symmetry between $0.2 \leq y/\delta_L \leq 0.8$ contained 5 large eddies. The most probable number of eddies near the surface and at $y/\delta_L > 0.8$ is slightly lower (at $y/\delta_L \simeq 1$ the most probable number is 4) because the initial breakdown to turbulence occurs at $0.6 \leq y/\delta_L \leq 0.8$ (see also Kovasznay Komoda and Vasudeva, '962) and some of the eddies did not arrive perhaps at the maesuring station.

The eddy detection scheme shown in fig. 2 renders not only the number of eddies in a given realization but also the time of their arrival at the location of measurement. These times were stored and the probability density of their distribution was examined. It appears that the eddies arrive at preferred times at the measuring station (fig. 4). Thus if one selects only those spots which contain a given number of eddies the histogram showing their time of arrival will contain identical number of peaks; each peak corresponds to the preferential time of arrival of the specific eddy. Since the probability density distribution of the number of eddies in a spot is narrow, by choosing only those spots which contain the most probable number of eddies for further analysis are selects between 25% - 50% of the total number of events; such a large fraction justifies the subdivision of transitional spots into groups containing an equal number of eddies.

The abvementioned information can be used obtain the detailed flow field in a spot which contains a prescribed number of eddies. The procedure is illustrated schematically in fig. 5 showing its inherent advantages in mapping the flow field of a "young" spot containing 3 eddies

only:

(i) The number of eddies in a spot is detected and a simple ensemble-averaged velocity conditioned on the perturbation is calculated (fig. 5a). Since only the spots containing 3 eddies were selected for the averaging, the ensemble averaged velocity contains 3 local minima. It is clear, however, that the amplitude of these minima is not representative of the velocity record in a single realization drawn to the same scale in fig. 5f.

(ii) Each realization is shifted in time in order to align the location of its last minimum before averaging. The ensemble averaged velocity resulting from the alignment procedure is shown in fig. 5b. The amplitude of the trailing fluctuation in the ensemble is enhanced by the alignment process and is comparable to the amplitude of the single realization shown in fig. 5f. The neighbouring minimum was hardly affected by the alignment while the first minimum disappeared.

(iii)Repeating the alignment procedure for the first and the second minimum enhanced the amplitude of the particular minimum concerned (fig. 5c, 5d).

(iv) A composite, ensemble-averaged velocity perturbation record is generated by subdividing the overall temporal record into 4 sections (fig.5c). This subdivision suggests that each large eddy

has a limited zone of influence. The velocity perturbation in regions (1) and (4) are under the total influence of minima A and C respectively. The velocity perturbation in regions (2) and (3) have been weighted proportionally to the distance (time elapsed) from points A, B and C respectively before averaging. Thus the velocity preturbation at points A; B; C; are identical to the velocity-perturbations shown in figs. 5d, 5c, 5b respectively. The velocity in region 2 is a weighted average of the records shown in fig. 5c and 5d respectively while the velocity in region 3 is the weighted average of records 5c and 5b.

This procedure can be applied to any number of eddies existing in a most probable spot at a given coordinate in space. The ultimate purpose of the process is to reconstruct a detailed 3 dimensional flow field in the most probable realization from a large number of point measurements, accepting the fact that consecutive realizations are only broadly similar. The success of the procedure is determined by comparing the reconstructed velocity perturbation contours in a spot with the contours measured by an array of wires during a passage of a single realization. The comparison is made at the largest distance from the location of the perturbation for which data is available (i.e. at X-Xpert = 375mm). At this distance the spot is already quite large and may be considered fully turbulent ($Rex_{LE} > 3.3*10^5$ or $Re_{\delta^*} \simeq 10^3$). The comparison thus reprsents the most severe test of the procedure based on the available data.

A simply ensemble-averaged velocity perturbation record is shown in fig. 6a. The velocity perturbation is entirely positive near the surface and entirely negative at large distances from the wall. This record, however, differs somewhat from similar data reported by Wygnanski Haritonidis and Zilberman (1980) because the measurements were made at much lower Re. The most obvious difference concerns the existance of two minima at an intermediate distance from the wall, $(0.25<y/\delta_L<0.6)$ which are marked by arrows in fig. 6a. Another difference is concerned with the existance of a positive velocity perturbation near the leading edge of the spot which extends to $y/\delta_L \simeq 0.6$, while it no longer exists at $y/\delta_L = 0.25$ at higher Re (see Wygnanski Haritonidis and Zilberman 1980).

The same data was reprocessed according to the procedure outlined earlier and plotted in fig. 6b. This data represents a velocity perturbation resulting from the sole influence of the large eddies, in the most probbable realization, on the plane of symmetry of the spot at a given Re, and X. The most probable spot contains 5 large eddies at $0.15 \leq y/\delta_L \leq 0.6$; 4 eddies near the surface and at $0.65 < y/\delta_L \leq 0.85$ and only 3 eddies at $y/\delta_L \simeq 1$. The perturbations shown in fig. 6b contain detailed information about the interior structure of the flow which is not visible in fig. 6a. Heavy filtering of the data in fig. 6b reproduces the regular ensemble averaged velocity perturbations. Velocity perturbations recorded during the passage of the first spot in the experiment are shown in fig. 6c. The velocity record contains high frequencies associated with small turbulent eddies which are simply filtered and replotted on the same figure. The filtered signal is dis-

placed vertically for convenience of comparison, and although it is not identical to the most probable realization, the latter appears to contain the most relevant information which is missing in fig. 6a.

Velocity perturbation contours corresponding to figs. 6a,b,c are plotted in fig. 7. The vertical scale in this figure corresponds to a distance from the wall while the horizontal scale is time. Using a representative convection speed it appears that the vertical scale is approximately stretched by a factor of 60. The similarity between the velocity perturbation contours recorded during a single event and the educed most probable perturbation contours shown in fig. 7b is impressive, while the contours shown in figure 7a contain no such detail.

3) THE SPANWISE STRUCTURE IN A TRANSITIONAL SPOT

There are objective difficulties in obtaining reliable data near the wall using a rake of hot wires oriented in the spanwise (Z) direction, because any small surface positioned parallel to the wall may produce lift when inserted into a boundary layer resulting in the shedding of trailing vortices. One may not overcome this difficulty by positioning the rake parallel to the direction of the mean streamline at every level from the surface because the rake may still lift periodically while interacting with the large coherent structures in the boundary layer and shed, in addition to streamwise vorticity, a starting vortex which is equivalent in strength to the bound vortex associated with the lift. Thus, all present experiments were made with a rake of wires

which are normal to the surface (see figure 1 of Wygnanski, Haritonidis and Kaplan 1979). The flow was traversed from the plane of symmetry outwards at intervals of ΔZ=2mm in order to provide sufficient spatial resolution of the longitudinal substructure.

Measurements in favorable pressure gradient (Wygnanski 1980) have shown that the velocity perturbation at a given distance from the wall is not homogenously decaying across the span of the spot. Positive velocity-perturbation regions near the solid surface were separated by areas of decelerated flow, pointing to the possible existence of longitudinal vortices. The number of the structures increased initially in the downstream direction untill the longitudinal substructure became indistinguishable in the mean, giving an appearance of a single large horse-shoe eddy. It was then realized that the individual spots vary considerably in width, so that the averaging process includes realizations which do not extend as far in Z as the line of measurement and do not contribute to the velocity perturbation. The same data was then reprocessed after the smaller spots were excluded from the averaging, and the spanwise structure re-emerged in the mean. The procedure is biased towards the larger spots but it has the advantage of sifting out irrelevant data.

A simple ensemble-averaging procedure conditioned to the perturbation was used in the present experiment to educe the spanwise structure 150mm downstream of the origin. The incipient spot (Fig. 5) contains three longitudinal structures situated in a Λ formation (see also Wyg-

manski 1980). The spanwise distance between the centers of these structures near the surface in terms of wall coordinates $\Delta z^+ = \frac{\Delta z U^*}{\nu} = 90$ (where the friction velocity U^* was estimated from fully developed turbulent boundary layer data). The number $\Delta z^+ = 90$ is interesting, because it is approximately equal to the distance measured between longitudinal streaks in a fully turbulent boundary layer. Repeating the same measurements in a developed turbulent spot (at x-xper$_t$=300mm) but biasing the averaging towards the larger events indicates that the spot contains 5 structures in the spanwise direction. There is an increase in the number of the structures with downstream distance but there is also an increase in the distance between the centers of adjacent structures. It is believed that the increase in the number of structures is dominating the lateral growth of the spot.

REFERENCES

1. Cantwell,B Coles,D Dimotakis,P (1978) J.F.M. 87, 641.

2. Gad El Hak,M Blackwelder,R.F Riley,J.J. (1980). in Laminar Turbulent Transition edited by Eppler and Fasel, Springer Verlag Berlin, Proceedings of IUTAM Symposium Stuttgart (1979).

3. Kovasznay,K.S.G., Komoda,H. and Vasudeva,B.R. (1962) Proc. Heat Transfer and Fluid Mechanics Instit. Stanford Univ. Press.

4. Matsui,T (1980), in Laminar Turbulent Transition edited by Eppler and Fasel Springer Verlag Berlin, Proceedings of IUTAM Symposium Stuttgart

(1979).

5. Wygnanski,I. Sokolov,M. Friedman,D. (1976) J.F.M. 78, 785.

6. Wygnanski,I. Haritonidis,J. Kaplan,R.E. (1979) J.F.M. 92, 505.

7. Wygnanski,I. (1980) in The Role of Coherent Structures in Modelling Turbulence and Mixing, Lecture Notes in Physics 136, Springer Verlag-Berlin, (Proceeding, Madrid 1980).

8. Wygnanski,I. Haritonidis,J. Zilberman,M. (1980) On the Spreading of a Turbulent Spot in the Absence of Pressure Gradient, to be published in J.F.M.

FIGURE CAPTIONS

1. Velocity signals during a passage of the spot.

2. The detection of significant minima within a spot.

3. A Histogram showing the number of eddies in a spot.

4. A Histogram showing the times of arrival of the large eddies at the measuring station.

5. The eduction of the large coherent eddies.

   (a) Simple ensemble average. (b) Ensemble averaged velocity aligned on the most rearward eddy. (c) Ensemble averaged velocity aligned on the middle eddy. (d) Ensemble averaged velocity aligned on the leading eddy. (e) A weighted composite average. (f) The velocity in a single realization.

6. Velocity records in a spot.

   (a) A simple ensemble averaged record. (b) A composite ensemble averaged record showing the most probable distribution of the large eddies. (c) The velocity perturbation during a single event.

7. Contours of velocity perturbation corresponding to fig.6 a, b, c.

8. The ensemble averaged spanwise structure in a spot.

(a) (X-Xpert)=150mm. (b) X-Xpert=300mm. (c) A schematic plan view of a spot.

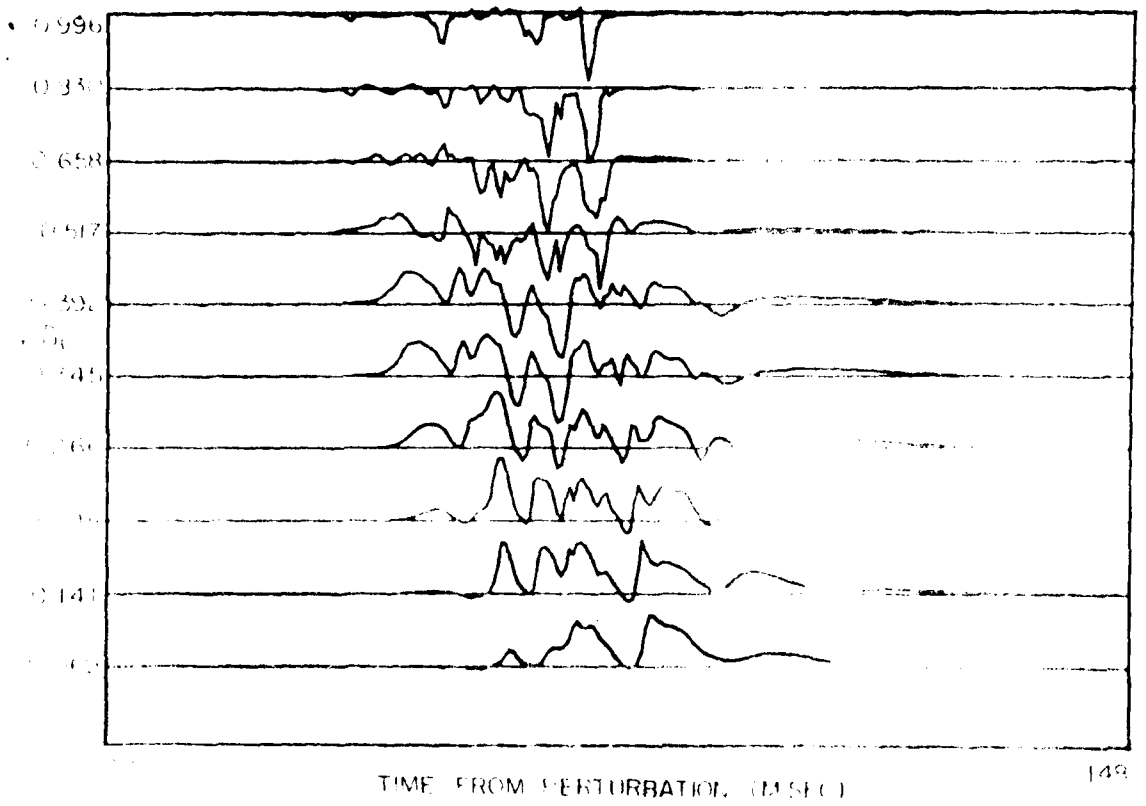

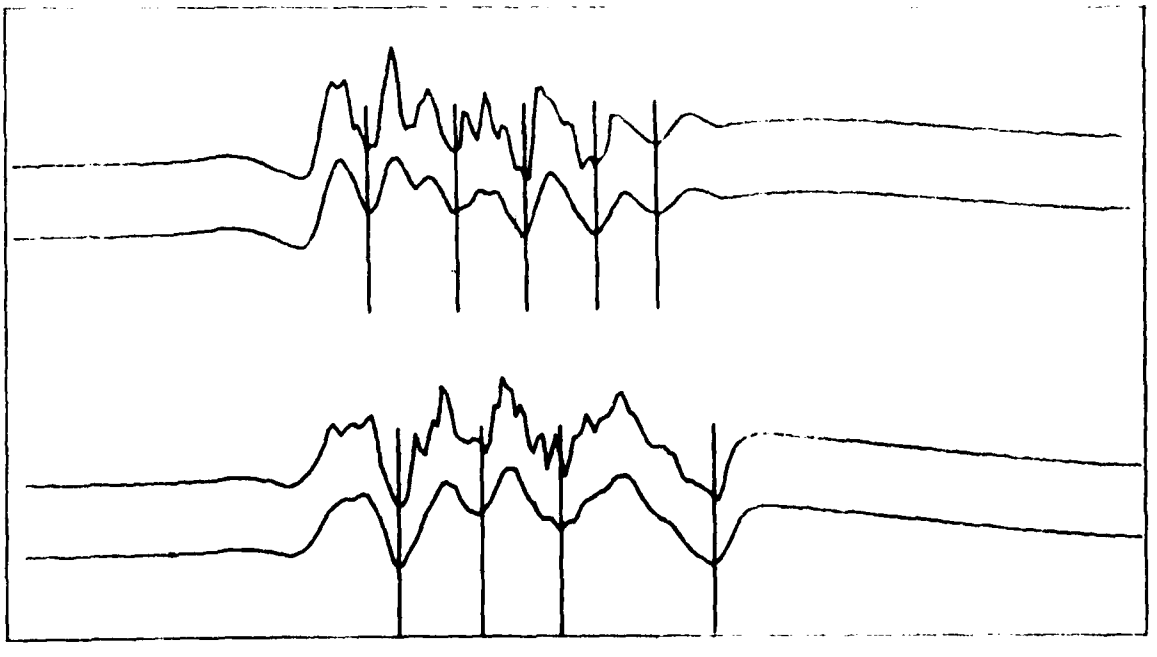

FIGS. 1 & 2

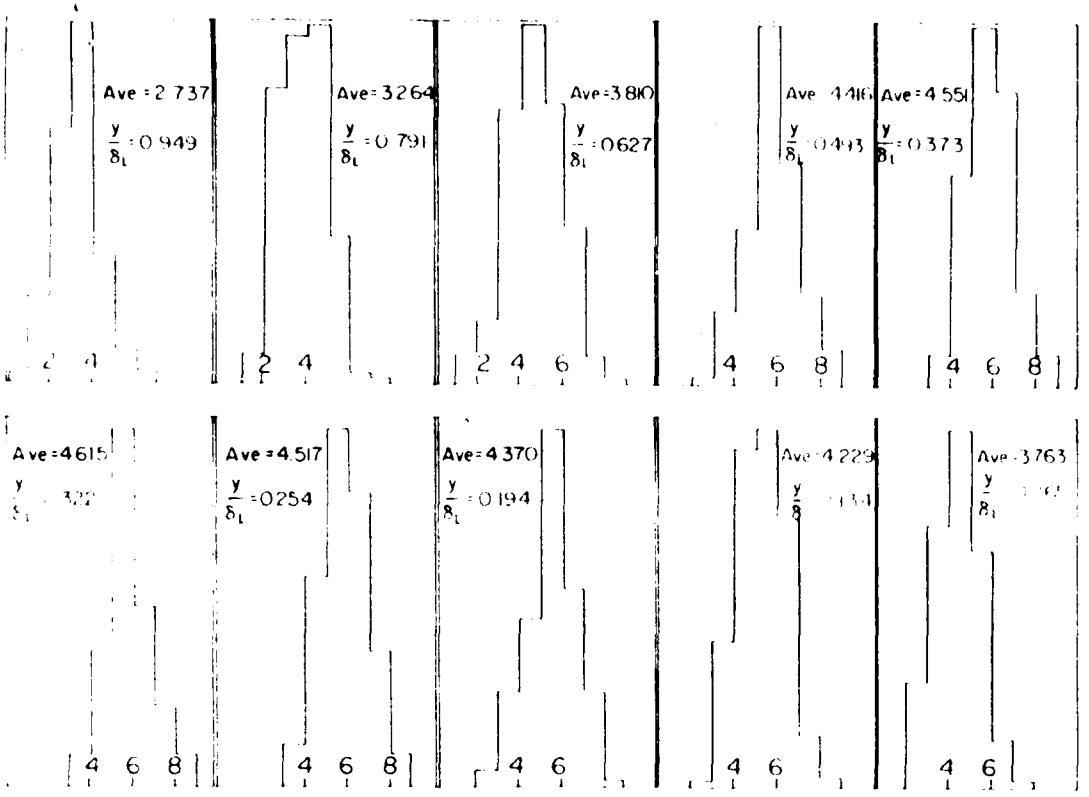
Ave = 2.737
$\frac{y}{\delta_L}$ = 0.949
Ave = 3.264
$\frac{y}{\delta_L}$ = 0.791
Ave = 3.810
$\frac{y}{\delta_L}$ = 0627
Ave = 4.416
$\frac{y}{\delta_L}$ = 0493
Ave = 4.551
$\frac{y}{\delta_L}$ = 0373
Ave = 4.615
Ave = 4.517
$\frac{y}{\delta_L}$ = 0254
Ave = 4.370
$\frac{y}{\delta_L}$ = 0194
Ave = 4.229
Ave = 3.763

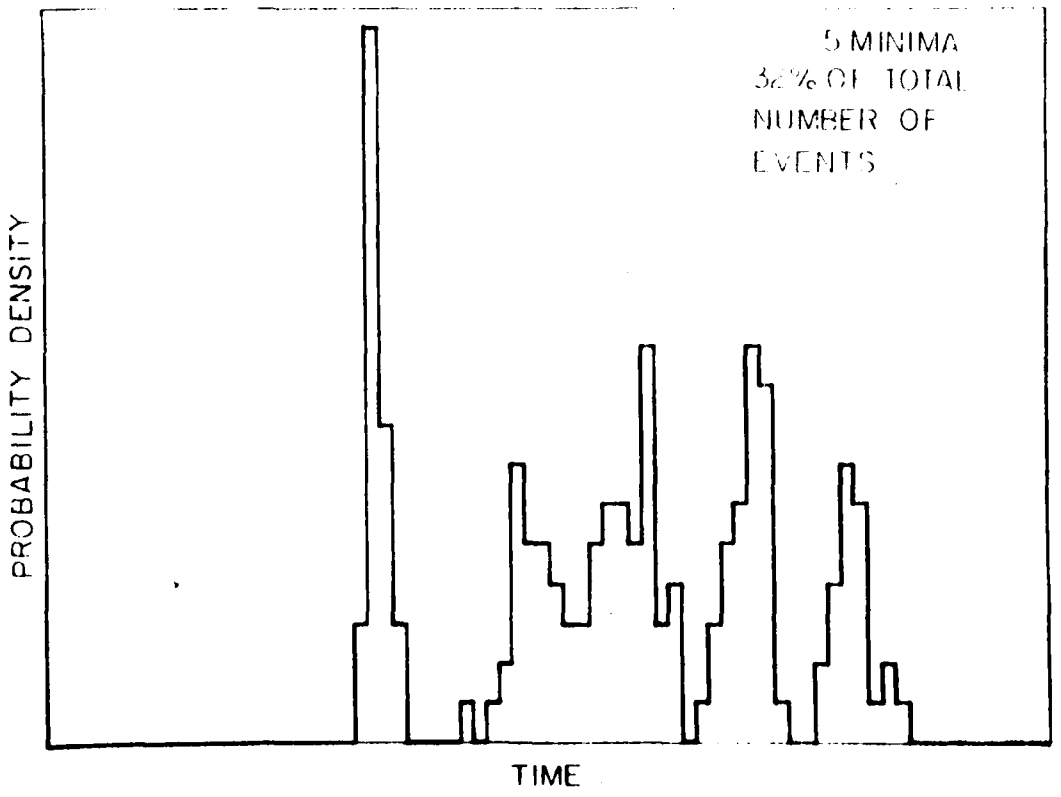
5 MINIMA
3c% OF TOTAL
NUMBER OF
EVENTS
PROBABILITY DENSITY
TIME

FIGS 3 & 4

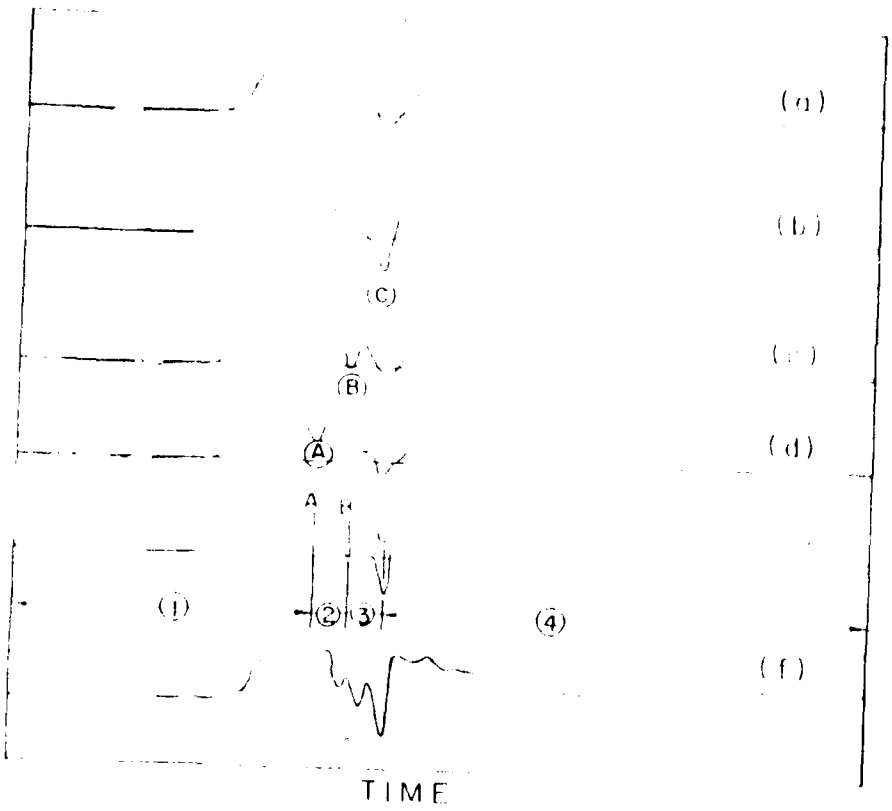
(a)
(b)
(c)
(B)
(d)
A
B
(1)
(2)
(3)
(4)
(f)
TIME

FIG. 5

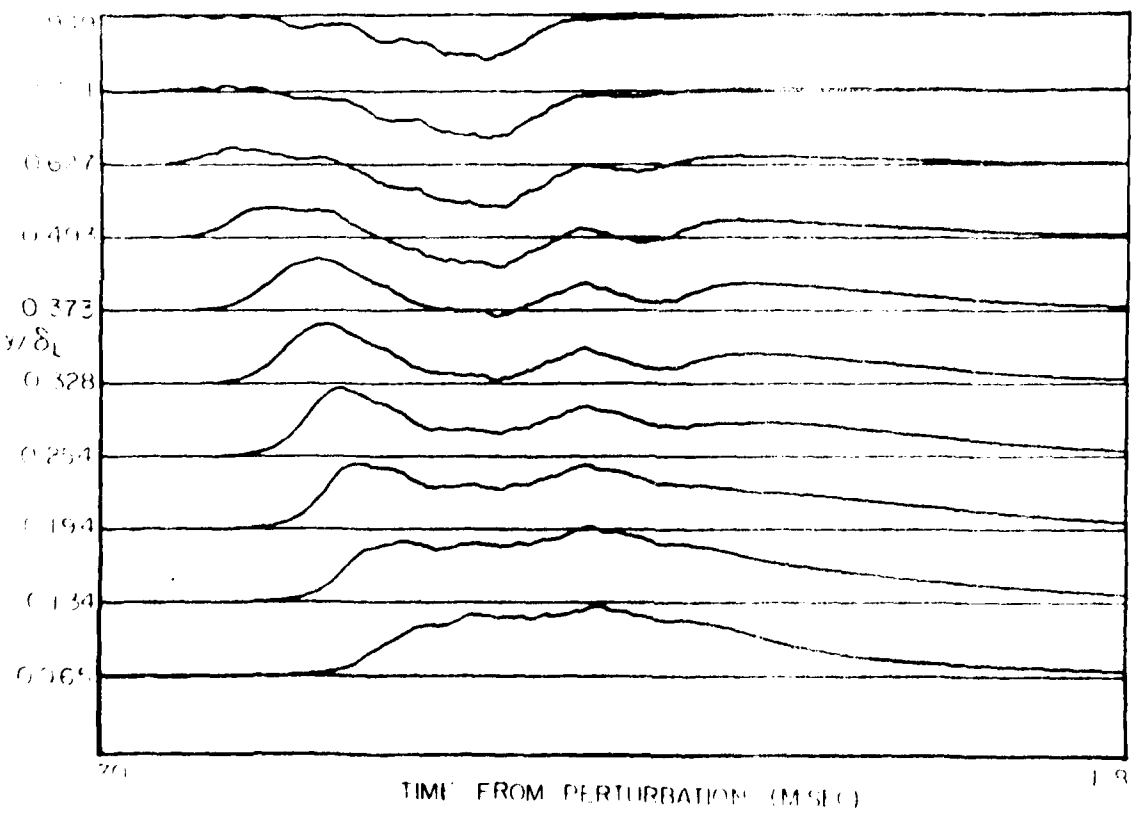
0.373
y/δL
0.328
TIME FROM PERTURBATION (MSEC)

FIG. 6a

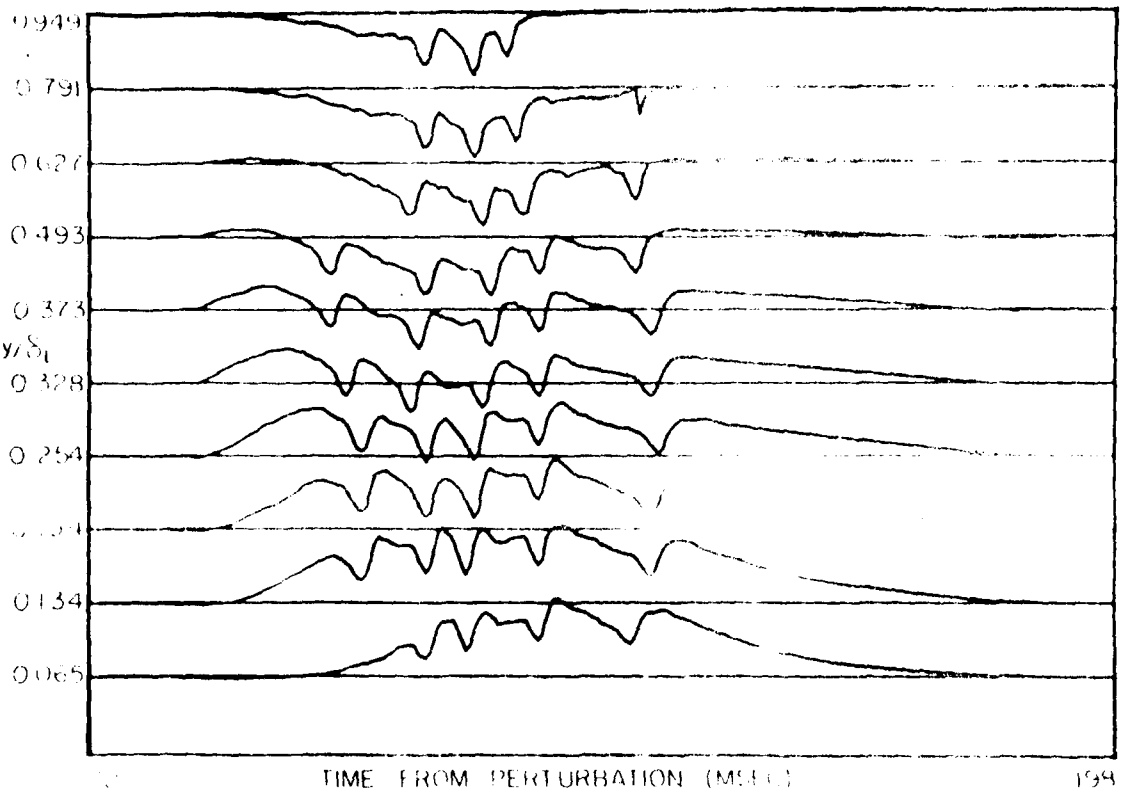
0.949
0.791
0.627
0.493
0.373
y/δ1
0.328
0.254
0.134
0.065
TIME FROM PERTURBATION (MSEC)

FIG. 6b

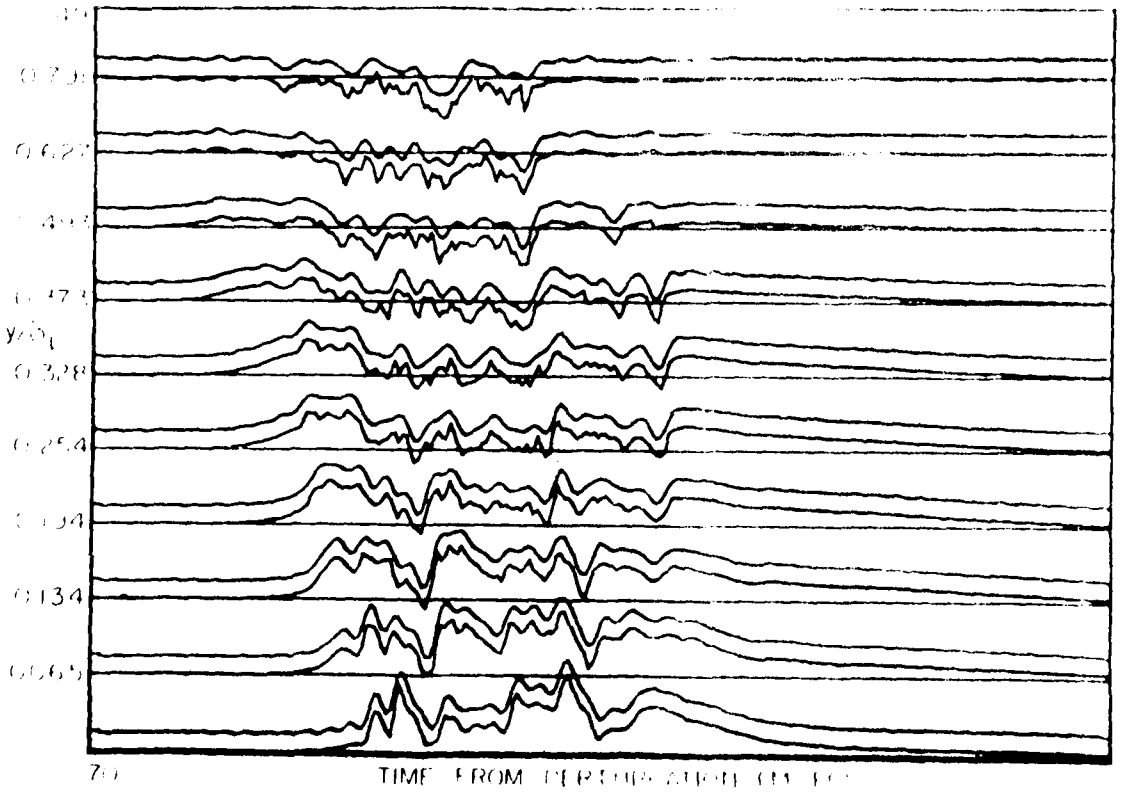
0.622
0.134
y/δ1
0.328
0.134
TIME FROM PERTURBATION (MSEC)

FIG. 6c

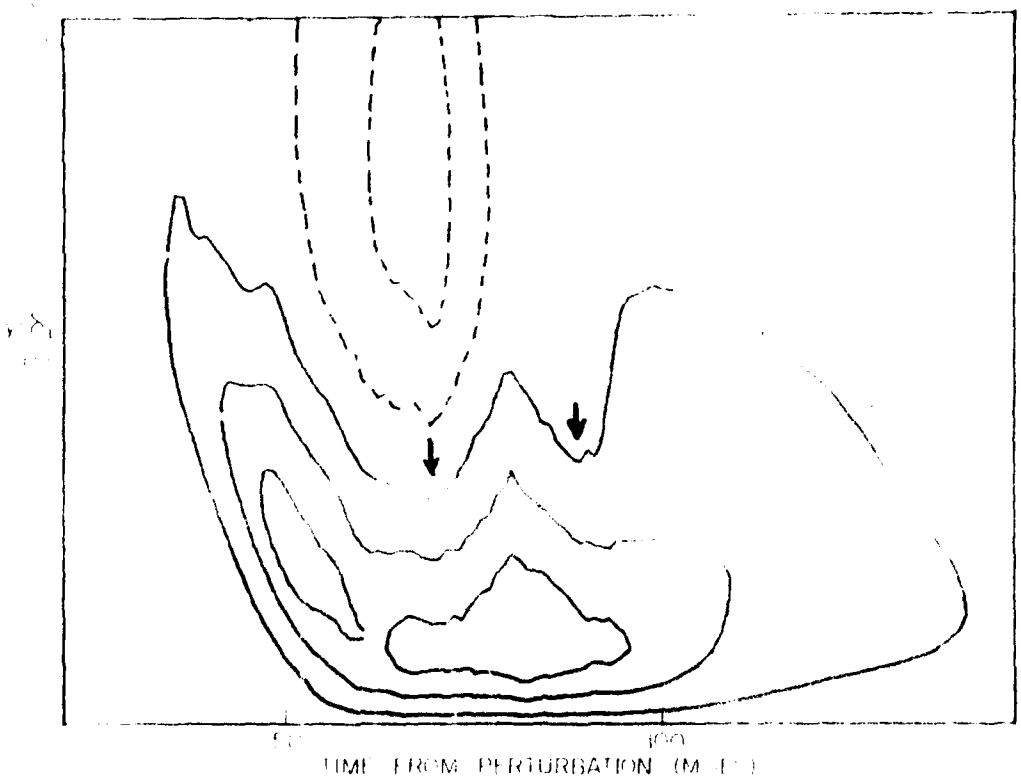
TIME FROM PERTURBATION (M

FIG 7a

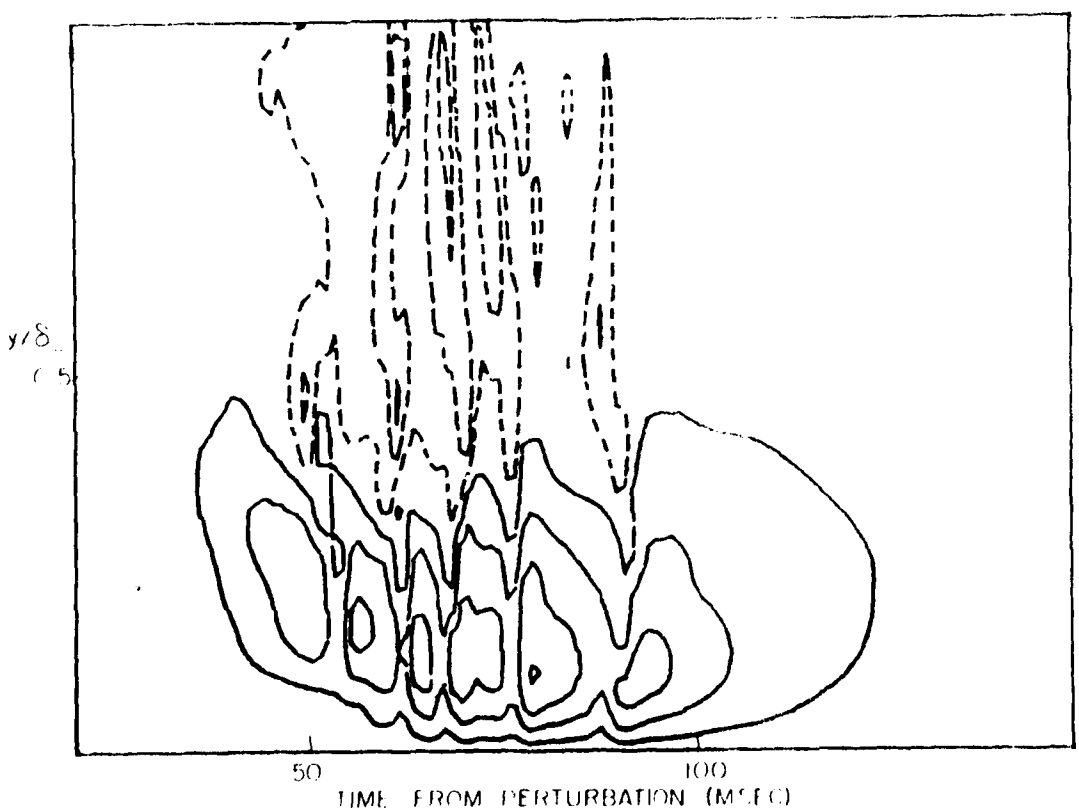
y/δ
50
100
TIME FROM PERTURBATION (MSEC)

FIG 7b

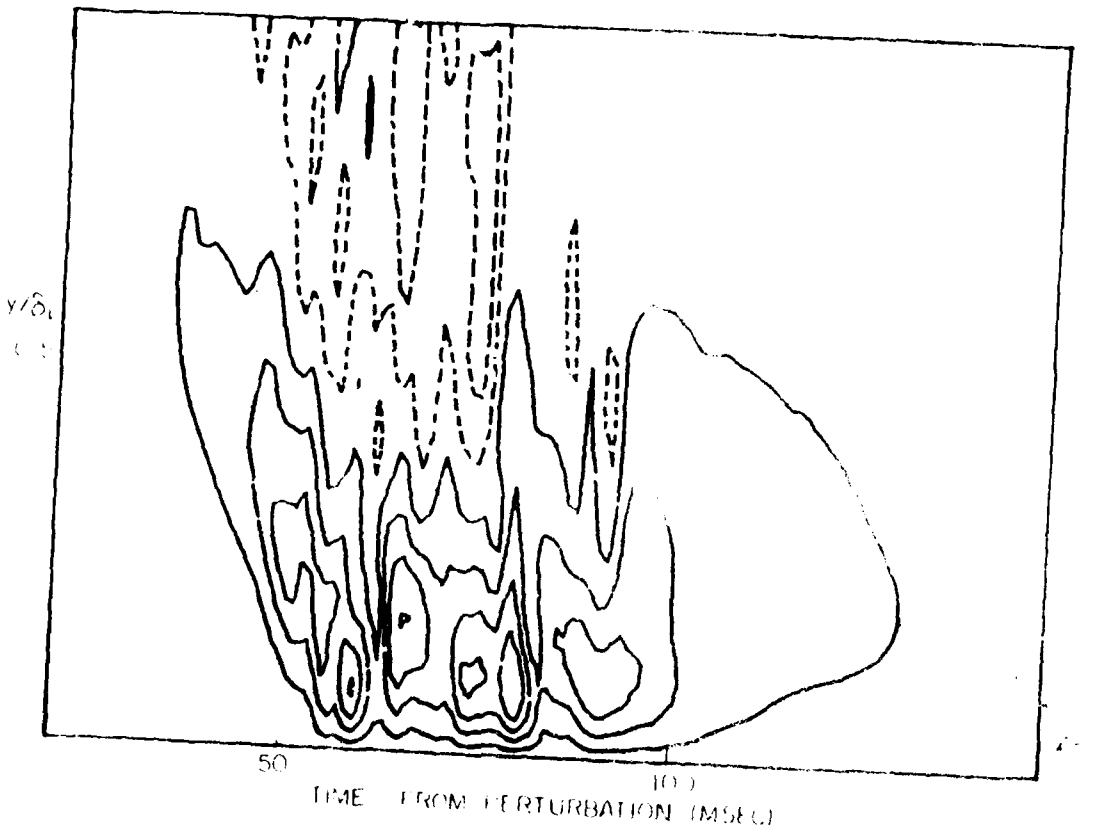

FIG

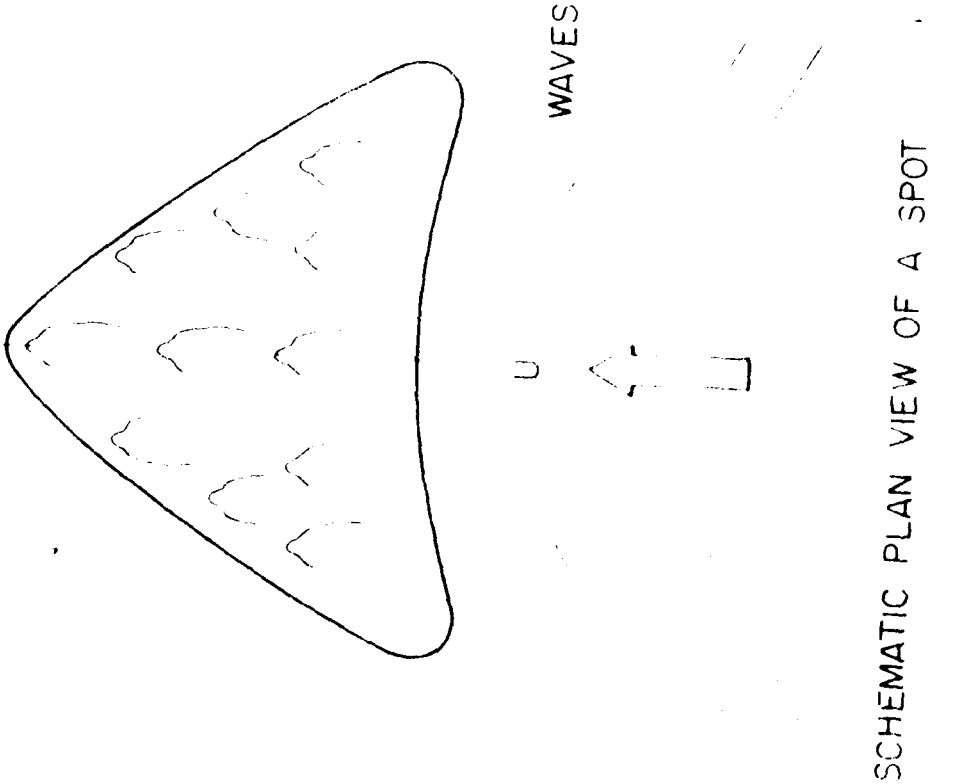

SCHEMATIC PLAN VIEW OF A SPOT

FIG

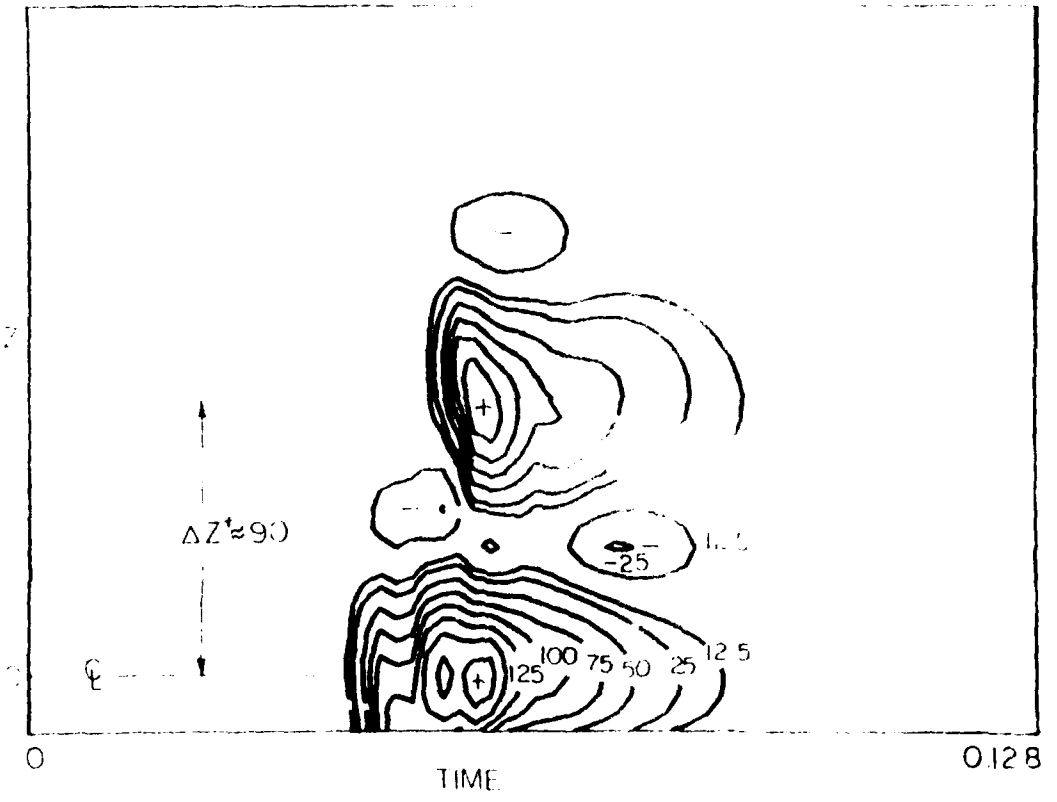
ΔZ⁺≈90
-25
125
100
75
50
25
12.5
0
0.128
TIME

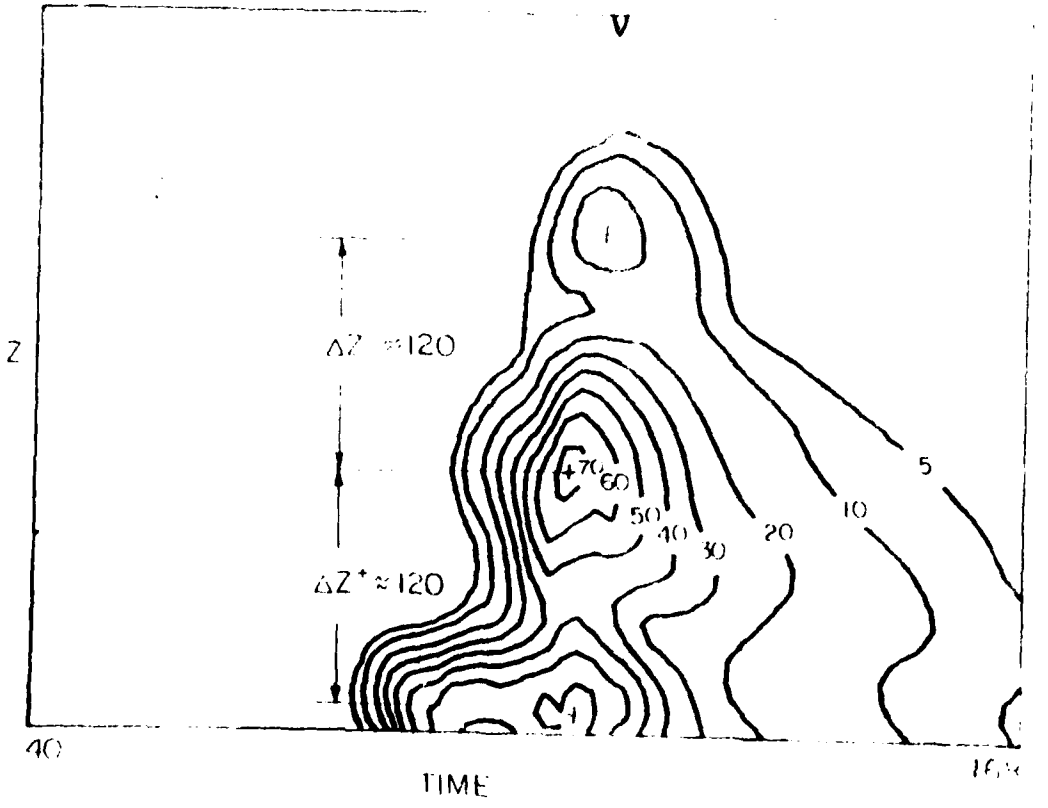
V
Z
ΔZ ≈120
ΔZ⁺≈120
70
60
50
40
30
20
10
5
40
TIME

INVESTIGATION OF THE TURBULENT CHARACTERISTICS OF A PULSATING PIPE FLOW

THESIS SUBMITTED FOR THE DEGREE "DOCTOR OF PHILOSOPHY"

BY

LEV SHEMER

SUBMITTED TO THE SENATE OF TEL-AVIV UNIVERSITY

JUNE 1981

This work was carried out under the supervision of

Professor Israel Wygnanski

ACKNOWLEDGMENTS

I wish to express my deep gratitude to Prof. I.Wygnanski for introducing me the problem, for his interest in the work, encouragement and readiness to share his experience and knowledge during the course of this investigation.

Special thanks are also due to Dr. E.Kit for endless discussions and numerous enlightening suggestions, which had a great influence on the general approach accepted in the present work.

I wish to thank Prof. R.Narasimha from Indian Institute of Science, Bangalore, India, for the opportunity to discuss with him the problem during his visit to Tel-Aviv and for usefull remarks.

I am also grateful to all my colleagues in the Laboratory of Fluid Mechanics, and espessially to Dr. S.Einav for his help at early stages of the work, to Dr. D.Oster, whose experience was widely used in the data processing, and to Mr. I.Weisbrot for his help in constructing the experimental facility and in data processing.

The typing of Miss R.Kurtzman and the draftsmanship of Mr. Y.Ben-Aharon are deeply appreciated.

Finally, I want to thank my wife, Sophie, and my children, Gaby and Michal, for tolerating the many hours I spent in the lab instead of devoting them to the family.

ABSTRACT

Pulsating flow of air in a straight smooth pipe was investigated experimentally. Most measurments were made at a mean Reynolds number of 4000, but the influence of Re was checked for 2900<Re<7500. The period of forcing ranged from 0.5 sec to 5 sec which resulted in the change in the non-dimensional frequency parameter $\alpha = R\sqrt{\omega/\nu}$ of 4.5 to 15. Velocities at the exit of the pipe and pressure drop along the pipe were measured simultaneously; velocity measurments were made using arrays of hot-wire anemometers consisting either of normal wires or an x array. Signals from the anemometers or pressure transducers were digitized and processed by a minicomputer before being recorded on a magnetic tape.

The introduction of periodic surging had no effect on the time mean quantities. The present data was compared in detail with the theory of Uchida (1956) in the laminar flow regime. The time dependent components at the forcing frequency were represented by the radial distribution of amplitude and phase. An integral momentum equation in a time dependent flow requires a force triangle to be maitained at any instant. The triad of forces are: pressure, inertia and shear. All terms of the force balance equation were measured independently providing a good check of data. The measured turbulent characteristics of the flow, including the RMS values of the velocity fluctuations, Reynolds stress and short time power spectra are dependent on the phase of the forced oscil-

lations.

The radial distribution of the phase angle of velocity is qualitatively different in laminar and turbulent flows. In order to explain this difference the concept of a relaxation time of the turbulent flow was employed. A simple eddy viscosity model for time dependent flow, which takes into account the "memory" of turbulence is proposed, and numerical solution of the Navier-Stokes equation for the turbulent pulsating pipe flow utilizing the proposed model were obtained.

TABLE OF CONTENTS

NOMENCLATURE

a	=sound velocity
a_n, b_n	=Fourier transform coefficients
A_1, A_2	=integration constants (Eq.(2.20))
A^+	=26.0 empirical constant in eddy viscosity model
c	=power spectra coefficients
D	=diameter
E	=anemometer output (volt) (Chapter 2)
E	=turbulent energy (Chapter 3)
f	=frequency
f_E	=dissipation frequency
g,h	=arbitrary functions
k	=0.4 empirical constant in eddy viscosity model
ℓ	=mixing length
ℓ_p	=length of the scotch-yoke
L^p	=length of the pipe
m	=mass of the gas in the settling chamber
p	=pressure
p_o	=atmospheric pressure
$\vec{p}$	$= \omega V_o p_1$ vector of pressure (Chapter 2)
$\vec{p}$	$=0.5\,\partial p_1/\partial x$ vector of pressure (Chapter 4)
Q	=flow rate
$\vec{Q}$	$=p_o Q_1 \exp(-i\phi_q)$ ' vector of flow rate (Chapter 2)
$\vec{Q}$	$=Q_1(r)\exp(-i\phi_q)$ ' vector of flow rate (Chapter 4)
r	=radial coordinate
r_p	=piston displacement
R^p	=pipe radius
Re	$=UD/\nu$ Reynolds number
St	$=fD/U$ Strouhal number
t	=time
T	=period of pulsations
T	=absolute temperature (deg K)(in Eq.(2.7) only)
u	=axial velocity
u_*	=friction velocity
U	=bulk velocity
$\vec{U}$	=velocity vector
u', v'	=turbulent velocity fluctuations
v	=radial velocity
V	=volume of the settling chamber
$\vec{V}$	$=\omega\rho_o V_1 \exp(i\phi_v)$ vector representing the change in volume
W	=mechanical power
x	=radius-vector
x	=axial coordinate
Y_1	=defined in p.29
Z_1	$=i\,\omega/\rho_o$
Z_0	$=Z_1\lambda_1$

Greek Letters

α	$=R\sqrt{\omega/\nu}$ frequency parameter
β	=hot-wire inclination angle

γ =[illegible]
δ =boundary layer thickness
$\delta\nu$ =viscous sublayer thickness
ϵ_{St} =Stokes layer thickness
ϵ =kinematic eddy viscosity
ϵ_o =kinematic eddy viscosity in steady flow
ϵ_1 =kinematic eddy viscosity in oscillating flow
$\bar{\epsilon}_1$ =complex eddy viscosity
θ =relaxation time
λ =friction coefficient (Chapter 3)
λ =acoustic wave length (Chapter 2)
μ =dynamic viscosity
ν =kinematic viscosity
Π =1.02 empirical constant in eddy viscosity model
ρ =density
σ_u =$(u_1/\bar{u})/(p_1/\bar{p})$
σ_τ =$(\tau_{b1}/\bar{\tau}_w)/(p_1/\bar{p})$
τ =shear stress
τ =$(\tau_1/r)\exp(i\phi_\tau)$ shear stress vector
τ_E =dissipation time scale
ϕ =phase angle
ω =$2\pi f$ cyclic frequency (Hz)

Subscripts and Symbols

cr =critical value
p =piston
1 =amplitude of oscillations
w =value at the wall
$\langle ... \rangle$ =denotes phase average
=(overbar) denotes time mean value

CHAPTER 1

INTRODUCTION AND REVIEW OF LITERATURE

1.1 General Introduction

The pulsating pipe flow is considred a "simple" time dependent flow. It is "simple" both spatially and temporally. In the absence of swirl the pipe flow is two-dimensional spatially, and in the fully developed region all mean quantities are functions of the radius only. Nevertheless, the theoretical solution for the problem of the linear stability of the stationary pipe flow was only recently obtained (see Goldshtick and Shtern (1977) and the process of transition from the laminar to turbulent flow is still an enigma although it has been investigated experimentally (Wygnanski and Champagne (1973), Rubin, Wygnanski, and Haritonidis (1979)). The spatial "simplicity" of the flow is therefore somewhat delusive. The superposition of simple harmonic oscillations on the steady mean flow adds a temporal dependence which considerably complicates the detailed analysis.

The importance of studying time dependent flows in general, and pulsating pipe flow in particular, is obvious. Most biological flows are pulsating, may be because the peristaltic pump is the simplest pump which can be employed by a biological system. Pulsating pipe flows were

therefore extensively studied by investigators associated with medicine and life-sciences (for references see Caro, Pedley and Schroder (1976), Hussain (1977)). Non-steady flows occur also in many engineering applications, for example: the discharge of any piston pump is pulsating, thus the flow in an intake or exhaust manifold of internal comoustion engine is pulsating; the flow in hydraulic lines and control systems often pulsates etc.

1.2 The Analysis of Periodic Data

The periodic nature of the turbulent flow suggests the decomposition of any flow variable $g(\vec{x},t)$ into 3 components (Hussain and Reynolds (1970))

$$g(\vec{x},t)=\overline{g(\vec{x})}+\langle g(\vec{x},\phi)\rangle+g'(\vec{x},t) \qquad 1.1$$

where $\overline{g(\vec{x})}$ is time mean value of the variable $g(\vec{x},t)$ at point $\vec{x}$

$$\overline{g(\vec{x})} = \lim_{T\to\infty} 1/T \int_{-T/2}^{T/2} g(\vec{x},t)dt$$

$\langle g(\vec{x},\phi)\rangle$ is the contribution of the periodic part at a phase angle ϕ at the same point $\vec{x}$ and is defined by

$$\langle g(\vec{x},\phi)\rangle = \lim_{N\to\infty} 1/N \sum_{i=1}^{N} (g_i(\vec{x},\phi)-\overline{g(\vec{x})})$$

and $g'(\vec{x},t)$ is the random nonperiodic part. Experimentally, the value of $\langle g \rangle$ is determined by averaging the data at a fixed phase angle and subtracting from the result the time mean value $\bar{g}$. The flow is pulsating provided the quantity $\langle g \rangle$ does not vanish. From the definition of the phase mean component $\langle g \rangle$ it is clear that the following relations must hold for the temporal mean values

$$\overline{g'} = \overline{\langle g \rangle} = \overline{g' \langle h \rangle} = 0 \qquad 1.2$$

A distinction is sometimes made between "pulsating" and "oscillating" flows; the former term implies that oscillations are superimposed on a non-vanishing steady velocity, while the term "oscillating" flow refers to $\overline{g(\vec{x})} = 0$. The phase dependent part of the flow $\langle g \rangle$ is referred to as the oscillating part.

Assuming that the flow is not only periodic, but also harmonic, and defining the phase angle $\phi = \omega t$, the periodic component may be represented by the real part of the exponential

$$\langle g(\vec{x}, \phi) \rangle = Re(g_1(\vec{x}) \exp(i(\omega t + \phi_g)) \qquad 1.3$$

where $g_1(\vec{x})$ is the amplitude of pulsations and ϕ_g is a reference phase angle. All phase angles referred to in this work are measured relative to pressure. Whenever a periodic motion is not simply harmonic, the time dependent variable can always be expanded in Fourier series, so that the right hand side of Eq.(1.3) becomes the leading time dependent

term in the expansion.

In the analysis of the harmonically pulsating flows it is often convenient to use vectorial notation, which is generally accepted in electrical engineering, and represents graphically the periodic component of the variable <g> by a vector of the length g_1 and angle ϕ_g relative to a reference direction (in our case the pressure). This presentation will be used later for further elucidation of phase and amplitude relationships in a pulsating pipe flow.

1.3 Governing Equations

In the absence of swirl the circumferencial component of velocity w vanishes thus only the axial u and radial v velocity components has been considered.*) The continuity equation for the incompressible flow in cylindrical coordinates has the following form:

$$\partial u/\partial x + 1/r\ \partial/\partial r(vr) = 0 \qquad 1.4$$

Decomposing the axial and the radial velocities into three distinct components according to (1.1), and averaging, we obtain that the contin-

*) The full set of equations for the nonstationary flow in the cylindrical coordinates was given by Cheng (1971).

uity equation in the form of (1.4) is valid for each of three components seperately: time mean, periodic, and random.

The Navier-Stokes equations for axial and radial velocity components (see Hinze (1975)) are

$$\frac{\partial u}{\partial t} + u\frac{\partial u}{\partial x} + v\frac{\partial u}{\partial r} = -\frac{1}{\rho}\frac{\partial p}{\partial x} + \nu\left(\frac{\partial^2 u}{\partial x^2} + \frac{\partial^2 u}{\partial r^2} + \frac{1}{r}\frac{\partial u}{\partial r}\right) \qquad 1.5$$

$$\frac{\partial v}{\partial t} + u\frac{\partial v}{\partial x} + v\frac{\partial v}{\partial r} = -\frac{1}{\rho}\frac{\partial p}{\partial r} + \nu\left(\frac{\partial^2 v}{\partial x^2} + \frac{\partial^2 v}{\partial r^2} + \frac{1}{r}\frac{\partial v}{\partial r} - \frac{v}{r^2}\right) \qquad 1.6$$

Decomposing the velocity and pressure terms in (1.5) and (1.6) according to Eq.(1.1) and averaging with respect to time taking into account the definitions (1.2) yields:

$$\bar{u}\frac{\partial \bar{u}}{\partial x} + \bar{v}\frac{\partial \bar{u}}{\partial r} = -\frac{1}{\rho}\frac{\partial \bar{p}}{\partial x} + \nu\left(\frac{\partial^2 \bar{u}}{\partial x^2} + \frac{1}{r}\frac{\partial}{\partial r}\, r\frac{\partial \bar{u}}{\partial r}\right) - \frac{\partial}{\partial x}\left(\overline{\langle u\rangle^2} + \overline{u'^2}\right) - \frac{1}{r}\frac{\partial}{\partial r}\, r\left(\overline{\langle u\rangle\langle v\rangle} + \overline{u'v'}\right) \qquad 1.7$$

$$\bar{u}\frac{\partial \bar{v}}{\partial x} + \bar{v}\frac{\partial \bar{v}}{\partial r} = -\frac{1}{\rho}\frac{\partial \bar{p}}{\partial r} + \left(\frac{\partial^2 \bar{v}}{\partial x^2} + \frac{1}{r}\frac{\partial}{\partial r}\, r\frac{\partial \bar{v}}{\partial r}\right) - \frac{1}{r}\frac{\partial}{\partial r}\, r\left(\overline{\langle v\rangle^2} + \overline{v'^2}\right) - \frac{\partial}{\partial x}\left(\overline{\langle u\rangle\langle v\rangle} + \overline{u'v'}\right) \qquad 1.8$$

Equations (1.7) and (1.8) indicate that the Reynolds stress in pulsating turbulent flow can be regarded as a sum of the oscillating and random parts. The Reynolds equations for the oscillating component may be deduced by phase averaging of the time dependent equations (1.5) and (1.6) and substracting from the result equations (1.7) and (1.8), respectively.

When the pipe flow is fully developed, all the time and phase mean parameters are independent of the streamwise coordinate x; thus it follows from the continuity equation that the temporal and phase averaged radial components of velocity vanish in the fully developed region.

$$\bar{v}=\langle v\rangle=0$$

The Reynolds equations for the stationary and oscillating components of the axial velocity are then:

$$0=-1/\rho\ \partial\bar{p}/\partial x+1/r\ \partial/\partial r(\ \nu r\partial\bar{u}/\partial r-\overline{ru'v'}) \qquad 1.9$$

$$\partial\langle u\rangle/\partial t=-1/\rho\ \partial\langle p\rangle/\partial x+1/r(\ \nu r\partial\langle u\rangle/\partial r-r\langle u'v'\rangle) \qquad 1.10$$

and for the fully developed laminar flow, equation (1.9) is reduced to

$$\partial u/\partial t=-1/\rho\ \partial p/\partial x+1/r\ \partial/\partial r(\ \nu r\partial u/\partial r) \qquad 1.11$$

As a result of linearity of (1.11), the solution is a superposition of two independent parts: the steady parabolic velocity profile calculated by Poiseuille and the time dependent oscillating part.

1.4 Review of Pertaining Literature

Velocity measurements in oscillatory pipe flow were first made by

Richardson (1927/28) and Richardson and Tyler (1929). They found, that in a pulsating laminar flow the maximum of time-mean velocity occurs near the wall of the pipe rather than on the centerline as it does in stationary flow. The location of the maximum velocity approached the surface with increasing the frequency of pulsation. This phenomenon was called "annular effect".

1.4.1 Laminar Flow

Sexl (1930) gave theoretical explanation to the annular effect in laminar flow by solving equation (1.11). The fully developed laminar oscillating velocity profile was found to be controlled by a single non-dimensional frequency parameter $\alpha = h\sqrt{\omega/\nu}$. For low values of the frequency parameter ($\alpha \ll 1$) the velocity profile is nearly parabolic in accordance with the instanteneous value of the pressure gradient. For higher values of the velocity profile deviates from the Poiseuille form and the annular effect appears.

Womersley (1955) and Uchida (1956) extended the solution of Sexl for the velocity distribution and calculated the phase and amplitude relationship among the pressure gradient, the mean bulk velocity, and shear stress in oscillating or pulsating pipe flows. The paper of Uchida gives the solutions in the most convenient form and this will be used as the main reference. Atabek and Chang (1961) tried to solve equations (1.5) and (1.6) for the developing pulsating flow in the entrance region of the pipe. They estimated the non-linear inertia terms by assuming

them to be proportional to the local value of $\partial u/\partial x$ and to the instantaneous value of the velocity entrance at the $\bar{U}(1+a_\kappa \cos \omega t)$, where $\bar{U}$ is the value of the uniform velocity at the entrance of the pipe, and a_κ is relative amplitude of velocity pulsations. The results are not presented in an analytical form but a procedure is developed which provides a solution for any given set of parameters.

Linford and Ryan (1965) measured the relation between the pressure gradient and the flow rate in an oscillatory flow of a mixture of water with glycol. They used only flow visualization techniques for measuring velocity and the accuracy of the results was poor. They concluded however, that the measured velocities agreed with the theoretical calculations of Womersley within the estimated experimental error.

Denison (1970) and Denison et al (1971) reported on measurments made in pulsating laminar flow with directionally sensitive laser velocimeter. Their apparatus was 500 diameters long, so their measurments could be made both in the entrance region and the fully developed region of the pipe. The viscosity of the working fluid was variable in order to produce the desired flow parameters (mean Reynolds number about 1000, and frequency parameter $4 \leq \alpha \leq 6$). The results obtained in the fully developed region were in good agreement with theory but in the entrance region discrepancies were found between the measurements and the predictions of Atabek and Cheng. The measured velocity profile developed significantly slower, than predicted theoretically.

Ohmi et al (1976) investigated both theoretically and experimentally the laminar pulsating pipe flow in air, taking into account, that the fluid is slightly compressible. They concluded that for $R\omega \ll 3a$, where a is the velocity of sound, the radial velocity and cross sectional variations of pressure are negligibly small. This result implies that the compressibility of the fluid does not change the radial distribution of velocity as long as the radius of the pipe is much smaller than the sound wave length produced by the oscillations.

1.4.2 Turbulent and Transitional Flows

One of the interesting features in the laminar pulsating pipe flow is that it may contain temporarily an inflection point at some phases of the motion. At high values of the frequency parameter α, points of inflection exist at all phase angles. It is well known that an existence of the inflection point is a necessary condition for the instability of unviscid flows (Rayleigh criterion). Sarpkaya (1966) tried to correlate the instability of oscillating pipe flow with the existence of an inflection point in the velocity profile. He found, that... "the flow has maximum stability, when the duration of the inflection period reaches about 53% of period of pulsations". (Sarpkaya (1966), p.598). It should be noted that Sarpkaya used erroneously a plane criterion ($d^2u/dr^2=0$) for instability, i.e., instead of a criterion applicable to cylindrical coordinates, namely: $d/dr(r\ d/dr(ru))=0$ (Batchelor and Gill (1962)). Nevertheless, these errors could not affect his conclusions significantly. The stability of bounded periodic flows seems to have

little in common with the Rayleigh criterion for an inviscid fluid. In contrast to free shear flows, like mixing layers, wakes and jets, whose instability is governed by an inviscid process, the appearance of an inflection point in an oscillatory bounded flow is a result of viscosity. Thus it seems inappropriate to use the Rayleigh criterion on these types of flow.

Stability calculations for the plane-oscillating boundary layer (von Kerszeck and Davis (1974), Davis (1976)), or the plane oscillating Poiseuille flow (Grosch and Salwen (1968)) or the round oscillating flow in a pipe (Yang and Yih (1977)) indicate that the imposed pulsations do not make the flow less stable. Yang and Yih have found, that the oscillating pipe flow is stable to axisimmetric disturbances at all frequencies and at all Reynolds numbers (based in this case on the amplitude of the velocity oscillations). No theoretical analysis is available for the stability of a pulsating pipe flow, in which oscillations are superimposed on a steady parabolic profile. The linear stability analysis applied separately to the mean and oscillatory components of the flow is incapable of predicting the outcome because the velocity profile enters into Orr-Sommerfeld equation in a nonlinear way.

The first experimental investigation of velocity and pressure in turbulent, pulsating pipe flow in water was made by Schultz-Grunow (1940). The velocity was measured by a Pitot tube, and was limited to time averaged values. It was concluded that the instantaneous velocity profiles were similar to the steady profiles in a converging channel

during the acceleration stage of a period, and to the steady profiles, existing in a diversent channel. It appeared that the intensity of turbulence increased during the decceleration stage, this observation was based on large increase in the scatter of the data during deceleration.

Cheng (1971) used hot-wire anemometry for velocity measurments in pulsating pipe flow in air. He has found, that there is a strong increase in the Reynolds stress and the turbulent kinetic energy, resulting from the addition of pulsations to the steady flow. A strong nonlinear interaction was found to play an important role in the distribution of the turoulent energy. It should be noted however, that the pipe used in Cheng's experiment was very short, about 30 diameters only, and the pulsations were not simply harmonic because of the awkward manner in which they were introduced. Consequently it is impossible to obtain reliable phase averaged information from these results.

Gerrard (1971) investigated the turbulent pulsating pipe flow by flow visualization technique which enabled him to obtain mainly qualitative data. He found a similarity between laminar and turbulent oscillating velocity profiles. Gerrard also observed the phase dependence of turbulent intensity and found, that all turbulence nearly disappears during the acceleration stage. The similarity between laminar and turbulent oscillating velocity profiles was noticed also by Emsmann (1973), who used six thermistor probes for instantaneous velocity measurments at different radial positions.

A number of investigators (Sergeev (1966), Clarion and Pelissier (1975), Merkli and Thomann (1977), among others) tried to determine the transition Reynolds number in oscillating pipe flow, whenever the flow becomes turbulent during a portion of the cycle only. A large scatter in the results indicates, that the instability has a nonlinear character and depends strongly on the experimental facility. In the work of Merkli and Thomann, for example, a pipe which was closed from both sides was used; that resulted in the appearance of shock waves and the pressure gradient was not spatially uniform. Their results seem to be relevant to the specific experimental set-up only. All the above mentioned experiments show that the flow can be turbulent during some part of the cycle, and laminar during another part of the cycle.

Clamen and Minton (1977) investigated experimentally oscillating and pulsating pipe flow in water by a hydrogen-bubble technique. A good agreement with theory was observed in laminar flow at low Reynolds number; at higher Reynolds numbers, their pipe which was only 170 diameters in length was far too short for the flow to become fully developed. They observed that the intermittency of the pulsating flow at higher Re (Re≈2900) depended on both the mean Re and amplitude of velocity oscillations.

Mizushina et al (1973[a], 1973[b], 1975) and Maruyama (1974) investigated a pulsating turbulent flow by electrochemical method, which enables measurments of instantaneous velocity. The measured data was recorded on a magnetic tape for subsequent processing on digital computer.

they found a critical value of the pulsation period T_{cr}, so that for slow pulsations (i.e. for $T>T_{cr}$) there is no significant change in turbulent intensity at different phase angles, and the flow behaves like a "steady" turbulent flow. For higher frequencies ($T<T_{cr}$), the turbulent characteristics are strongly dependent on the phase angle. A calculated eddy viscosity $\varepsilon=\tau/(\partial u/\partial r)$ attained negative values at certain phase angles, when relaminarization took place during the acceleration. An empirical relation for critical period of pulsations T_{cr} was determined to be:

$$T_{cr}\bar{U}/D=0.10Re^{2/3} \qquad 1.12$$

where $\bar{U}$ is the time mean bulk velocity. It is not clear from these results whether the change in the flow behaviour results from the different frequencies of pulsations, or there might be an influence of the amplitude of the pulsations at higher frequencies.

Kirmse (1975) used laser Doppler velocimeter to measure pulsating turoulent pipe flow in water at high values of the dimensionless frequency parameter ($55<\alpha<137$). The phase shift between pressure and velocities at all radial positions and at all frequencies was found to be 90^{o}. An eddy viscosity model was used to calculate the time-dependent velocities in this type of flow, and a reasonable agreement was obtained for velocity profiles at two phase angles.

Ramaprian and Shuen-Wei Tu (1980) observed laminarization of ini-

tially turbulent flow of oil in a pipe when pulsations were introduced. They observed that the maximum amplitude of the velocity pulsations near the surface of the pipe is attained before the maximum amplitude occurs in the central region of the pipe whenever the flow is fully turbulent. Poor angular resolution of the data in their experiment did not allow them to get quantitative information about phase shift angles. The velocity profiles, measured in laminar pulsating flow, were in good agreement with the theoretical results of Uchida. Similarity was noted between laminar and turbulent flows at the same frequency, and it was concluded that the imposed oscillations have no effect on the time mean properties of the flow.

CHAPTER 2

A DESCRIPTION OF THE APPARATUS, THE INSTRUMENTATION AND THE EXPERIMENTAL TECHNIQUES

2.1 General Description of the Experimental Apparatus

A straight and smooth aluminium pipe 33 mm in diameter and 17×10^3 mm long was used. The facility, shown schematically on Fig.2.1, was originally used by Wygnanski and Champagne (1973), and described in detail in their paper. The pipe was carefully alligned to within 1 mm over it's entire length. The contraction was made of two subsections, giving an overall area ratio of .340:1. As a result of the careful alignment and the smooth inlet, laminar flow could be retained at the Reynolds numbers exceeding 20000 without the addition of screens. The mean flow was supplied by a high pressure source (6 atm compressor) and controlled by a precise pressure regulator. This arrangement insured that that the flow rate was independent of the superimposed pulsations and the flow regime, whether laminar or tubulent, in the pipe.

Pressure oscillations were introduced by a valveless piston pump, connected to the settling chamber. The piston diameter D_p was 90 mm, and it's displacement r_p could be changed from about r_p=5 mm to r_p=75 mm in 17 steps. The length of the scotch-yoke was ℓ_p=500 mm. The bulk rate of change of the settling chamber for the circular frequency ω is

given by

$$dV/dt = \pi D^2/4 r_p \omega (\cos \omega t - r_p/2\ell_p \sin 2\omega t)$$

the amplitude ratio in the bulk displacement between the fundamental frequency ω and it's first harmonic 2ω is therefore $r_p/2\ell_p < 0.1$ at the highest possible displacement amplitude. The oscillations at the harmonic frequency could thus be neglected. The pump was driven by 1.5 hp variable speed motor, permitting a change in the period of pulsations between 0.5 sec to 5 sec. The repeatability of the period was better than 0.3%.

2.2 The Piston Pump as a Source of Pressure and Velocity Pulsations

The velocity and pressure pulsations in the pipe, resulting from the movement of the piston, can be easily analyzed by assuming that the flow in the pipe is laminar and fully developed. The amplitude of the pulsations of the bulk velocity is $U_1 = Q_1/\pi R^2$, where R is the radius of the pipe, and Q_1 is the amplitude of the oscillations in the flow rate. U_1 is proportional to $\partial p_1/\partial x$, where p_1 is the amplitude of pressure pulsations at the entrance of the pipe. For fully developed flow $\partial p_1/\partial x = p_1/L$, where L is the length of the pipe. For a given amplitude of pressure oscillations the amplitude of the bulk velocity U_1 depends strongly on frequency. If $\bar{U}$ is the steady part of the volumetric velo-

city ($\bar{u}=\bar{Q}/\pi R^2$, where $\bar{Q}$ is the mean flow rate) and $\bar{p}$ is the steady pressure, then the relationship between the ensemble averaged time dependent parts $\langle u\rangle$ and $\langle p\rangle$ can be expressed by the equation

$$\langle u\rangle/\bar{u}=\langle Q\rangle/\bar{Q}=\sigma_Q(\langle p\rangle/\bar{p})\cos\phi_Q \qquad 2.1$$

where the amplitude coefficient $\sigma_Q=(Q_1/\bar{Q})/(p_1/\bar{p})$ and phase lag angle ϕ_Q were calculated for the fully developed laminar flow by Uchida (1956) and reproduced in Fig.2.2. The abscissa in this figure is $\log\alpha=\log R\sqrt{\omega/\nu}$. It can be seen from Fig.2.2, that at very low frequencies ($\alpha<1$) $\sigma_Q \approx 1$ and the phase lag $\phi_Q \to 0$. Thus, when the frequency of the imposed pulsations is low, the flow at any instant behaves like a Poiseuille flow at the appropriate instantaneous pressure gradient. Inertia effects become noticeable with increasing frequency when the flow cannot follow after the rapid changes in pressure anymore. An increase in α causes a corresponding increase in the phase angle between the volumetric velocity and the pressure ϕ_Q, and dampens the amplitude of the velocity pulsations, as well. At very high frequencies ($\alpha >>1$) the inertial term becomes dominant in comparison with the viscous term, and the resulting acceleration ($dQ/dt=i\omega Q_1$) is proportional to the driving force (instantaneous pressure). The quantity iQ_1 is thus in phase with the pressure, while the pulsations in flow rate have 90° phase lag behind p_1.

Consider the control volume in which the movement of the piston causes a corresponding change in the volume of the settling chamber.

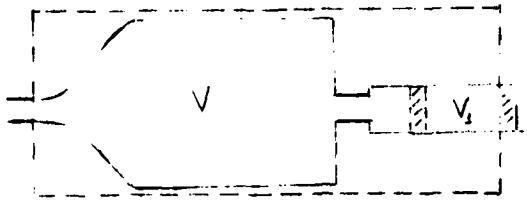

If $\langle Q \rangle$ is the time dependent component of the volume flow, the continuity equation for the control volume may be expressed by:

$$dm/dt = d/dt(\rho V) = -\langle Q \rho \rangle \qquad 2.2$$

where V is the volume, ρ is the density, and $\langle Q \rangle$ is assumed to be positive when the fluid leaves the settling chamber through the pipe.

For small amplitudes of volume oscillations, V_1, (relative to the total volume of the settling chamber V_o) and pressure oscillations, p_1, (relative to the atmospheric pressure p_o) equation (2.2) can be linearized to give

$$\rho_o dV/dt + V_o d\rho/dt = -\rho_o \langle Q \rangle \qquad 2.3$$

Equation (2.3) is a linear homogeneous equation, having solutions of the form

$$V = V_o + V_1 \exp(i(\omega t + \phi_v)) \qquad 2.4$$

$$p = p_o + \bar{p} + p_1 \exp(i\omega t) \qquad 2.5$$

$$\langle Q \rangle = Q_1 \exp(i(\omega t - \phi_q)) \qquad 2.6$$

where ϕ_v and ϕ_q represent the phases of the volume and flow pulsations, respectively, relative to the phase of the pressure oscillation which was arbitrarily set to be zero. Assuming that air obeys the ideal gas law

$$p = \mathbb{R}\rho T \qquad 2.7$$

where $\mathbb{R}$ is gas constant, and that the process is isothermal, and substituting equations (2.4) to (2.7) into (2.3) one obtains

$$p_o i\omega V_1 \exp(i(\omega t+\phi_v)+V_o i\omega p_1 \exp(i\omega t)+p_o Q_1 \exp(i(\omega t-\phi_q))=0 \qquad 2.8$$

Eq.(2.8) contains two unknown amplitudes, p_1 and Q_1, but the assumption of fully developed laminar flow provides an additional equation relating the two quantities. Substituting (2.1) into (2.8) and cancelling $\exp(i\omega t)$ yields

$$i\omega p_o V_1 \exp(i\phi_v)+p_1(i\omega V_o - 1/\bar{p}\ \bar{Q} p_o \sigma_q \exp(-i\phi_q))=0 \qquad 2.9$$

Equation (2.9) can be separated into real and imaginary parts and solved for ϕ_v and p_1. In laminar pipe flow $\bar{Q}/\bar{p} = \pi D^4/128\ \mu L$ is a known quantity fixed by the flow geometry and the viscosity of the fluid. Substituting it into (2.9) and taking real part of the equation gives

$$-\omega V_1 \sin\phi_v+(\bar{Q}/\bar{p})p_1 \sigma_q \cos\phi_q=0 \qquad 2.10$$

and imaginary part of (2.9) provides the second equation

$$\cos \phi_v = - \frac{p_1}{V_1} \left(\frac{V_o}{\bar{p}_o} + \frac{\bar{Q} \sigma_q \sin \phi_q}{\bar{p} \omega} \right) \qquad 2.11$$

One may now express ϕ_v and p_1 in terms of the piston displacement V_1 and frequency of pulsations ω

$$\operatorname{tg} \phi_v = - \frac{p_o \frac{\bar{Q}}{\bar{p}} \sigma_q \cos \phi_q}{(\omega V_o + p_o \frac{\bar{Q}}{\bar{p}} \sigma_q \sin \phi_q)} \qquad 2.12$$

$$p_1 = \frac{\omega V_1 \sin \phi_v}{\frac{\bar{Q}}{\bar{p}} \sigma_q \cos \phi_q} \qquad 2.13$$

The amplitude of the oscillations in the flow rate Q_1 can be expressed in terms of p_1 and Eq.(2.1)

$$Q_1 = (p_1/\bar{p}) \sigma_c \bar{Q} \qquad 2.14$$

For a given amplitude of the volumetric change of the system V_1, amplitudes of the oscillations in the flow rate Q_1 and in pressure p_1 were calculated from equations (2.12) to (2.14) as functions of the period (Fig.2.3[a]). At low frequencies (large values of the period T, $\alpha < 1$) $\sigma_c \approx 1$, and the pressure amplitude in the settling chamber is adequate to "push" through the pipe nearly all the mass flow supplied by the piston pump to the settling chamber. At these frequencies the amplitude in flow rate is thus proportional to the rate of change in the volume of the settling chamber V_1. For $\alpha < 1$ therefore the relation $Q_1 \sim 1/T$ is

obtained.

At higher frequencies ($\alpha > 1$) σ_q decreases with increasing frequency (see Fig.2.2), and the amplitude of the pressure oscillations in the settling chamber, resulting from the oscillations in the volume of the system grow more steeply than the flow rate. In order to understand the physical meaning of the mutual interaction between the oscillations in the pressure and in the flow rate, equation (2.8) is rewritten in vector form, using the notation $\vec{V}=\omega c_o V_1 \exp(i\phi_v)$; $\vec{P}=\omega V_o p_1$, and $\vec{Q}=p_o Q_1 \exp(-i\phi_q)$:

$$i\vec{V}+i\vec{P}+\vec{Q}=0 \qquad 2.8^a$$

The calculations indicate, that the oscillations in pressure and volume are nearly 180^o out of phase ($\phi_v \approx 180^o$), i.e. pressure increases when the piston pushes air into the settling chamber, and vice versa. At frequencies corresponding to $\alpha \approx 5$ the resulting oscillations in the flow lag behind the pressure by more than 70^o (see Fig.2.2). Taking into account these phase relations, and the fact, that multiplication by i adds 90^o to the phase angle, two sketches can be drawn, the first showing the relative direction of each vector, and the second representing the mass balance in accordance with Eq.(2.8^a):

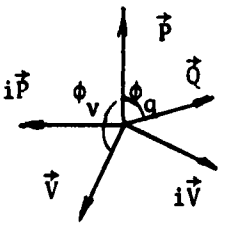

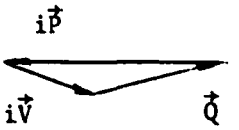

It follows from the diagram, that the pressure vector $\vec{P}$ is inclined to the flow rate vector $\vec{Q}$ by about 180°. When the pressure in the settling chamber is maximum, the time dependent portion of the flow rate is directed towards the settling chamber, causing a further increase in pressure amplitude. The phase relations between pressure and flow rate thus lead to a kind of a positive feedback, resulting in curves $Q_1=Q_1(\alpha)$ and $p_1=p_1(\alpha)$ (Fig.2.3[a]), which resemble a resonance phenomenon. The amplification of pressure oscillations has however nothing in common with resonance, since in this case the system has no eigen frequency.

At even higher frequencies ($\alpha > 6$) σ_q is small, and the pressure amplitude is insufficient to provide strong oscillations in the flow rate, thus Q_1 decreases, and the amplification influence of the flow rate on the pressure fluctuations weakens; so the pressure amplitude decreases together with the amplitude of flow rate. Further increase in frequency ($\alpha > 10$) results in $\sigma_q \to 0$, and vanishing oscillations in flow rate. In this case the entrance from the settling chamber to pipe may be regarded as closed for the time dependent flow, and the amplitude of the pressure oscillations tends to a constant value $p_o V_1/V_o$ which corresponds to the ideal gas law pV=const.

The results of Fig. 2.3[a] were calculated for the geometrical data appropriate to the existing experimental facility. The total volume of the settling chamber was approximately equal to 1 m^3, and the maximal changes in volume were 100 cm^3. The preceeding calculations show, that

the maximum responce of the system to the volume oscillations occur at T=3.25 sec (α=5.7) (Fig.2.3^a). In reality, the maximum amplitude of pressure pulsations occured at T=2.4 sec, corresponding to α =6.7. (Fig.2.3^b). The discrepancy between theory and experiment is attributed to the influence of the entrance region which was not considered in the calculations, and some difference in the geometrical parameters. Fig.2.3^a shows that the calculated maximum amplitude of the pressure oscillations is about three times higher, than it would have been if the settling chamber was closed (i.e. $\Delta p(\alpha=5.7)/\Delta p(\alpha\to\infty) \approx 3$) The maximum amplification in pressure oscillations realized in laminar flow was approximately 2.5, and the absolute value of Δp at α=6.7 agrees fairly well with the calculations (see Fig.2.3^b).

Some amplification exists in turbulent pulsating flow also, as it can be seen from the Fig.2.3^b, but the maximum amplitude is reduced. The mechanism of the amplification in turbulent flow is qualitatively identical to the mechanism in laminar flow. It will be shown in Section 3.2, the oscillating parts of the bulk velocity <U> in both laminar and turbulent flow behave alike, but the phase lag angle ϕ_q is notably less in the turbulent flow, than in the corresponding laminar case. The component of the flow rate vector $\vec{Q}$, which is collinear with the pressure vector $\vec{P}$ and thus causes the amplification (see the sketches), has the length $|\vec{Q}|\sin\phi_q$; and thus a lower value of ϕ_q in the turbulent case causes a reduction in pressure amplification. The maximum of the curve $p_1=p_1(\alpha)$ is shifted in α relative to its position in the laminar flow obviously due to different amplitude $\sigma_q=\sigma_q(\alpha)$ and phase $\phi_q=\phi_q(\alpha)$ rela-

tions in this case.

2.3 The Influence of the Length of the Pipe on the Pulsating Flow

It is usually assumed that in a fully developed region of a pulsating pipe flow the pressure gradient depends on time only, and consequently the radial component of the pulsating velocity has to vanish. Only recently Richardson (1980) raised this question in his discussion of the paper of Kirmse (1979). Richardson argued that applying a pulsating pressure at one end of the pipe does not necessarily result in a linear pressure distribution along the pipe; acoustic waves may make pressure gradient dependent on the axial coordinate and resulting in the generation of a radial component of velocity. It was noted in Section 1.4, that the fully developed, laminar pulsating flow is independent of the axial coordinate because the inertial term in the Navier-Stokes equations (1.4) $(\vec{u}\nabla)\vec{u}$ dissapears, making the equation linear and enabling a separation of the steady from the oscillating flow components. The pressure gradient is independent of the axial coordinate whenever any change in pressure at the inlet of the pipe is felt "instantly" in the entire pipe. Since a weak pressure pulse travels at the speed of sound, a, the assumption of spatially constant pressure gradient may only be valid for a limited length of the pipe L.

In order to obtain an estimate of the highest permissible pulsation

frequency and the longest pipe length L for which the pressure drop $\partial p/\partial x$ may be assumed constant the flow is considered to be incompressible (i.e. $\bar{U}<<a$). The pressure is prescribed at both ends of the pipe: $p=0$ at the open end of the pipe at $x=L$; and $p=\bar{p}+p_1\cos(\omega t)$ at the inlet to the pipe at $x=0$. When $\bar{U}<<a$ and can be neglected, one obtains the wave equation for the spatial and temporal pressure distribution

$$\partial^2 p/dt^2 = a^2 d^2 p/dx^2 \qquad 2.14$$

The solution of (2.14) for the given boundary conditions is:

$$p(x,t) = \frac{\bar{p}}{L}(L-x) + p_1 \frac{\sin\frac{\omega}{a}(L-x)}{\sin\frac{\omega}{a}L}\sin\omega t \qquad 2.15$$

Pressure gradient therefore becomes:

$$\frac{\partial p}{\partial x}(x,t) = -\frac{\bar{p}}{L} - \frac{\omega}{a}\frac{\cos\frac{\omega}{a}(L-x)}{\sin\frac{\omega}{a}L}\sin\omega t \qquad 2.16$$

The pressure gradient may be regarded as spatially constant provided $x\,\omega/a<<1$ for all x concerned, or that the lenth of the pipe L is much shorter than the acoustic wave lenth $L<<2\pi a/\omega$.

A more accurate estimate of the limitation on the frequency of oscillations of a slightly compressible fluid in a pipe of a given length is obtained by considering the continuity equation for the pulsating part of the bulk velocity $\langle u\rangle$

$$\frac{\partial}{\partial t}(\rho_o+\langle\rho\rangle) + (\rho_o+\langle\rho\rangle)\frac{\partial\langle u\rangle}{\partial x} = 0 \qquad 2.17$$

and the momentum equation

$$\partial(\rho_o+\langle\rho\rangle)/\partial\langle u\rangle/\partial t = -\partial\langle p\rangle/\partial x - 2\langle\tau_w\rangle/h \qquad 2.18$$

where $\langle\tau_w\rangle$ is the oscillating part of the wall shear stress $\langle\tau_w\rangle = -\mu(\partial\langle u\rangle/\partial r)_w$. By assuming that the fluid is only slightly compressible, (i.e. $\langle\rho\rangle/\rho_o << 1$), equations (2.17) and (2.18) can be linearized to give

$$\frac{\partial\langle\rho\rangle}{\partial t} + \rho_o\frac{\partial\langle u\rangle}{\partial x} = 0 \qquad 2.19$$

and

$$\rho_o\frac{\partial\langle u\rangle}{\partial t} = -\frac{\partial\langle p\rangle}{\partial x} - \frac{\partial\langle\tau_w\rangle}{R} \qquad 2.20$$

The pressure term can be eliminated from (2.20) using the adiabatic sound velocity

$$\frac{\partial\langle p\rangle}{\partial x} = a^2\frac{\partial\langle\rho\rangle}{\partial x} \qquad 2.21$$

The wall shear stress $\langle\tau_w\rangle$ may be eliminated by following the equation

$$\frac{\langle \tau_w \rangle}{\bar{\tau}_w} = \sigma_\tau \frac{p_1}{\bar{p}} e^{i\phi_\tau} \qquad 2.22$$

and equation (2.1), where $\bar{\tau}_w$ and $\bar{p}$ are the steady wall shear stress and pressure, respectively. Shear stress and pressure pulsations amplitude ratio σ_τ and relative phase shift ϕ_τ were calculated using the analitical solution of Uchida for the laminar pulsating flow. From the equations (2.1) and (2.22)

$$\frac{\langle \tau_w \rangle}{\bar{\tau}_w} = \frac{\sigma_\tau}{\sigma_q} \frac{U_1}{\bar{U}} e^{i(\phi_\tau + \phi_q)}$$

The steady bulk velocity U and the steady wall shear stress $\bar{\tau}_w$ are related by the equation

$$\bar{\tau}_w = \frac{16}{Re} \frac{\rho_o \bar{U}^2}{2} = 8 \frac{\rho \nu \bar{U}}{R}$$

We therefore obtain

$$\tau_w = 8 \rho_o \nu / R \, (\sigma_\tau / \sigma_q) \exp(i(\phi_\tau + \phi_q)) \qquad 2.23$$

By assuming harmonic oscillations, the time derivatives can be replaced by the operator $i\omega$, so that $\partial\langle\rho\rangle/\partial t = i\omega\rho_1$, and $\partial\langle U\rangle/\partial t = i\omega U_1$. Equations (2.19) and (2.20) were therefore rewritten in the form:

$$\frac{dU_1}{dx} = - \frac{i\omega}{\rho_o} \rho_1 \qquad 2.24$$

and

$$\frac{d\rho_1}{dx} = -\frac{1}{a^2}\left(i\omega\rho_o + \frac{8\rho_o\nu}{R}\frac{\sigma_\tau}{\sigma_q}e^{i(\phi_\tau+\phi_q)}\right)U_1 \qquad (2.24)$$

[illegible] equation gives

$$\partial^2 U_1/\partial x^2 = \alpha_1\lambda_1 U_1 \qquad (2.25)$$

and

$$\partial^2 \rho_1/\partial x^2 = \alpha_1\lambda_1\rho_1 \qquad (2.27)$$

where

$$\alpha_1 = i\omega/\rho_o$$

and

$$Y_1 = \frac{i\omega\rho_o}{a^2}\left(1+\frac{8i\nu}{R}\frac{\sigma_\tau}{\sigma_q}e^{e(\phi_\tau+\phi_q)}\right)$$

introducing $\gamma=\alpha_1\lambda_1$ the solution of (2.25) can be presented in the form

$$b_1 = A_1\exp(-\gamma x) + A_2\exp(\gamma x) \qquad (2.26)$$

using (2.25) and (2.26) the density distribution becomes

$$\rho_1 = A_1/\alpha_o\exp(-\gamma x) - A_2/\alpha_o\exp(\gamma x) \qquad (2.28)$$

where $\alpha_o = \alpha_1/\lambda_1$.

To determine the integration constants A_1 and A_2 the boundary conditions at both ends of the pipe are used. At the outlet the amplitude of the pressure pulsations vanishes and so does thus the amplitude of density pulsations $\rho_1(x=L)=0$. For the given amplitude of pulsations in the flow rate, Q_1, the boundary condition on the amplitude of the bulk velocity pulsations at the inlet is: $U_1(x=0)=Q_1/\pi R^2$. Taking into account the boundary conditions the final form of the solution is:

$$U_1 = \frac{Q_1}{\pi R^2} \frac{\cosh \gamma(L-x)}{\cosh \gamma L} \qquad 2.30$$

$$\rho_1 = \frac{Q_1}{\pi R^2} \frac{\sinh \gamma(L-x)}{\cosh \gamma L} \qquad 2.31$$

As a quantitative measure of the flow dependence on frequency a phase shift between the bulk velocity pulsations at both ends of the pipe was chosen. It is obvious that for the flow to be independent of x this phase shift has to vanish. The complex parameter which governs the phase of U_1 at different locations along the pipe is γ, which in itself depends both on the length of acoustic wave $\lambda=2\pi a/\omega$ and on the frequency parameter α. The parameter is dependent on the radius of the pipe and on the viscosity of the fluid. The major factor governing the phase shift was found to be the ratio λ/L (i.e. the acoustic wave length to the lengtn of the pipe). Fig.2.4 gives numerical results of solution (2.30) for the parameters used in this experiment (R=1.65 cm, L=1700 cm) and $\nu=0.16$ cm^2/sec. It can be seen from Fig.2.4 that for $L/\lambda<0.08$ the resulting phase shift is less than $1^\bullet$. Accepting this

value as the upper limit for which one may assume $\partial p/\partial x$=const. gives the maximum permitted frequency parameter α=15, and pulsation period longer than 0.5 sec. It is worth noting that for $L/\lambda > 0.2$ the flow can no longer be regarded as one-dimensional, even by a crude approximation.

2.4 Calibration of Velocity and Pressure Sensors

Velocity measurments were made with a rake of 9 hot wires, distributed evenly in the radial direction at distances equivalent to $\Delta r/R=0.12$ between the neighbouring wires; so that when the first wire was on the center line of the pipe, the 9-th wire was located at a distance 0.5 mm from the wall (i.e. at $r/R=0.97$). All velocity measurments were taken at the exit plane of the pipe. A 10 channel constant temperature hot-wire anemometer and 10 channel amplifier, both built by the electronic shop of the School of Engineering of Tel-Aviv University were used in the experiment. The outputs of the amplifier were connected via an analog to digital converter to a DEC PDP 11/60 minicomputer.

The calibration of the hot wires is done in a wind tunnel, which provided a stable velocity stream between 30 cm/sec and 15 m/sec. Although flow reversal was avoided in the experiment, very low velocities occured in the pipe as a result of the superimposed pulsations. It was thus necessary to calibrate the wires at the lowest velocities anticipated in the experiment.

It is well known, however, that standard Pitot tube is not a proper instrument for measuring air velocities below 1.5 m/s. An alternative way for accurate measurment of low velocities may be based on the frequency of vortices shed behind a circular cylinder. Insert in Fig.2.5 (Kovazsnay (1949)) shows the dependence of the frequency of shedding, i.e. the Strouhal number St=fD/U, on the Reynolds number of the cylinder suggesting that St is independent of Re for Re>300. The later measurments by Roshko (1955, 1961) confirmed the results shown in Fig.2.5 for Re>300. At Re<300 St decreases with decreasing Re; and the scatter in the data collected by various investigators is very large in this area. Different empirical formulae showing the dependence St=f(Re) (see, for example, Goldstein (1965), Berger and Wille (1972)) are not very accurate and may cause significant errors at low Reynolds numbers.

In this experiment a cylinder 1.269 cm in diameter was used for the velocities under consideration (U>35 cm/sec); Re thus was larger than 300 and Strouhal number therefore could be regarded as a constant. The dependendence of St on Re was measured for Re>1700, where a Pitot tube could provide accurate measurments of velocity, and it was assumed that the mean value of St could be extrapolated to lower Reynolds numbers.

A hot wire was placed several diameters downstream of a cylinder at a radial location at which the vortex shedding frequency is detected most clearly on an oscilloscope, and the output of the anemometer was sampled digitally by the computer. The sampling frequency was fixed by the signal frequency, which was roughly estimated from monitoring the

oscilloscope. The minimum sampling frequency chosen was approximately twice the expected signal frequency. A buffer of 2040 sampled data points was Fourier transformed, and the power spectrum of the signal was calculated. The procedure was repeated several times (usually 4 to 10, depending on sampling frequency), the average specrum was calculated, and the frequency of the most energetic component was assumed to be the signal frequency. The repeatability of the frequency measurment was better than 0.2% which seems equivalent to the resolution of the method.

On the Fig.2.5 the measured dependence of St on Re is shown; Fig.2.6 gives the calibration curve for the dependence of flow velocity on the vortex shedding frequency.

The detailed description of the hot wire calibration procedure may be found in the thesis of Oster (1980) and in wygnanski and Oster (1981). Seven calibration velocities, determined by the vortex shedding method, were used. A 4-th order polinomial, giving the dependence of the flow velocity u on the output voltage E was found by a least square method from the 7 measured points:

$$u=a_1E^4+a_2E^3+\ldots+a_5$$

The calibration curve was further checked for several additional velocities.

In order to calibrate an x-wire the output voltage was sampled at

11 different angles (in the range of $27^{\circ}>\beta>-27^{\circ}$) at each one of 7 velocities used. The output of each wire depends on both absolute value of the velocity vector $\vec{U}$ and its angle : $E_1=E_1(|\vec{U}|,\beta)$ and $E_2=E_2(|\vec{U}|,\beta)$. It was assumed that from the measured values of E_1 and E_2, U and β can be uniquely determined. From the measured 77 calibration points the 4-th order polinomials, giving the dependence of the absolute value of the velocity vector $|\vec{U}|$ and its angle β on the output voltages of both wires E_1 and E_2 were found

$$|\vec{U}|=a_1E_1^4+a_2E_2^4+\ldots+a_{13}E_1+a_{14}E_2+a_{15}$$

$$\beta=b_1E_1^4+b_2E_2^4+\ldots+b_{13}E_1+b_{14}E_2+b_{15}$$

With $|\vec{U}|$ and β known, the velocity components were calculated from the equations $u=|\vec{U}|\cos\beta$ and $v=|\vec{U}|\sin\beta$.

A Validyne model DP215-30 pressure transducer with CP15 Sine Wave Carrier Demodulator was used to measure the pressure. The pressure transducer was connected by a 5 cm long tygon tube to the second section of bell-shaped nozzle. For the calibration of the Demodulator output a Fuess micromanometer was connected in parallel with the transducer. The pressure transducer provides linear responce in the whole range of pressures. The dynamic responce of the pressure transducer (1000 Hz) was more than adequate for the present purpose.

2.5 Data Aquisition

A D.C. voltage corresponding to the output of the anemometer in absence of flow was subtracted from the signal before amplification in order to take advantage of the full range of the A/D converter which accepts signals between ± 5 volt. The converter having a 12-bit presision provides a resolution of about 2.5 mv. The amplified anemometer signals together with the output from the pressure transduser were sampled at a predetermined frequency, the sampled data was converted into 16-bit words and arranged in buffers.

At the initiation of a measurment the period of pulsations was determined by the computer. Two different methods to measure the period were used in this work, the first based on the 50 Hz clock of the computer, and the second on 1 MHz clock. An optical switch (Monsanta MCA8) was used to obtain trigger signal. A cylinder 1.5 mm in diameter, connected to the driving motor of the piston pump, passed at each revolution trough a narrow gap of the optical switch, causing change in the output current, which operated TTL Schmidt trigger. In the first method the time ellapsed between two neighbouring trigger signals, supplied to the interrupt input of the computer, was measured by 50 Hz clock. The resolution of a single measurment is 20 msec, the final result was obtained by averaging 10 measurments. In the second method the trigger signal served as input to the A/D converter and was sampled at a predetermined sampling rate, controled by the 1 MHz clock. The period was der-

ived from the number of sampled points between two consequent trigger p[illegible] and the time interval between samples. The resolution of this method depends on sampling frequency and was in principle orders of magnitude more accurate than in the first method. In this case too, the final period was determined by averaging over 10 cycles.

With the period of pulsations known, the sampling frequency was fixed so that 1024, 2048 or 4096 points were sampled per channel per period in order to facilitate the processing of data using a Fast Fourier Transform (FFT). An estimate of the repitability of the period from one event to another was made counting the number of sampled points over many cycles, and it was found to be better than 0.3%.

Two different sampling methods were used. In the first method a trigger signal, supplied to the interrupt of the computer, initiated the sampling which lasted precisely for 1 period. From the sampled data points appropriate velocities and presssure were calculated and the results were recorded on a magnetic tape. After the data recording was completed the computer was ready to accept new information. All x-wire, and some of normal-wire rake data was acquired using this method, which has the advantage that it does not constrict the sampling frequency. There are, however, two drawbacks. Firstly, the overall acquisition time is much longer than the time of measurment, because the computer requires additional time to convert the signals to velocities and pressure and to record the processed data on tape. The overall duration of the measurment increasd thus by a factor of 2 in the case of the normal

wires and by a factor of 4 for the single x-array. The second drawback stems from the fact that the duration of the measurments corresponds exactly to one period of pulsations, thus no spectral information can be obtained for frequencies which are lower than the frequencies of pulsations.

A different sampling method was used therefore in conjunction with a rake of normal wires. The data points were sampled continuously during more than 8 periods of pulsations. The memory was divided into two buffers, and while one buffer accepted the information sampled, the contents of the other buffer was recorded on a magnetic tape, thus providing the possibility of essentially unlimited in length continuous sampling. The output of the optical switch was connected to an additional input channel and provided phase information. A total of 11 data channels were thus sampled: 9 channels contained velocity information, 1 pressure and 1 phase information. This method does not have the two drawbacks of the mentioned before, but it is limited to a sampling frequency which could not exceed 1800 Hz. This frequency however was quite adequate in the range of Re considered. It should be noted that in this method the "raw" data was recorded on the tape, and the calculations of velocity and pressure were made at a later stage.

In the latter type of sampling single continuous record consists of more than 8 periods. In laminar flow 7 recordes were usually acquired, providing 56 measured periods of pulsations containing 1024 sampled points in each period. In turbulent flow, the number of records was usu-

ally 30, giving 240 periods with the number of points in each period ranging from 1024 to 4096, depending on the duration of the period. In laminar flow, therefore, 57344 points were sampled for each data channel per measurment, while in the turbulent case the number of sampled points per channel varied from $2.5*10^5$ to 10^6.

2.6 Preliminary Measurments

In most cases velocity measurments were taken in laminar and turoulent flow regimes consecutively while keeping all the flow parameters, (e.g. mean Reynolds number, period of pulsations and piston stroke) constant. Before recording the data on magnetic tapes, preliminary measurments were made, in which the data was sampled at the rate of 1024 points per channel per period for several periods. The time mean velocity was calculated for each channel by averaging, and mean Reynolds number and flow rate were calculated by numerical integration using a Simpson formula. The exact distances between the wires were measured with a microscope and were used in the integration procedure. In laminar pipe flow the center line velocity is double the mean bulk velocity. This fact, coupled with independence of the mean flow rate from the state of the flow (whether laminar or turbulent) was used to allign the rake at the exit of the pipe. The preliminary measurments also served as a simple check of the drift in the output of the anemometers.

It was observed that the hot-wire which was placed at a distance of 0.5 mm from the wall overestimated velocity values because of heat

transfer to the metal wall which was absent in the calibration conditions in the wind tunnel. At the Reynolds numbers used, the velocities near the wall were usually less than 0.7 m/sec. Thus, the heat transfer was greatly influenced by free convection, which is strongly dependent on the flow geometry. For this reason the mean output of the last wire was ignored in the integration procedure and served only for obtaining information on the oscillating and turbulent components of velocity. The non-slip condition at the wall was taken as an additional point for the purpose of integration. The hot wire placed on the center line of the pipe did not contribute to the flow rate because of its vanishing radial distance.

For all radial-rake data, only seven measured velocities were used to determine the mean flow rate. The relatively small number of data points and absence of reliable information near the wall, contributed to a discrepancy between the Re calculated from the velocity profile and measured with a rotameter of about $\pm 5\%$ This estimate was obtained using the fact, that the flow rates were independent of the flow regime, and compairing the results obtained in laminar and turbulent flows with the constant rotameter reading. The accuracy of this measurment did not appreciably changed by changing the flow regime in the pipe from laminar to turbulent.

CHAPTER 3

EXPERIMENTAL RESULTS

3.1 Mean Flow: Steady vs. Pulsating Velocities and Pressure

Fig.3.1[a] represents time mean velocity profile measured by an x-wire probe in laminar pulsating flow and normalized by the center-line velocity. The velocity profile presented was taken at Re=4000, period T=1.34 sec, relative amplitude of bulk velocity $U_1/\overline{U}$=20%. In Fig.3.1[b] three measured turbulent velocity profiles are shown, one of the profiles was taken in steady flow at Re=4000, while for the other two the amplitude of pulsations was varied. No significant difference can be observed between steady and pulsating time mean velocity profiles whether in laminar or turbulent flow. This result could be anticipated in fully developed laminar flow, because of the resulting linearity of the Navier-Stokes equations, but in turbulent pulsating flow it indicates, that the time mean Reynolds stresses are not affected by the oscillations.

The friction coefficient λ , calculated from Darcy's formula

$$\overline{p}/\rho = \lambda L/D\ \overline{U}^2/2$$

did not show any difference between steady and pulsating flows for both laminar and turbulent regimes. The measured friction coefficient in laminar flow was higher by about 10%, than the theoretically predicted value of 64/Re. In turbulent flow the value of λ obtained is in fair agreement with the values quoted in the literature for smooth pipes (see H.Schlichting (1975)).

A number of factors might have influenced the accuracy at which λ was defined. 1) The accuracy of the measurment of the mean bulk velocity, as discussed above. 2)Pressure was measured in the entrance nozzle rather than in the developed region of the pipe in order to increase the resolution of the measurment. Pressure differences at Re=4000 along the entire pipe were approximately 2 mm of water in laminar flow and 4 mm of water in turbulent flow. The measured pressure therefore included the influence of the developing flow in the entrance region and the dynamic head component $\rho\overline{U}^2/2$. 3) It is difficult to null the output of the pressure transducer because of relatively low values of mean pressure, as compared to the pick pulsation values.

3.2 Phase Mean Values: Laminar vs. Turbulent Flow

Phase-averaged data is obtained from the measurments discussed for both laminar and turbulent flow regimes thus providing the first two terms in the decomposition (1.1). Fig.3.2 shows a typical dependence of

phase averaged velocities in a tuoulent pulsating flow during one period. The concommitant reference pressure oscillations are shown at the top of the Figure. Each velocity trace is normalized on the time mean velocity on the center line of the pipe. The uppermost velocity trace corresponds to r/R=0 (i.e. the velocity was measured on the center line) and the bottom trace represents the velocity at r/R=0.97. During a fraction of the period the pressure at the inlet of the pipe is lower than at the exit, pointing to the existence of an adverse pressure gradient. The velocity however does not reverse itself at all radial positions and at all phase angles. The relations between the amplitudes and the phase angles of pressure and velocity oscillations may thus lead to a situation when at a portion of the period the direction of the flow is opposite to the instantaneous direction of the pressure gradient.

The validity of the assumption that pressure and velocity oscillations are harmonic may be checked by representing the ensemble averaged signals in Fourier series. The "power" spectra were calculated, and the ratio of the two first coefficients $c(2\omega)/c(\omega)$, i.e. for the coefficient of the fundamental frequency and its first harmonic, was determined. For moderate amplitudes of velocity pulsations, this ratio was less than 3% thus providing the justification for the harmonic assumption. At high amplitudes, in turbulent pulsating flow, relaminarization occurs making the contribution of the second harmonic more significant.

3.2.1 Oscillating Part of the Velocity Profile

Phase locked velocity profiles can be obtained from the phase averaged velocity records. Since the time mean velocity profiles are independent of the pulsations, it is more instructive to plot the oscillating part of the velocity profile only (i.e. the part represented by the second term in equation (1.1)). In the laminar case a comparison with tne theoretical predictions of Uchida is performed. Although at least 1024 points, sampled in each period, made it possible to plot phase locked velocity profiles at 0.3^{o} intervals, it suffices to plot eight profiles, with phase difference of 45^{o} for the purpose of the following discussion.

In laminar flow the shape of the velocity profiles depends only on frequency parameter α . The oscillating part of the laminar velocity profiles corrsponding to pulsation periods T=0.78 sec (α =11.8) and T=2.4 sec (α=6.7), respectively, are shown in Fig.3.3^{a} and Fig.3.3^{b}. The symbols represent the measured values of the oscillating velocity while the solid lines represent the theoretically calculated profiles, normalized and matched to the measured velocity on the center line. The agreement with the theory is good. It may be seen, that for short periods of pulsation the flow is quite uniform in the central core of the pipe at all phases of the cycle. Sharp velocity gradients occur near the wall. The extent of the wall region is proportional to $\sqrt{\nu/\omega}$. This region is referred to in the literature as the Stokes layer in view of the analogy with the oscillating plane boundary layer which was analysed by Stokes. For large α the Stokes layer becomes narrow causing the velocity gradients to increase.

In the turbulent flow important parameter is the ratio between the thickness δ_{St} of the Stokes layer and viscous sublayer δ_ν . If one assumes that the effects of pulsations are limited to the Stokes layer while the effects of turbulence are excluded from the viscous sublayer (i.e. from $0<yu_*/\nu<5$) then for $\delta_{St}/\delta_\nu<1$ the pulsating part of the velocity profile in laminar and turbulent flows should be identical. This hypothesis may be checked by assuming that the thickness of the viscous sublayer is equal to $\delta_\nu=5\,\nu/u_*$, and the friction velocity u_* may for the sake of convenience be related to the mean velocity $\bar{U}$ by the power law (see Schlichting p.508)

$$u_*^2=0.0225U^{7/4}(\nu/R)^{1/4}$$

one obtains the following expression for δ_ν :

$$\delta_\nu=5\,\nu/u_*=60R/Re^{7/8}$$

which renders the desired thickness-ratio between of the two layers

$$\delta_{St}/\delta_\nu=Re^{7/8}/60\,\alpha$$

At Re=4000 $\delta_\nu/R=0.04$ thus for T=0.78 sec, $\delta_{St}/\delta_\nu=2.0$, and the effects of oscillations on the radial velocity distribution are visible (Fig.3.4[a]). At lower frequencies turbulence penetrates into the Stokes layer and destroyes it, and the frequency parameter α is no longer im-

portant resulting in a much more uniform velocity profile (Fig.3.4[b] recorded at T=2.4 sec, giving δ_{St}/δ_{ν} =3.5. In order to reduce furtner the thickness ratio δ_{St}/δ_{ν} the Re was reduced to 2900 for T=0.55 sec resulting in δ_{St}/δ_{ν} =1.2. The measured oscillatory velocity profiles are plotted in Fig.3.4[c]. There is a reasonable similarity between the measured turbulent (symbols) and calculated theoretically laminar (solid line) oscillating velocity profiles for this case.

3.2.2 Radial Distribution of Velocity Phase Angle and Amplitude

The harmonic character of pulsations enables one to represent the instanteneous velocity by an exponential form (Eq.(1.3)), and aleviates the necessity of describing the temporal and spatial changes in velocity by plotting a large number of phase averaged velocity profiles. Two functions can fully describe the oscillating component of velocity at the imposed frequency: (i) the amplitude distribution $u_1(r)$; (ii) the phase angle $\phi_u(r)$ relative to the phase of the pressure oscillations. In order to obtain these functions, the phase averaged velocity was Fourier transformed

$$u(r,t)=a_o(r)+\sum_{n=1}^{N}(a_n(r)\cos(nt/T)+b_n(r)\sin(nt/T)) \qquad 3.1$$

where N is half of the number of points sampled at each period, and T is period of pulsations. The coefficients, that describe the oscillations at the forcing frequency 1/T, were then used to find the amplitude fuction $u_1(r)=\sqrt{a_1^2(r)+b_1^2(r)}$ and the initial phase angle

$\phi_o(r)=\arctan((b_1(r)/a_1(r))$. From the initial phase of the velocity oscillations, the initial phase of the pressure oscillations was substracted, giving phase angles $\phi_u(r)$ relative to the pressure.

In the absence of viscosity, the pressure, being the only driving force, is in phase with the acceleration of the fluid. The velocity lags by 90^o behind the acceleration, and thus also lags behind the pressure. The radial distribution of the phase angle is shown in Fig.3.5 for Re=4000 and various periods of oscillations. The solid lines show the theoretical prediction of Uchida, while the crosses and the triangles give the measured phase angles in fully developed laminar and turbulent flows, respectively. A good agreement with the theory was obtained in the laminar case, with the exception of very low frequencies for which the influence of the entrance region becomes more pronounced, as it will be described later. The phase lag on the center line in laminar flow is usually 90^o, and it decreases to approximately 45^o near the wall.

In turbulent flow the results appear to be very different. The frequency parameter $\alpha = R\sqrt{\omega/\nu}$ no longer controls the flow because the relevant viscosity becomes some kind of turbulent exchange coefficient ε, which is orders of magnitude larger than ν. The effective frequency parameter α is thus much lower, and the phase lag of the velocity in the central region of the pipe decreases more quickly with increasing the period than in the corresponding laminar flow. In contrast to the laminar flow, the phase lag increases towards the wall. The qualitative na-

ture of the result was noticed by Ramaprian and Tu (1980). A more detailed explanation of this phenomenon which is based on a simple turbulent model for the pulsating pipe flow will be discussed later.

The radial distribution of the phase lag in velocity in the turbulent flow is both amplitude and mean Re dependent. The dependence on the amplitude of pulsations is rather weak. The radial distribution of the phase lag for two amplitudes of pulsations at two frequencies is presented in Figures 3.6[a] and 3.6[b]. For longer periods of pulsations (T=2.4 sec) changes in amplitude cause no concommitant change in the central region of the pipe. At higher frequencies (T=1.25 sec) the influence of the amplitude on the phase angle is felt accross the entire pipe. Nevertheless, a large increase in the amplitude causes a relatively small change in the phase angle (about 3°).

The dependence of the phase angle on the mean Reynolds number is more pronounced. A representative viscosity increases with increasing Re, reducing effective α. The velocity phase-lag therefore also decreases with increasing Re (Fig.3.7). On the other hand, the viscous sublayer becomes thinner with increasing Re, and the radial distribution of the phase-lag at Re=7500 is practically constant.

A qualitative difference between laminar and turbulent pulsating flows also exists in the radial distribution of the amplitudes of the velocity oscillations. In laminar flow, the maximum amplitude of the velocity oscillations occurs in the Stokes layer near the wall, as no-

ticed by Richardson (1927/28), while in turbulent flow the maximum amplitude occurs in the center of the pipe. The radial distribution of the measured amplitudes of velocity oscillations in laminar and turbulent flows resulting from identical forcing is shown in Fig.3.8. The theoretically calculated amplitudes in laminar flow which were matched on the center line (Uchida (1956)) are shown also in Fig.3.8 for comparison.

The amplitude distribution of the axial component of velocity in the turbulent flow is nearly uniform in the central region of the pipe, but decreases rapidly near the wall. The amplitude of pulsations in laminar flow also decreases near the wall. Increasing the mean Re or decreasing the frequency of oscillations lead in turbulent flow to more uniform distribution of the velocity amplitudes for the reasons already discussed in conjunction with the radial distribution of the phase lag.

3.2.3 The Influence of the Entrance Region

The disagreement between the calculated and measured phase angles of velocity at low frequencies may be attributed to the influence of the entrance region on the flow. To check this further, a second pressure transducer was placed 100 diameters upstream the exit of the pipe, (i.e. 400 diameters from the first one, which was located at the entrance of the pipe). The flow at x/D=400 is considered to be fully developed, thus the comparison between the two measured pressures could provide information about the development of pressure gradient along the pipe.

A phase shift in pressure pulsations was found to exist between these two positions and is shown in Fig.3.9[a] as a function of the pulsation period in both laminar and turbulent flows. No notable amplitude dependence was found in the measurments which were made at mean Re=4000. At long periods of forcing, pressure at the exit leads the pressure pulsations at the inlet of the pipe. The phase difference is much higher in laminar, than in turbulent flow, and decreases in both cases with decreasing period of pulsations.

The calculated values of the same phase shift are shown also in Fig.3.9[a]. The calculations were made for the appropriate values of Re and T according to the theoretical calculations of Atabek and Chang (1961) for the laminar pulsating flow in the entrance region of a pipe. It is clearly seen that the phase shift angles are underestimated by the theory. These results support the conclusion of Denison (1970), who found that the theory of Atabek and Chang predicts a faster evolution of the pulsating flow to the asymptotic, fully developed form, than observed experimentally. The conclusion of Denison is based on measurments of pulsating velocity profiles in the laminar entrance region of the pipe. It should be noted, however, that qualitatively the prediction is correct: the pressure at inlet lags behind the pressure in the fully developed region, and the phase difference increases with increasing the period of pulsations. The influence of the entrance region in the turbulent pulsating flow is much weaker, than in laminar flow, and phase differences are therefore less pronounced.

At higher frequencies (T<0.7 sec), the sign of the phase difference changes. The finite value of the sound velocity becomes important at these frequencies, and the pressure downstream lags behind the changes in upstream pressure as predicted in Section 2.3. The measured phase differencies are slightly higher than the theoretically calculated. The discrepancies may stem from the finite angular resolution in the experimental setup (about 0.3^{o} for each transducer) and the hydraulic approximation, used in the theory. It is interesting to notice, that there is practically no difference in the measured pressure phase lags between laminar and turbulent pulsating flows at this range of frequencies (T<1 sec).

An additional way to check the influence of the entrance region is to compare the amplitudes of the pressure pulsations at different streamwise locations. As it was mentioned earlier, one transducer was placed at inlet of the pipe which is 500 D long, while the second transducer was placed 100 D from the exit. Thus for a linear distribution of pressure along the pipe the ratio of the pressure amplitudes should therefore be equal to 0.2. This ratio would be reduced as a result of the influence of the entrance region. The accuracy of measuring the amplitude is much better than the accuracy in measuring the absolute steady pressure because the former is independent of the error in the zero setting.

Fig.3.9[b] showes the measured ratio of the pressure amplitudes in both laminar and turbulent flows. There is no significant difference

between these flow regimes; the results suggest, however, that the influence of the entrance region diminishes with increasing frequency. It is worth noting that the effects of the entrance region are much stronger on the steady, than on the oscillating parts of the flow. This stems from the fact that the oscillating velocity profile in fully developed laminar, or turbulent flows, does not differ significantly from the slug-type velocity profile, which enters the pipe from the settling chamber. The theory of Atabek and Chang does not predict notable nonlinearity in the distribution of the pressure amplitude along the pipe.

3.2.4 The Relation between the Pulsations of Pressure and Flow Rate

The mechanical power W, neccessary to push the flow at a rate Q through a pipe in which the pressure drops by Δp is proportional to the product $Q\,\Delta p$. In pulsating flow the power is time dependent, and the amplitude of power oscillations is determined by the amplitudes and phase relations between the pulsations of the pressure and flow rate: $W=p_1Q_1\cos\phi_q$. In order to compare the amplitudes of power pulsations in laminar and turbulent flows the relation between p_1 and Q_1 has to be known.

Fig.3.10 shows the dependence of the measured amplitude of pulsations of bulk velocity on the amplitude of the imposed pressure oscillations for two frequencies. Only small differences can be noticed in the responce of the velocity amplitude to the imposed forcing in laminar and turbulent flows.The bulk velocity amplitude is proportional to that of

pressure, and the difference between the slope of the laminar and the turbulent dependence is within the experimental error. For a given amplitude of pressure pulsations the amplitude of the bulk velocity is higher at lower frequency as it follows from the expected dependence of σ_q on the frequency (see Fig.2.2).

At a given frequency of pulsations only the phase difference ϕ_q can contribute to the difference in the amplitude of power pulsations between the laminar and the turbulent flows. In laminar flow the phase angle does not differ appreciably from 90° (it changed from about 85° at T=0.56 sec to about 78° at T=2.4 sec). In the turbulent flow, changes in frequency cause a more significant decrease in the phase lag of the flow rate behind the pressure, as it qualitatively can be concluded from Fig.3.5. At high frequencies, however, there is only a small difference in ϕ_q between laminar and turbulent flows; at T=0.56 sec it is about 85° in both cases. In turbulent flow ϕ_q decreases fast with decreasing frequency (at T=2.4 sec $\phi_q=50^\circ$), and cos ϕ_q therefore becomes larger, than in the corresponding laminar flow.

There is thus no significant difference in the amplitude of the power pulsations between laminar and turbulent flows at high frequencies, where the oscillating velocity prifiles are very much alike (see Section 3.2.1). Decreasing the frequency increases the amplitude of the flow rate for given pulsations of pressure and the amplitude of the power pulsations grows in both laminar and turbulent flows; the growth in the turbulent case is faster because of stronger dependence of ϕ_q on

frequency.

3.3 Turbulent Characteristics

There is no doubt, that a lot of information about the structure of the turbulent flow is lost by the conventional and phase locked averaging procedure. In Fig.3.11 the instantaneous axial u and radial v velocities, measured during a single period are shown and compared with the phase averaged values; the dependence of the pressure on time is shown in the upper curve. Several conclusions could be drawn from this Figure: 1) the phase averaged value of the radial velocity vanishes, so there is no Reynolds stress component, connected with the orderly pulsating part of flow as expected in the fully developed pipe flow; 2) the intensity of radial velocity fluctuations is of the same order of magnitude, as the intensity of axial velocity fluctuations; 3) there is some evident dependence of the turbulent activity on the phase of imposed oscillations which is expressed in the changes in both amplitude and frequency of the turbulent velocity fluctuations (see also Fig.3.12).

The turbulent activity becomes increasingly dependent on the phase of forcing at higher amplitudes of the pulsations. The oscillating part of velocity during a single period, measured by the hot-wire rake and compared with the signature of the pressure oscillations, is shown in

Fig.3.12. A partial laminarization of the flow is observed during the time corresponding to the minimum velocities produced by the forcing. A "breakdown" seems to occur at a time corresponding to the maximum instanteneous velocity, when the amplitude of turbulent fluctuations increases quite suddenly. The decrease in the amplitude of the fluctuations on the decelerating portion of the cycle is relatively gradual.

At even higher amplitudes of pulsations the flow becomes completely laminar. At these amplitudes the instantaneous Re falls below its critical value during a fraction of the period. When the duration of the flow at the subcritical Re is sufficiently long, a complete relaminarization occurs. The mean velocity of the flow at Re=4000 is about 1.0 m/sec, so that even at lowest frequency of pulsations (T=4.5 sec) each fluid particle remained in the pipe for several periods. The flow is naturally laminar at Re=4000, and the transition to turbulence was triggered artificially by a perturbance, which was purposely placed at the entrance to the pipe. Thus if the flow relaminarizes further downstream, it will remain laminar throughout the pipe. This effect was noticed by a number of investigators, cited earlier (e.g. Sarpkaya (1966) and Hamaprian and Tu (1980)).

3.3.1 The Intensity of Velocity Fluctuations

The distribution of the time averaged, root-mean squared, turbulent fluctuations in the axial and radial directions for steady and pulsating flows is compared in Fig.3.13. The velocity fluctuations are normalized

by the friction velocity u_* which was calculated from the time mean value of the pressure drop (u_*=15.1 cm/sec at Re=4000). There is no significant difference between time mean values of $\sqrt{u'^2}$ and $\sqrt{v'^2}$ in steady and pulsating flows. A small but consistant decrease in $\overline{v'^2}$ can be noticed (Fig.3.13^D), with increasing amplitudes of pulsations. The distribution of $\sqrt{u'^2}$ and $\sqrt{v'^2}$ is in good agreement with the results, obtained for steady turbulent pipe flow by Laufer (1954) and by Wygnanski and Champagne (1973).

Measurments of Laufer were made at Re=50000, which is higher by order of magnitude, than the prevailing Re used in the present investigation. Nevertheless, the comparison of the normalized results is still possible, because RMS values of the turbulent velocity fluctuations normalized by the friction velocity are practically independent of Re. On the other hand, u_* is dependent on Re, and its instanteneous values change in the pulsating pipe flow. Thus, u' and v' are phase dependent. This conclusion was reached by examining the recorded velocity dependence on time, as shown on Figures 3.11 and 3.12.

The phase dependence of the RMS values of velocity fluctuations is plotted in Fig.3.14, after the calculated data was smoothed slightly by a running average procedure. The smoothing was necessary because of relatively short length of the ensamble used in the averaging process (200 measured data points at each phase angle). A number of conclusions can be drawn from the examination of this Figure: 1) the RMS values of axial and radial velocity fluctuations are phase dependent; 2) the

phase angle of the intensity of the axial and radial velocity fluctuations is not identical; 3) the phase dependence of $\sqrt{\langle u'^2 \rangle}$ and $\sqrt{\langle v'^2 \rangle}$ is obviously non-harmonic, the growth is notably faster than the decay, as it was noted previously while examining the instanteneous velocity records over a single period.

In order to compare the radial dependence of the phase of $\sqrt{\langle u'^2 \rangle}$ and $\sqrt{\langle v'^2 \rangle}$ with the phase of the mean velocity, it was decided to limit the analysis to the fundamental frequency only, inspite of the non-harmonic behaviour of this ensemble averaged data.

Figure 3.15 shows the phase lag of $\sqrt{\langle u'^2 \rangle}$ behind the pressure and compares it to the phase of the mean velocity, for three different frequencies of pulsations but approximately for identical amplitude of the bulk velocity. The higher the frequency, the larger is the phase lag of $\sqrt{\langle u'^2 \rangle}$ behind the fundamental oscillation of the flow velocity. It is interesting to note, that the phase angle of $\sqrt{\langle u'^2 \rangle}$ changes significantly with the change in the radial position, being maximum at the center of the pipe, and attaining a minimum in the region corresponding to the maximum turbulent production. At lower frequencies the pulsations (T>2 sec) $\sqrt{\langle u'^2 \rangle}$ at r/R=0.7 may even lead the phase averaged velocity. In Fig.3.15 the phase distributions of $\langle u \rangle$ and $\sqrt{\langle u'^2 \rangle}$ are compared for a constant frequency of forcing (T=2.4 sec) and the Reynolds numbers ranging from 3300 to 7500. The phase difference between $\langle u \rangle$ and $\sqrt{\langle u'^2 \rangle}$ decreases with increasing Re; the location of minimum in the phase difference approaches the wall at high values of the Reynolds

number.

The phase angle of $\sqrt{\langle v'^2 \rangle}$ is practically independent of the radial position (Fig.3.16). The phase-lag of $\sqrt{\langle v'^2 \rangle}$ behind pressure is very close to that of $\sqrt{\langle u'^2 \rangle}$ in the center of the pipe, but it does not decrease at larger r/R. The magnitude of the phase-lag in $\sqrt{\langle u'^2 \rangle}$ and $\sqrt{\langle v'^2 \rangle}$ relative to the pulsating velocity depends on the amplitude of the velocity pulsations, but the radial distribution of the phase is unaffected.

The qualitative difference in the phase behaviour of $\sqrt{\langle u'^2 \rangle}$ and $\sqrt{\langle v'^2 \rangle}$ can be explained by considering the budget of the turbulent energy (see Hinze, p.325). The rate of change in the intensity of the longitudinal fluctuations (i.e. $\partial \langle u'^2 \rangle / \partial t$) is governed by the production term $-\langle u'v' \rangle \partial \langle u \rangle / \partial r$, so that simultaneous existence of the oscillating velocity gradient and Reynolds stress is necessary for the production, as it was pointed out by Rotta (1962). The temporal change in the phase-mean velocity gradient produces a most pronounced change in $\sqrt{\langle u'^2 \rangle}$ at the location where the product of the oscillating Reynolds stress with $\partial \langle u \rangle / \partial r$ attains maximum. The phase difference between $\langle u \rangle$ and $\sqrt{\langle u'^2 \rangle}$ is thus minimal in the region of maximum production and occurs approximately at r/R=0.7 at time-mean Re=4000; at higher values of Re the location of the minimum in the phase difference approaches the wall. Once generated, the longitudinal velocity fluctuations are transferred accross the pipe by energy redistribution mechanisms, which are connected to pressure fluctuations. The phase lag between $\langle u \rangle$ and

$\sqrt{\langle u'^2 \rangle}$ increases therefore with the increasing distance from the region of maximum production. This is the direct production of the turbulent energy in the central region of the pipe resulting in a maximum phase lag there.

The radial velocity fluctuations do not extract energy directly from the mean flow but rather from $\langle u'^2 \rangle$ through pressure redistribution terms. Thus the phase-lag in $\sqrt{\langle v'^2 \rangle}$ is similar to the phase-lag of $\sqrt{\langle u'^2 \rangle}$ in the center of the pipe, but the phase-lag of $\sqrt{\langle v'^2 \rangle}$ is independent of radial location.

In addition to the phase behaviour of the RMS of the turbulent velocity fluctuations, the radial distribution of their amplitudes was checked as well. The dependencies of the dimensionless amplitudes of $\sqrt{\langle u'^2 \rangle}$, normalized by the amplitudes of the pulsating bulk velocity for three periods of forcing, are plotted in Fig.5.17. Increasing the frequency of the pulsations results in higher dimensionless amplitudes of $\sqrt{\langle u'^2 \rangle}$. A large change in the amplitude of the bulk velocity produces a small growth in the amplitude of $\sqrt{\langle u'^2 \rangle}$. The data presented in Fig.5.16 reflects a change of approximately 300% in the amplitude of the bulk velocity pulsations which lead to a change of 20% in the dimensionless amplitude of $\sqrt{\langle u'^2 \rangle}$.

In order to check the non-harmonic behaviour of $\sqrt{\langle u'^2 \rangle}$ and $\sqrt{\langle v'^2 \rangle}$ the ratio of the first two power spectral coefficients $c(2\omega)/c(\omega)$ was calculated for the phase averaged RMS values. The first coefficient

$c(\omega)$ corresponds to the fundamental frequency of pulsations, while $c(2\omega)$ to its first harmonic. No significant frequency or radial dependence of $c(2\omega)/c(\omega)$ was observed. This ratio was about 18% for $U_1/\bar{U}$=15%, and increased to $c(2\omega)/c(\omega)$=40% at $U_1/\bar{U}$=35%. The non-harmonic behaviour of $\sqrt{\overline{<v'^2>}}$ was similar. The phase dependence of $\sqrt{\overline{<u'^2>}}$ is becoming more harmonic when Re is increased. At Re=5800 and Re=7500 $c(2\omega)/c(\omega)$ is less than 5% at all radial locations. The conclusion thus can be made that the non-harmonic behaviour of the turbulent characteristics at Re<4500 is caused by the onset of the relaminarization process at low instanteneous values of the bulk velocity.

3.3.2 Reynolds Stresses

Time averaged Reynolds stresses $-\overline{u'v'}$ which were measured by an x-wire, are essentially independent of the flow pulsations (Fig.3.19), as is the case of the RMS values of turbulent velocity fluctuations. This conclusion was inferred earlier from the similarity of time mean velocity profiles (Section 3.1). The fact that the time mean pressure drop along the pipe is independent of forcing also indicates, that the pulsations have nearly no effect on the mean Reynolds stresses.

The radial distribution of the oscillating part of the Reynolds stresses for two amplitudes of pulsations is shown in Fig.3.20. The measured values of $<u'v'>$ were rendered dimensionless when divided by the amplitude of the pulsations of u_s which in turn were deduced from the oscillatory component of the pressure drop. Normalized in that way,

the amplitudes of the Reynolds stress appear to be independent of the amplitude of the pulsating bulk velocity. Qualitatively, the radial distribution of the amplitude of $\langle u'v' \rangle$ resembles the time mean $\overline{u'v'}$ dependence, both grow linearly with the radius in the central region of the pipe, but the pulsating $\langle u'v' \rangle$ attains its maximum value closer to the wall, than the time mean Reynolds stresses.

The phase lag of $\langle u'v' \rangle$ behind pressure (Fig. 3.21) is similar to the phase-lag of $\sqrt{\langle u'^2 \rangle}$ at comparable amplitudes and radial positions (compare with Fig.3.16). The phase-lag of $\langle u'v' \rangle$ is minimal not far from the wall, at $0.7<r/R<0.8$; with the location of minimum depending on the amplitude of the forcing. The resemblence between the radial distribution of the phase-lag of $\sqrt{\langle u'^2 \rangle}$ and $\langle u'v' \rangle$ stems from the fact that u'v' fluctuations can extract energy directly from the mean flow through the production term $-\langle v'^2 \rangle \, \partial \langle u \rangle / \partial r$ (Hinze p.325). The minimum in the radial distribution of the phase angle of $\langle u'v' \rangle$ is much less pronounced than for the longitudinal velocity fluctuations, because of the uniform distribution of both amplitude and phase angle of $\sqrt{\langle v'^2 \rangle}$.

The Reynolds stresses, as the RMS values of velocity fluctuations, are not changing harmonically in time. The "power spectrum" of the phase averaged $\langle u'v' \rangle$ was calculated, and the coefficients, corresponding to the fundamental frequency of pulsations and its first harmonic, were compared. Their ratio was found to be similar to that, obtained for $\sqrt{\langle u'^2 \rangle}$, i.e. about 20% when the amplitude of forcing was $U_1/\bar{U}=20\%$ and about 40% for $U_1/\bar{U}=35\%$.

AD-A108 367 TEL-AVIV UNIV (ISRAEL) DEPT OF FLUID MECHANICS AND --ETC F/G 20/4
ON THE RELATIONSHIP BETWEEN TRANSITIONAL AND FULLY TURBULENT SH--ETC(U)
MAY 81 I WYGNANSKI AFOSR-77-3275

UNCLASSIFIED AFOSR-TR-81-0764 NL

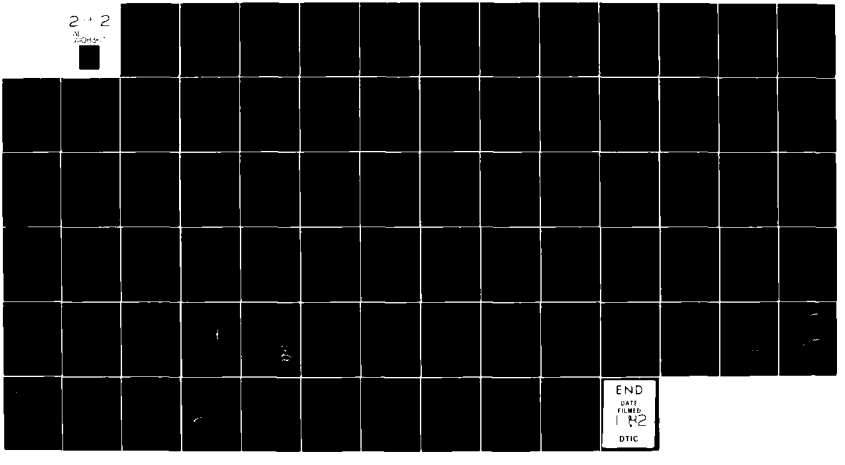

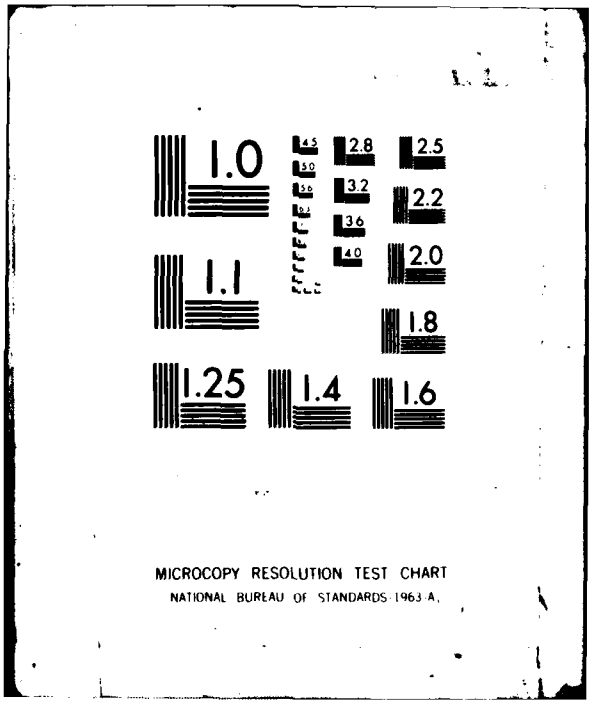
1.0
1.1
1.25
1.4
1.6
1.8
2.0
2.2
2.5
2.8
3.2
3.6
4.0
4.5
5.0
5.6
MICROCOPY RESOLUTION TEST CHART
NATIONAL BUREAU OF STANDARDS 1963 A.

3.3.3 Spectral Analysis

One of the interesting questions, concerning turoulent pulsating pipe flow, is the interaction of turbulence with the velocity oscillations generated by forcing. Cheng (1971), for example, states, that there is a strong amplification of the turbulent fluctuations at the frequency of the pulsations.

In order to check the spectral distribution of the energy of turbulent fluctuations at frequencies corresponding to the frequency of the imposed oscillations, the sampling period was increased to eight periods of forcing. The data was acquired in the following way. The first trigger pulse recognized by the computer initiated the record. From that point in time only every 8-th or 16-th data point was stored after the corresponding phase-averaged value of the velocity was substracted from it, thus leaving only the fluctuating turbulent component of the instanteneous velocity. One hundred and twenty eight (128) data points were obtained for each period, giving a total of 1024 points per record. The power spectra were calculated for each record and averaged over the number of records used.

A log-log plot of the spectra at 9 radial locations is shown in Fig.3.22[a] for unforced flow; and in Fig.3.22[b] and Fig.3.22[c] for forcing at a period equal to T=1.34 sec and at two amplitudes of oscillations $U_1/\bar{U}$=20% and $U_1/\bar{U}$=35%. The general shape of the spectra of the steady and pulsating flows is very similar. Forcing produces a strong peak in

the spectrum at the frequency of the pulsations in the nonstationary flow. In the central region of the pipe even the second and the third harmonic of the pulsating frequency are visible. This confirms, at the first sight, the conclusion of Cheng about the increase of the turbulent energy at the frequency of the pulsations. To check the matter further the same type of measurment was repeated in laminar pulsating flow at identical flow conditions; the ensued spectra had identical peaks at the frequency of the pulsations and its harmonics. Since the intensity of these spectral peaks relative to the background was identical to the intensity measured in turbulent flow and yet the flow was laminar, error in the processing of data was suspected.

As explained in Section 2.5, the sampling frequency was calculated by the computer in order, that 1024 or 2048 data points would be sampled per each channel per period. In reality, however, the desired number of sampled data points per period was not precisely achieved. The reason for the discrepancy stems from the fact that 11 channels were recorded at a total sampling rate of approximately 15 KHz. Thus, about 70 μsec elapsed between the consecutive data points while the resolution of the clock being only 1 μsec, resulted in a maximum possible error in the sampling frequency of approximately 1.5%. The sampled period might have been either longer or shorter than the real period of pulsations, resulting in a discontuinity at the end of each record. The absolute value of the discontinuity was not large, and it could not be noticed from observing the velocity signature on a "Tektronix" screen, but its periodicity caused the generation of the spectral peaks discussed in

conjunction with Fig.3.22 at the frequency of pulsations and its harmonics.

Examination of the low frequency spectra excluding the above mentioned spikes leads to the conclusion, that there is no significant interaction between the imposed oscillations and the turbulence. Thus the conclusion of Cheng might be in error.

In order to obtain spectral information at higher frequencies, the spectra of the axial and radial velocities during a single time period (T=1.34 sec) were calculated and averaged over 100 cycles. The spectra at two radial positions are shown in Fig.3.23: one on the center line (Fig.3.23^{a}) and one taken at r/R=0.73 (Fig.3.23^{b}). The lowest frequency of the spectra corresponds to the frequency of the pulsations, i.e. f=0.74 Hz.

The value of the leading coefficient of the axial velocity component power spectrum which corresponds to the forcing frequency grows with increasing amplitude of forcing, but the rest of the spectrum is not influenced by pulsations. The changes at the frequency of pulsations are assumed to result from the experimental error discussed earlier in the case of long time spectra. Turbulent energy is increasing towards the wall, as expected; most of the turbulent energy is contained in frequencies lower than 100 Hz; the value of power spectrum coefficients at frequencies higher, than 500 Hz, is at least four orders of magnitude below the coefficients corresponding to the energy contain-

ing eddies, so that the sampling frequency of about 1.5 kHz, used in the experiment, is adequate.

The spectra in Fig.3.23 are plotted in log-log coordinates. This presentation is necessary because of the wide range of parameters, but it conseals the relative contribution of different frequencies to the total turbulent energy. The connection between the spectral coefficients c(f) and turbulent energy E may be presented in the following form

$$E=\int_0^\infty c(f)df=\int_{-\infty}^{\infty} f^2c(f)d(\log f) \qquad 3.2$$

It is clear from this presentation, that when logf is used instead of frequency, the contribution to the total turbulent energy at the frequency f is proportional to $f^2c(f)$. The Fig.3.23^c gives the spectrum of the turbulent energy of the longitudinal velocity fluctuations on the center line of the pipe, as given in Fig.3.23^a, but instead of logc(f) the logarithm of the product $f^2c(f)$ is given on the ordinate. Fig.3.23^d presents the spectra of radial velocity fluctuations, calculated in the same way.

It can be seen from the Figure, that the main contribution to the total turbulent energy of axial velocity is at frequencies corresponding to a Strouhal number based on mean bulk velocity $\overline{U}$ and diameter of the pipe D ($St=fD/\overline{U}$) which is of the order unity (St=1 at f=55 Hz). The frequency of energy containing eddies increases near the center of the

pipe. The characteristic frequency of the energy containing eddies in the radial direction is about 100 Hz, and seems to be less dependent on radial position.

With power spectrum c(f) known, dissipation spectrum $f^2c(f)$ and dissipation integral $\int f^2c(f)df$ can be calculated. The log-log plot of dissipation spectra on the center line of the pipe for unforced flow and for two amplitudes of forced pulsations at T=1.34 sec ($U_1/\overline{U}$=20% and $U_1/\overline{U}$=35%) is presented in Fig.3.25. The maximum dissipation region is approximately at f=150 Hz. The difference between the regions of energy containing eddies and maximum dissipation is not very large, as can be expected for low Reynolds numbers considered. The dissipation spectra are practically uneffected by pulsations, and the slight increase in the value of the dissipation integral with increasing results from changes in spectra at the high frequency (f>200 Hz).

The spectra on Figures 3.23 give information which is averaged over the whole period. It was mentioned earlier, however, that in the pulsating flow the turbulent activity is phase dependent. It was decided therefore to divide each period into eight equal parts, and calculate the spectrum for each part separately. Each record thus included 256 measured data points and thus no spectral information could be obtained about frequencies lower than 8/T=6 Hz. The spectral resolution, which depends on the duration of the total record is also reduced by the subdivision of the period. Figures 3.24[a] and 3.24[b] show three out of eight possible spectral distributions at the initial pressure phases of 90°,

90^{o} and 270^{o} and for two amplitudes of bulk velocity pulsations (15.5% on Fig.3.24[a] and 55% on Fig.3.24[b]). The phase angles chosen show the maximum deviation (90^{o} and 270^{o}) of the short duration spectra from long time averaged spectrum which also resembles the spectrum at phase angle 90^{o}. At large amplitudes of pulsations, the difference between the specral coefficients measured at $\phi=90^{o}$ and $\phi=270^{o}$ for a given frequency may be as large as decade. It is intersting to note that effect of pulsations on the spectra is most pronounced at high frequencies (20 Hz<f<100 Hz) rather than in the immediate neighbourhood of the forcing frequency (i.e. at f~1 Hz).

To evaluate the influence of forcing on the energy containing eddies same spectra were plotted once again in the coordinates log(f*c(f)) vs. log(f) (Figures 3.24[c] and 3.24[d]). It transpires that in addition to the effect on the amplitude of the turbulent fluctuations, the introduction of forcing also effects the energy containing eddies, as it was noticed from examining a single event in Section 3.3. At higher instanteneous Reynolds numbers (with a certain phase lag) the entire spectrum seems to shift towards higher frequencies which are appropriate perhaps to the instanteneous Reynolds number.

This behaviour is even more pronounced on the short duration dissipation spectra, calculated from the power spectra and presented in Fig.3.26. The values of the dissipation spectral coefficients differ by two orders of magnitude at different initial phase angles. The region of maximum dissipation also depends strongly on the phase angle.

3.3.4 Dissipation time scale

The multiple spectra, presented in the previous Section, show that the frequency of turbulent fluctuations is phase dependent. They cannot, however, provide "instanteneous" information about frequency, but rather an average over 1/8 of the period. An alternative way to obtain phase locked information on the characteristic frequency of the turbulent fluctuations is to calculate the ensamble averaged values of the Eulerian dissipation time scale $\overline{\tau}_E$, defined as

$$f_E = 1/\tau_E = \sqrt{\overline{(\partial u'/\partial t)^2}/\overline{2u'^2}}$$

(Hinze, p.45). Although Townsend (1956) was very sceptical about the phisical meaning of the so called dissipation parameters, they still may serve as an indicator defining the most rapid turbulent fluctuations in the flow.

The radial distribution of time averaged values of $\overline{f}_E$ for three amplitudes of pulsations at T=1.34 sec is presented in Fig.3.27[a]. No significant influence of pulsations can be noticed up to the maximum amplitude used (i.e. $U_1/\overline{U}$ 30%). The average $\overline{f}_E$ attains a maximum on the center line of the pipe. The obtained maximum value of $\overline{f}_E$ (about 400 Hz) supplies one more indication, that the sampling frequency chosen in this investigation (about 1500 Hz) is quite adequate. The value of time averaged $\overline{f}_E$ increases sharply with decreasing distance from the wall.

The radial distribution of the amplitude of the oscillations in $\langle f_E \rangle$ (see Fig.3.27^b) resembles the distribution of the amplitude of phase averaged velocity oscillations. In the central region of the pipe the radial distribution of f_E is approximately uniform, as is the case for the amplitude of $\langle u \rangle$, the difference occurs in the vicinity of wall, where the reduction in the amplitude of f_E is steeper. The amplitude of oscillations in $\langle f_E \rangle$ is roughly proportional to that of $\langle u \rangle$.

The radial distribution of the phase lag of $\langle f_E \rangle$ behind the pressure (Fig.3.27^c) resembles that of $\phi_u(r)$, with the phase lag increasing towards the wall. The phase difference between $\langle u \rangle$ and $\langle f_E \rangle$ is about 20^o at all radial positions, and is practically independent of amplitude.

CHAPTER 4

DISCUSSION AND THEORETICAL CONSIDERATIONS

4.1 The balance of forces in a pulsating flow

In a steady fully developed pipe flow there are two types of forces, acting on every element of fluid and balancing one another: pressure forces, resulting from favorable pressure gradient in the direction of the flow, and shear forces, which are caused by friction on the walls and oppose the motion. In the case of non-steady flow a third force is added: an inertia force. At any instant, all three forces have to be balanced, forming triangle of forces for each frequency in the Fourier expansion. The leading term in the expansion is considered and the presentation of (1.3) is used (e.g. the analysis refers to the frequency of the pulsations only).

Eq.(1.10) may be rewritten in the following way:

$$\frac{\partial \langle u \rangle}{\partial t} = -\frac{1}{\rho}\frac{\partial \langle p \rangle}{\partial x} - \frac{1}{\rho r}\frac{\partial}{\partial r}\left(r\langle \tau(r) \rangle\right) \qquad 4.1$$

where $\langle \tau \rangle$ is the ensemble averaged pulsating part of the shear stress

$$\langle\tau\rangle = \mu \frac{\partial\langle u\rangle}{\partial r} - \rho\langle u'v'\rangle \qquad 4.2$$

Integrating Eq.(4.1) from the center-line to another radial position r yields after some manipulation

$$\frac{1}{r}\frac{\partial}{\partial t}\int_0^r \rho r'\langle u(r')\rangle dr' = -\frac{\partial\langle p\rangle}{\partial x} + \frac{\langle\tau(r)\rangle}{r} \qquad 4.3$$

The integral on the left hand side represents an instantaneous rate of mass flow through the central region of the pipe up to the radial position r, and will be designated further $\rho Q(r)$. Making use of Eq.(1.3) and considering the fundamental frequency only, the differential equation (4.3) reduces to an algebraic expression

$$\frac{i\omega}{r^2}\rho Q_1(r)e^{-i\phi_q(r)} = -\frac{1}{2}\frac{\partial p_1}{\partial x} - \frac{\tau_1(r)}{r}e^{i\phi_\tau(r)} \qquad 4.4$$

Eq.(4.4), being a complex one, represents in fact two independent equations, for the real and for the imaginary part. When the experimental information about flow velocities and pressures is available, Eq.(4.4) contains two unknown values: the amplitude of the shear stress τ_1 and its phase angle ϕ_τ. Both values can thus be determined from equations (4.4).

An alternative approach to Eq.(4.4) is to regard it as a vector equation representing a balance among three vectors: $\vec{Q}=Q_1(r)\exp(-i\phi_q)$, $\vec{P}=0.5\partial p_1/\partial x$ and $\vec{\tau} = (\tau_1/r)\exp(i\phi_\tau)$, where ϕ_q and ϕ_τ represent the phase angles of mass-flux and shear relative to the pressure. In turbulent

flow the mass flux-lags behind the pressure by an angle ranging from 0° to 90°, depending on frequency and mean Reynolds number (see Sections 3.2.2 and 3.2.4). The fact that the mass flux term on the left hand side of Eq.(4.4) is multiplied by i means that an angle of 90° is added to this phase angle in order that the mass flux term on the left hand side of Eq.(4.4) will lead the pressure term. The following sketch shows qualitatively the relevant vectors and phase angles.

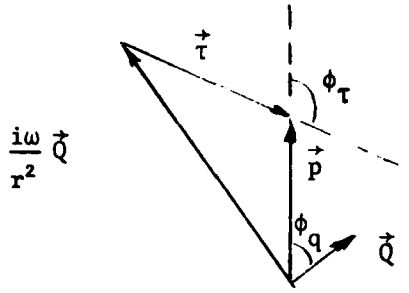

It is seen from the sketch, that both amplitude τ_1 and phase angle ϕ_τ of the shear stress vector are critically dependent on the relative length of $\vec{P}$ and $\vec{Q}$ and on the phase angle between them, consequently even a relatively small error in one or both quantities which are measured experimentally, can lead to a significant error in the shear stress vector.

In laminar pulsating flow the radial distribution of the shear stress has been calculated theoretically (Uchida (1956)), and the solution for the amplitude of $<\tau>$, normalized by the length of the pressure vector, is represented by a solid line in Fig.4.1 for $\alpha = 9$. (T=1.3 sec). The slope of the curve in the central region of the pipe is very small, and it differs notably from zero only inside the Stokes layer. This behaviour of the radial dependence of τ_1/r in the laminar flow

follows from the fact, that in the central region of the pipe the acceleration term is practically in phase with pressure, and both terms balance one another. The viscous term becomes more important in the Stokes layer, where the radial gradients in the amplitude and phase of velocity pulsations increase (Fig.3.6 and Fig.3.5). The increased amplitude of the velocity oscillations renders a longer acceleration vector; the changes in the velocity phase-lag increase the angle between the acceleration vector and the pressure vector; thus the shear stress term which closes the force triangle increases. Near the wall the amplitude of velocity oscillations decreases causing the acceleration vector to become shorter than the pressure, and the phase lag of the shear stress behind the pressure tends approximately to 45^{o}. The following sketch shows qualitatively (but not to scale) the force triangles in laminar flow at three radial locations: in the central region, in the Stokes layer and at the wall.

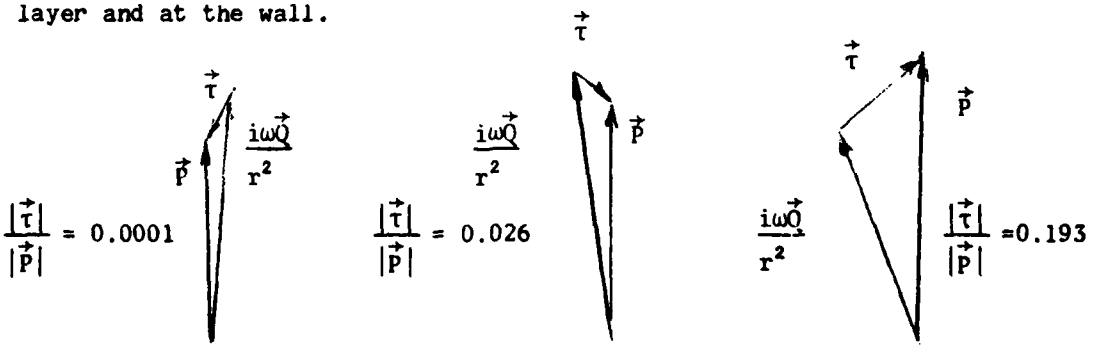

center(r/R=0.24) Stokes layer (r/R=0.85) wall (r/R=1)

The relative length of the shear stress vector in laminar flow is small with the exception of the wall region and consequently the pressure and acceleration are collinear and equal. This identity provides an opportunity to check the consistency of the measurments and correct

the pressure vector which in all probability contains the largest error. The measured values of $\vec{P}$ and $i\,\omega\vec{\zeta}/r^2$ in the central region of the pipe in laminar flow were equated, and a coefficient of the correction for the length of the pressure vector was determined. This coefficient was used to correct the length of the pressure vector in the turbulent flow at otherwise identical parameters (i.e. Re, T, piston displacement). The value of the corection coefficient was usually about 1.15. It is worth noting here, that the shear stress term appears in the form τ/r. This term does not vanish in the center of the pipe, contrary to the shear stress itself, and therefore there is no way to correct the relative length of the other two experimental vectors using the known value of $\tau=0$ in the center of the pipe.

The shear stresses calculated from Eq.(4.4) with the aformentioned correction factor for the pressure can be checked experimentally by comparison with the measured Reynolds stresses. Fig.4.1 represents the calculated radial distribution of τ_1/ρ, normalized by the modulus of the pressure vector $\vec{P}$, as compared with the theoretically calculated laminar distribution. Four different amplitudes of pulsations are shown in Fig.4.1 for the period T=1.34 sec.

An identical way of normalization was used in Section 3.3.2 for the radial distribution of the amplitudes of pulsations of Reynolds stresses shown in Fig.3.20. The vector diagrams provide a reason for it. As it was mentioned in Section 3.2, the amplitude of velocity pulsations is proportional to the amplitude of pressure for both laminar and turbulent

flows, as long as this amplitude is not too high, ϕ_u is practically independent of amplitude. This implies, that the force triangles for different amplitudes of pulsations at a constant frequency are similar, and thus the amplitude of pulsations of the shear stress is also proportional to the pressure.

It is seen from Fig.4.1, that this way of normalization leads to radial distribution of τ_1 which collapse fairly well on the same curve provided the very large amplitudes of forcing are excluded ($U_1/\overline{U}$=35%). The comparison of the measured Reynolds stress with τ_1 callculated according to Eq.(4.4) is fairly satisfactory. In the central region of the pipe $\partial\langle u\rangle/\partial r \approx 0$ (see Section 3.2.1), thus $\langle\tau\rangle/\rho = -\langle u'v'\rangle$, yet the measured $\langle u'v'\rangle_1$ are consistently below τ_1. The maximum discrepancy however, is less than 20% (Fig.4.1) thus giving an estimate of the error in the use of Eq.(4.4). If one does not correct the pressure vector the discrepancy between the measured and calculated τ_1 incresases slightly without affecting the qualitative results.

Fig.4.2 presents the radial distribution of the amplitude of the pulsations of the shear stress, normalized in the same way as in the previous Figure, for four different frequencies. The relative lengths of the shear stress vector and of the pressure vector are obviously strongly dependent on frequency. At low frequency the length of $\vec{\tau}$ at the wall nearly equals to that of $\vec{P}$, as it is in steady flow, and the contribution of the acceleration term is manifested mainly in the phase shift between $\vec{\tau}$ and $\vec{P}$. It is natural to assume, that at frequencies

lower than the ones measured this phase lag eventually vanishes, and the behaviour of the pulsating turbulent pipe flow does not differ from the steady flow. The length of $\vec{\tau}$ relative to the amplitude of the pressure pulsations decreases with increasing frequency, and the behaviour of the flow in the central region of the pipe resembles the laminar case, where the influence of the shear stress is negligible.

It should be noted however that the amplitude of the shear stress does not change notably with frequency when normalized by the flow rate amplitude Q_1 rather than the pressure. This is also the case for the RMS values of the longitudinal velocity oscillations (see Fig.3.17). It may be concluded that the oscillations in shear stress and RMS values of velocity fluctuations are functions of the oscillating Reynolds number.

There exists a phase difference between the oscillations in mass flux and in shear stress. The phase lag of $<\tau>\phi_\tau$ as calculated from the Eq.(4.4), shows only slight dependence on amplitude (Fig.4.3), with the possible exception at very high amplitude of forcing ($U_1/\overline{U}$=35%). In the latter case ϕ_τ increases notably. The dependence of the phase angle on frequency is considerable (Fig. 4.4). The phase angle ϕ_τ calculated from Eq.(4.4) and the angle ϕ_{uv} which was deduced from the measured Reynolds stresses are in very good agreement (Fig.4.3). The difference between the two quantities is less than 10^o. The phase angle between the pressure and the shear stress increases with increasing frequency. ϕ_τ decreases near the wall, this decrease is much more pronounced at higher frequencies.

The following sketch (which can not be drawn to scale) shows relative length and directions of the relevant vectors at a given radial location (r/R=0.61) for three frequencies (all vector moduli are normalized by the modulus of $\vec{P}$), as calculated from experimental data in accordance with Eq.(4.4):

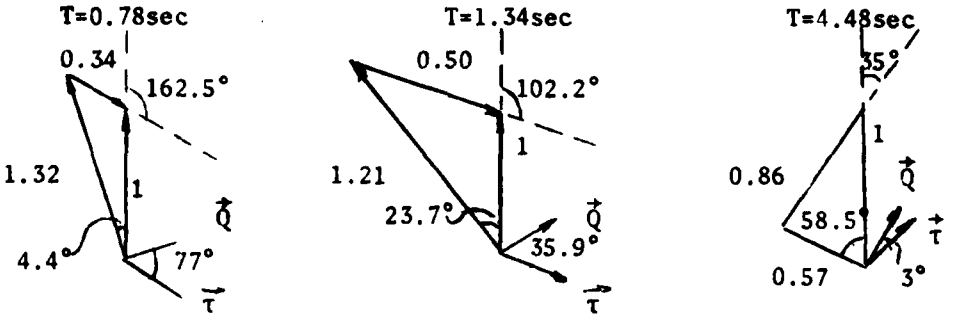

Increasing the frequency results in smaller phase angles between the pressure and the acceleration vector. The length of $\vec{Q}$ relative to the pressure decreases with increasing frequency (in analogy to the behaviour of σ_q, α) in laminar flow (Fig.2.2)), but the product ωQ_1 which corresponds the the acceleration vector increases with increasing frequency. Thus, while examining the instanteneous force balance, $\vec{\tau}$ oeing related to the acceleration should be compared with a characteristic $\omega\vec{Q}$ term, while in examining the influence of forcing on the turbulent intensities or Reynolds stress should be compared with a characteristic amplitude of velocity and hence with Q_1. The phase lag of $\vec{\tau}$ behind $\vec{P}$ increases with frequency, as shown in Fig.4.4.

At a given radial position there is no practical difference between $\langle\tau\rangle/\rho$ and $-\langle u'v'\rangle$. The phase angle ϕ_τ of $\langle\tau\rangle$ may thus be considered to be equal to the phase angle of the Reynolds stresses. The phase lag of

the Reynolds stresses behind the mass flux thus ranges from nearly zero at low frequencies to approximately 60° at T=0.70 sec. At high frequencies Reynolds stress is nearly in antiphase with the acceleration vector. Since the radial dependence of the phase angle of the longitudinal velocity fluctuations is similar to the dependence of the Reynolds stresses (because of production term), it follows from the force triangles, that at high frequencies the acceleration is associated with reduction in the turbulent activity. This fact is widely recognized in the literature (e.g. Narasimha and Sreenivasan (1979)) and a causality of relaminarisation by acceleration was suggested, but the present experimental results suggest a different interpretation.

At long periods of pulsations (T=4.48 sec), the rate of change of the bulk velocity is small enough for the turbulent structure to accomodate itself to the instanteneous value of the phase-locked average velocity distribution. The changes in the turbulent characteristics of the flow are therefore in phase with the mass flux and with the pulsating Reynolds number. The situation resembles laminar pulsating pipe flow, where at $\alpha<1$, the velocity at any instant has a Poiseuille distribution corresponding to the instanteneous value of the pressure gradient. The period of pulsations for which the turbulent structure responds to the instanteneous mean flow (T=4.5 sec) is still very short in terms of the frequency parameter ($\alpha=4.9$ rather than 1). Thus the characteristic responce time of turbulent fluctuations to a change in mean flow, is much shorter than the time needed for the laminar flow to accomodate itself to the changing pressure gradient.

When the frequency of pulsations increases, the phase lag of the mass flux relative to the pressure tends to 90°, and all three vectors in the force triangle tend to be collinear. This implies that the Reynolds stresses lag behind the mass flux by 90° and cannont exceed this angle under any condition. At high enough frequencies the turbulent activity is minimum when the acceleration is maximum because the relative contribution of the shear stresses to the total balance of forces decreases. The "laminarizing" effect of the acceleration is thus obtained in the limiting case of very rapid oscillations.

4.2 The Eddy Viscosity Model in the Time Dependent Flow

In pulsating pipe flow amplitudes and phase angles of the oscillating pressure, velocity and shear stress are mutually dependent. Therefore the qualitative difference in the radial distribution of ϕ_u in laminar and turbulent flows (Fig.3.5) results from the different behaviour of the oscillating part of the shear stress in both flows. The oscillating parts of the laminar and turbulent velocity profiles at high values of α are vaguely similar, suggesting that a proper use of an eddy viscosity model may provide a qualitative answer for the behaviour of the oscillating turbulent flow, including in particular the vastly different radial distrubution of the phase. The eddy viscosity model has to be modified in order to provide a qualitatively correct description of the time dependent turbulent flow.

The suggested expression of the kinematic eddy viscosity for the time dependent portion of the flow is based on the steady flow model of Van-Driest (1956) with the correction of the wake function of Coles (1954), as proposed by Yahalom-Dimant (1974). The kinematic eddy viscosity ε_o for steady flow is given by

$$\varepsilon_o(r) = \frac{(r/R)u_*^2}{\partial u/\partial r} \qquad 4.5$$

The velocity gradient $\partial u/\partial r$ is composed of two parts, the first represented by Van-Driest model:

$$\frac{\partial u_1}{\partial r} = \frac{(r/R)u_*^2/\nu}{1+[1+4k^2(\frac{R-r}{\nu})u_*^2\,\frac{r}{R}\,(1-\exp(-\frac{(R-r)u_*}{\nu A^+}))]^{\frac{1}{2}}} \qquad 4.6$$

for which the empirical constants are: $A^+=26$; $k=0.4$; and the second part is the wake correction for the central region of the pipe:

$$\frac{\partial u_2}{\partial r} = \frac{\Pi\pi}{2k}\,[1-\exp(-2Ru_*/\nu A^+)\sin(\pi(1-\frac{r}{R})] \qquad 4.7$$

where the additional empirical constant Π was chosen to be $\Pi=1.02$.

The eddy viscosity for the time dependent part of the flow is different from that for the steady flow. Following Maruyama (1974) and using the Prandtl's mixing length approach, the expressions for the shear stress and the eddy viscosity are:

$$\tau = \rho\varepsilon_o\frac{\partial u}{\partial r}\;;\quad \varepsilon_o = \rho\ell^2\frac{\partial u}{\partial r} \qquad 4.8$$

where ℓ is the mixing length. Introducing the decomposition for the steady and time dependent parts of the phase averaged velocity $u=\bar{u}+\langle u\rangle$, substituting it into Eq.(4.8), and neglecting terms of second order yields:

$$\tau = \rho\ell^2\left(\frac{\partial u}{\partial r}\right)^2 = \rho\ell^2\left(\frac{\partial \bar{u}}{\partial r}\right)^2 + 2\rho\ell^2 \frac{\partial \bar{u}}{\partial r} \frac{\partial\langle u\rangle}{\partial r} \qquad 4.9$$

thus implying for the eddy viscosity of the oscillating flow ε_1

$$\varepsilon_1 = 2\rho\ell^2 \frac{\partial \bar{u}}{\partial r} = 2\varepsilon_o = \frac{\partial \tau}{\partial(\partial\bar{u}/\partial r)} \qquad 4.9^a$$

The simple model of Prandtl which uses a constant length scale, gives for the time dependent part of the shear stress an eddy exchange coefficient ε_1 which is twice the conventional, steady eddy viscosity.

For a more complex model, like the one given in equations (4.5) through (4.7), the relation between ε_o and ε_1 is not as simple. In order to obtain the eddy viscosity which represents the dependence of the shear stress on the velocity profile, the radial distributions of the velocity gradient and of the shear stress was calculated for two slightly different values of the friction velocity u_* from equations (4.6) and (4.7). The eddy viscosity for the oscillating flow was then calculated following (4.9^a) from the equation:

$$\varepsilon_1 = \frac{(r/R)\Delta u_*^2}{\Delta(\partial u/\partial r)} \qquad 4.10$$

Fig.4.5 presents so calculated radial distribution of the oscillating eddy viscosity as compared to the steady one.

It was tacitly assumed in this derivation, that the shear stress is corresponding to the instantaneous value of the local velocity gradient, irrelevant to the rate of change of the phase-averaged flow. The carefull examination of the experimental data however reveals, that this is not always true. From the Eq.(4.2) and the definition of the eddy viscosity one obtaines

$$(\varepsilon_1 - \nu)\ \frac{\partial \langle u \rangle}{\partial r} = -\langle u'v' \rangle \qquad 4.11$$

The phase angle of the Reynolds stresses is thus related to the velocity gradient $\partial\langle u\rangle/\partial r$. With the radial distribution of both amplitude $u_1(r)$ and phase angle of velocity oscillations $\phi_u(r)$ known, the time dependent velocity gradient is:

$$\frac{\partial \langle u \rangle}{\partial r} = \left[\frac{\partial u_1(r)}{\partial r} + i u_1(r) \frac{\partial \phi_u(r)}{\partial r} \right] e^{i(\omega t + \phi_u(r))} \qquad 4.12$$

The phase angle of $\partial\langle u\rangle/\partial r$ may thus be calculated from Eq.(4.12). The experimentally observed radial dependencies of $u_1(r)$ and $\phi_u(r)$, as presented in Section 3.2, are very slowly varying functions of r with the exception of the wall area, thus the differentiation of these curves will inevitably cause a very large experimental error. Consequently, the accurate calculation of the eddy viscosity for the oscillating part of the flow from the experimentally measured values of $\langle \tau \rangle$ and $\partial \langle u \rangle/\partial r$

seems impossible in practice.

There exists, however, a point, at which the phase lag $\phi_u(r)$ attains a minimum, so that $\partial\phi_u(r)/\partial r=0$ at this radial position, and the phase angles of $\partial\langle u\rangle/\partial r$ and $\langle u\rangle$ are identical (Eq.(4.12)). The experimental data of Section 3.3.2 show a difference in phases between $\langle u\rangle$ and $\langle u'v'\rangle$ at this, as well as at other radial positions. It follows therefore from Eq.(4.11), that the turbulent part of the eddy viscosity for the time dependent flow has to be a complex function which introduces a phase shift between $\partial\langle u\rangle/\partial r$ and $\langle u'v'\rangle$.

The complex nature of the eddy viscosity for the oscillating flow can be related to the finite relaxation time in turbulent flows (Nee and Kovasznay (1969), Narasimha and Prabhu (1972)). The concept of the relaxation time refers to the time period necessary for the turbulent structure to adjust itself to a step-function change in the mean flow. Nee and Kovasznay and Prabhu and Narasimha (1972) proposed model equations for calculating the shear stress in a flow with non-stationary mean values, based on the diffusion equation. A different aproach will be taken here. The equation relating the shear stress to velocity gradient is modified in order to include a responce time of the Reynolds stress:

$$\langle u'v'\rangle = (\varepsilon_1-\nu)\frac{\partial\langle u\rangle}{\partial r} - \theta\frac{\partial\langle u'v'\rangle}{\partial t} \qquad 4.13$$

The second term on the right hand side of the Eq.(4.13) represents the

"inertia" of the Reynolds stress, which may be large whenever the changes in $\langle u'v' \rangle$ are rapid in comparison with characteristic time θ, but vanishes for infinitely slow processes. Substituting into the Eq.(4.13) the presentation (1.3) for the time dependent part of the Reynolds stress $\langle u'v' \rangle = (u'v')_1 \exp(i\omega t + \phi_{uv})$, one obtains:

$$\langle u'v' \rangle = \frac{\varepsilon_1 - \nu}{1+i\omega\theta} \frac{\partial \langle u \rangle}{\partial r} = \frac{\varepsilon_1 - \nu}{\sqrt{1+\omega^2\theta^2}} e^{-i\,\mathrm{arctg}(\omega\theta)} \frac{\partial \langle u \rangle}{\partial r} \qquad 4.14$$

which gives an expression for the oscillating eddy viscosity:

$$\tilde{\varepsilon}_1 = \nu + \frac{\varepsilon_1 - \nu}{\sqrt{1+\omega^2\theta^2}} e^{-i\,\mathrm{arctg}(\omega\theta)} \qquad 4.15$$

Eq.(4.15) indicates that the argument of the complex eddy viscosity, as well as its' absolute value are frequency dependent. At high frequencies relative to the relaxation time θ ($\omega\theta >> 1$) the absolute value of the eddy viscosity for the oscillating flow decreases, and the Reynolds stresses become independent of the phase angle. Thus, the turbulence is "frozen" and depends on the mean flow only. The pulsations are governed by the molecular viscosity ν only, and are in this sense laminar, while the mean flow is fully turbulent.

As mentioned earlier, the phase difference between $\langle u'v' \rangle$ and $\partial \langle u \rangle / \partial r$ is known accurately at one radial position only, where the phase of the velocity gradient equals to the phase of the velocity itself. The experimentally measured ϕ_u at T=1.34 sec and $U_1/\bar{U}$=20% at-

tains minimum at r/R=0.72 (Fig.3.16), and the phase difference between the velocity and the Reynolds stress is at this radial position 30^{o} (Fig.3.21). The relaxation time θ , obtained from the Eq.(4.15) is therefore $\theta = (\pi/6)/(2\pi/T)=0.12$ sec. Although the relaxation time should in general depend on the radial position, it is convenient to assume it to be constant across the pipe. The relaxation time therefore is a universal constant for a given mean Reynolds number. Narasimha and Prahbu (1972) used a similar approach to calculate the influence of the finite relaxation time on the development of the turbulent wake in responce to a steep change in pressure gradient. Neglecting the dependence of the relaxation time on the transverse coordinate proved in their case to have no significant effect on the results of the calculations nor on the agreement with experimental results.

Following equation (4.15), one may define a critical frequency of pulsations $f_{cr}= \omega_{cr}/2\pi = 1/2\pi\theta = 1.3$ Hz. At $\omega < \omega_{cr}$ the modulus of $\tilde{\varepsilon}_1$ is practically independent of frequency and equals to the value of an eddy exchange coefficient for very slow pilsations. At $\omega=\omega_{cr}$ the oscillating eddy viscosity decreases to $1/\sqrt{2}$ of its value at $\omega \to 0$. When $\omega > 1/\theta$, and $(\omega\theta)^2 >> 1$, $|\tilde{\varepsilon}_1| \sim 1/\omega$, and thus the amplitude of oscillations in shear stress decreases rapidly with increasing frequency for a given value of $\partial\langle u\rangle/\partial r$. The corresponding critical period of the pulsations is in this case $T_{cr}=1/f_{cr}=0.75$ sec. For the turbulent structure to become frozen, i.e. for the oscillating eddy viscosity to vanish, the frequency of pulsations has to be much higher than f_{cr}, as may be deduced from Eq.(4.15). On the other hand, even at $f<f_{cr}$ the oscillating

eddy viscosity still introduces a significant phase angle between $\langle u'v' \rangle$ and $\partial \langle u \rangle / \partial r$, thus influencing on the total force balance in the oscillating part of the flow.

Ramaparian and Tu (1980) used a criterion, proposed by Rao et al (1971); Laufer and Badri Narayanan (1971) for the characteristic responce time in a turbulent boundary layer $U\theta / \delta = 5$, in order to distinguish slow pulsations from rapid ones. The adaptation of the criterion to the pipe flow required that the boundary layer thickness is replaced by a diameter D of the pipe. The direct adaptation of results obtained in the boundary layer to a pipe flow seems questionable, and the radius is probably a better substitute for δ, than D. Still, the use of the abovementioned criterion for the flow parameters, used in the present invesigation, gives a characteristic time $\theta = 5D/U = 0.06$ sec, which is in fair agreement whitnin an order of magnitude with the estimated value of $\theta = 0.12$ sec mentioned earlier. Ramaparian and Tu concluded that the turbulent structure is independent of the phase angle at $f \sim f_{cr}$, yet in the present investigation experimental results and model considerations indicate, that much higher frequencies are necessary in order to "freeze" the turbulence. The characteristic time θ, when calculated from the criterion $\theta = 5D/U$, decreases with increasing Re, thus the phase shift between the velocity and the turbulent structure has to decrease with increasing time-mean bulk velocity. The Reynolds number dependence of the phase shift between $\langle u \rangle$ and $\sqrt{\langle u'^2 \rangle}$ (Fig.3.15^b) confirms this conclusion.

It is intersting to note that the empirical relation of Mizushina et al (1973[a]) (Eq.(1.12) leads in our case to the same value of T_{cr}=0.75 sec. These authors also referred to the paper of Rao et al (1971); their conclusion is however opposite to the results obtained in the present work: Mizushina et al found that for $T>T_{cr}$ the pulsations do not effect the turbulent structure, and for very rapid pulsations ($T<T_{cr}$) turbulent intensities become phase dependent. This conclusion contradicts to the physical sense and experimental results and seems to be error.

The eddy viscosity calculated from the Eqs.(4.5) to (4.7), (4.10) and (4.15), was substituted into the Navier-Stokes equation for the oscillatory part of the flow to give:

$$i\omega\langle u\rangle = -\frac{1}{\rho}\frac{\partial\langle p\rangle}{\partial x} + \frac{1}{r}\frac{\partial}{\partial r}\left(r\tilde{\varepsilon}_1(r)\frac{\partial\langle u\rangle}{\partial r}\right) \qquad 4.16$$

with boundary conditions:

$$\left.\frac{\partial\langle u\rangle}{\partial r}\right|_{r=0} = 0 \; ; \qquad \left.\langle u\rangle\right|_{r=R} = 0$$

Eq.(4.16) was solved numerically using an implicit finite difference scheme by the Gaussian elimination method (Chow (1979), p.74).

The results of the calculations are presented in Fig.4.6, showing the radial distribution of the amplitudes and phase angles of the oscillations in velocity and shear stress. The calculations were performed

for mean Re=4000 and T=1.0 sec. A qualitative agreement with the experimental results was achieved in this way. The calculated phase lag of the velocity behind the pressure behaves as the experimentally observed. The calculated angle slightly decreases with the increasing distance from the center line, then increases near the wall. It should be noted that the efforts to use the real value of the oscillating eddy viscosity resulted in the calculated radial distribution of ϕ_u which resembled ϕ_u in laminar flow, and decreased monotonically with increasing r/R.

In the immediate proximity of the wall the rate of change of ϕ_u with radius decreases sharply. The comparison of the ϕ_τ which was calculated from the experimental data according to Eq.(4.4) and shown in Fig.4.4, with ϕ_u at the same large radial location (shown in Fig.3.5) reveals, that the phase difference between them is small. The turbulent (complex) part of the eddy viscosity being negligible in this region, the assumption can be made that $\langle\tau\rangle$ has to be in phase with $\partial\langle u\rangle/\partial r$, thus the phase angle gradient $\partial\phi_u(r)/\partial r$ has to be small near the wall as it follows from Eq.(4.12). The behaviour of $\phi_u(r)$ in the vicinity of wall calculated numerically seems therefore reasonable, but no direct experimental data is available in this region.

The calculated values of both $\phi_u(r)$ and $u_1(r)$ differ from the experimentally measured angles, implying that the theoretical model is not sophisticated enough to provide an exact balance between viscous, inertia and pressure forces, and perhaps is not valid for the low Reynolds number used.

CHAPTER 5

CONCLUSIONS

The pulsating flow in pipe was investigated experimentally. Measurments were carried out in fully developed laminar and turbulent flows consecutively while all other flow parameters were kept constant; enabling a detailed comparison between the laminar and turbulent flows at otherwise identical conditions. Most measurments were taken at a mean Re=4000, for the periods of pulsations from 0.5 sec to 5 sec corresponding to a dimensionless frequency parameter $5<\alpha=R\sqrt{\omega/\nu}<15$.

By considering the fundamental forcing frequency only, the regular time-dependent component of the flow parameters is represented by the radial distributions of amplitude and phase-angle of the oscillations. It seems, however, interesting and possible to expand the analysis to include higher harmonics, which are important whenever turbulence is considered. The restriction of the analysis to the fundamental frequency made it possible to represent the balance between the inertia, pressure and shear forces in pulsating flow by a vector triangle. The vector approach is helpful in understanding the physical process at hand.

The time mean properties of the flow were found to be practically indpendent of pulsations in both laminar and turbulent regimes. A small

increase in the turbulent energy at the high frequency end of the spectrum was observed at relatively high amplitudes of forcing. No accumulation of the turbulent energy at, or near the frequency of pulsations was observed in this investigation.

The theoretical analysis of the fully developed, laminar, pulsating pipe flow provides a good estimate for the measured quantities. The theory describing the laminar pulsating flow in the entrance region of the pipe (Atabek and Cheng (1961)) which uses a linear approximation for the inertial term in equation of motion underestimates the importance of this region in comparison with the experimental results.

The dependence of the bulk velocity oscillations on pressure was found to be similar in laminar and turbulent pulsating flows. The amplitude of the bulk velocity pulsations, depends linearly on the pressure in both flow-regimes; so that equal amplitudes of pressure pulsations, result in nearly identical amplitudes of velocity regardless of the flow regime. The phase-lag of the bulk velocity relative to the pressure is different in laminar and in turbulent flows, the phase lag in the turbulent flow being usually notably smaller than in the corresponding laminar flow. The radial dependence of the amplitude of the velocity oscillations was also found to be different in laminar and turbulent flows. In laminar flow, the maximum amplitude of the velocity oscillations occurs in the Stokes layer, resulting in an M-like shape of velocity profile. In the turbulent flow the amplitude of velocity oscillations decreases monotonically from the center towards the wall pro-

vided that the viscous sublayer is thinner than the Stokes layer. At high frequency of forcing in the turbulent flow regime, when the Stokes layer is thinner than the viscous sublayer, the radial distribution of the amplitudes of the velocity pulsations resmoles the distribution observed in the laminar flow. The radial distribution of the phase angle ϕ_u, changes significantly when the flow regime changes from laminar to turbulent. In the laminar flow, ϕ_u is approximately 90° in the central region of the pipe at all frequencies considered, and decreases to about 45° near the wall. In turbulent flow, ϕ_u is smaller in the center than in the corresponding laminar case, and increases with increasing frequency. At all frequencies considered, the phase angle, ϕ_u, in turbulent flow is higher near the wall of the pipe than near the center, in contrast to the distribution of ϕ_u in the laminar flow.

The turbulent structure in pulsating pipe flow was found to be phase dependent. The amplitude of the oscillations of longitudinal and radial velocity fluctuations, as well as the Reynolds stress, correspond roughly to the amplitude of pulsations of the bulk velocity. The angle between the intensity of the longitudinal component of the velocity fluctuations and the pressure attaines a minimum in the region where most turbulent energy is produced and increases towards the center line. The radial distribution of phase of the Reynolds stresses resembled that of the longitudinal velocity fluctuations, but the minimum is less pronounced. The phase lag of the radial velocity fluctuations is uniform acoross the pipe, and approximately equals to the phase angle of longitudinal velocity fluctuations in the center of the pipe. The phase lag

of the turbulent quantities behind the velocity of forcing increases with increasing frequency from zero to about 90^{o}. At high frequencies, the turbulent activity reduces to a minimum whenever the acceleration is high, the phase lag between the two leads to the suggestion that the turbulent structure needs time to accomodate itself to the everchanging mean flow, thus revealing properties of "memory". Measurments of phase between Reynolds stress and velocity oscillations at high frequency, enabled evaluation of a characteristic responce-time of a turbulent structure. This characteristic time was used in developing an eddy viscosity model for the oscillating part of the turbulent pulsating pipe flow. The model gave an expression for a complex eddy viscosity for the time-dependent component of the flow, for which both modulus and argument are frequency dependent. The argument of the eddy viscosity differs from zero at relatively low frequencies, and tends to 90^{o} with decreasing period of pulsations. The modulus of the oscillating eddy viscosity is independent of frequency whenever the period of pulsations is longer than the relaxation time of the turbulence, but decreases at higher frequencies. The relaxation time of the turbulent structure was evaluated from a single point.

The dependence of the eddy viscosity on the frequency leads to the suggestion that for a sufficiently high frequencies the modulus of the eddy viscosity vanishes, and the turbulent structure becomes independent of forcing. The turbulence therefore becomes "frozen", and the oscillating part of the flow may be considered laminar although the mean flow is turbulent. These high frequencies could not be achieved in the pre-

sent experimental setup.

Flow analysis notwithstanding, the responce of tne facility, consisting of a valvless piston pump, a large settling chamber and straight smooth pipe, to a periodic change in the volume of the settling chamber, was analysed theoretically and experimentally. It was found that for a given amplitude of oscillations in volume the resulting pressure oscillations depend on frequency. A maximum responce of the system to oscillations in volume occurs in both laminar and turbulent flows at approximately identical frequencies. The resonance type of behaviour of the pressure oscillations is caused by the phase relation between the pulsations in the flow rate and pressure for the specific facility. The influence of the finite sound velocity on the linearity of the pressure distribution along the pipe was investigated as well and a qualitative criterion was obtained for the range of frequencies at which a fully developed flow may be regarded to be independent of the axial coordinate.

LIST OF REFERENCES

1. Atabek,H.B., and Chang,C.C. (1961) ZAMP, vol.12, p.185

2. Batchelor,G.K., and Gill,A.E. (1962) Journ. Fluid Mech. vol.13,, p.529

3. Berger,E., and Wille,R. (1972) Ann. Rev. Fluid Mech., vol.4, p.313

4. Caro,C.G., Pedley,T.Y., Schroter,R.C., Seed,W.A. (1978) The Mechanics of the Circulation, Oxford Univ. Press, Oxford

5. Cheng,l. (1971) Ph.D Thesis, University of Utah

6. Chow,C.Y. (1979) An Introduction to Computational Fluid Mechanics, J.Wiley, New-York

7. Clamen,M., and Minton,P. (1977) Journ. Fluid Mech. vol.81, p.421

8. Clarion,C., and Pelissier,R. (1975) Journ. Fluid Mech., vol.70, p.59

9. Coles,D. (1954) ZAMP, vol.5, p.181

10. Davis,S.H. (1976) Ann. Review of Fluid Mech., vol.8, p.57

11. Denison,E.B. (1970) Ph.D Thesis, Purdue University

12. Denison,E.B, Stevenson,W.H., and Fox,R.W. (1971) AIChE Journ., vol.17, p.781

13. van Driest,E.R. (1956) Journ. Aero. Sci., vol.23, p.1007

14. Emsmann,S. (1973) Dr.-Ing. Thesis, Tech. Univ. Berlin

15. Gerrard,J.H. (1971) Journ. Fluid Mech., vol.46, p.43

16. Goldshtick,M.A., and Shtern,V.N. (1977) Hydrodynamic Stability and Turbulence, Nauka, Novosibirsk (in Russian)

17. Goldstein,S. (editor) (1965) Modern Developments in Fluid Dynamics, vol.2 Dover, New-York

18. Grosch,C.E., and Salwen,H. (1968) Journ. Fluid Mech., vol.34, p.177

19. Hino,M., Sawamoto,M., and Takasu,S. (1976) Journ. Fluid Mech., vol.75, p.193

20. Hinze,J.O. (1975) Turbulence, Mc-Grow Hill, New-York

21. Hussain,A.K.M.F., and Reynolds,W.C. (1970) Journ. Fluid Mech., vol.41, p.241

22. Hussain,A.K.M.F. (1977) in Cardiovascular Flow Dynamics and Measurments, University Park Press, Baltimore

23. von Kerczek,C., and Davis,S.H. (1974) Journ. Fluid Mech., vol.62, p.753

24. Kirmse,R.E. (1979) Trans. of ASME. Journ. Basic Eng., vol.101, p.436

25. Kovasznay,L.S.G. (1949) Proc. Roy. Soc. ser A. vol.198, p.174

26. Laufer,J. (1950) NACA Tech. Notes No.2123

27. Laufer,J., and Narayanan,M.A.B. (1971) Phys. of Fluids. vol.14, p.182

28. Lindford,R.G., and Ryan,N.W. (1965) Journ. Appl. Physiol., vol.20, p.1078

29. Maruyama,T. (1974) Transport Phenomena in Pulsating Pipe Flow, Kyoto University

30. Merkli,P., and Thomann,H. (1975) Journ. Fluid Mech., vol.68, p.567

31. Mizushina,T., Maruyama,T., Ide,S., and Mizukami,Y. (1973[a]) Journ. Chem. Eng. Japan. vol.6, p.152

32. Mizushina,T., Maruyama,T., and Shiozaki,Y. (1973[b]) Journ. Chem. Eng. Japan. vol.6, p.487

33. Mizushina,T., Maruyama,T., and Hirasawa,H. (1975) Journ. Chem. Eng. Japan. vol.8, p.210

34. Narasimha,R., and Prabhu,A. (1972) Journ. Fluid Mech., vol.54, p.1

35. Narasimha,R., and Sreenivasan,K.R. (1979) Advances in Appl. Mech. vol.19, p.221

36. Nee,V.W., and Kovasznay,L.S.G. (1969) Phys. of Fluids. vol.12, p.473

37. Ohmi,M., Usui,T., Fukawa,M., and Hirasaki,S. (1976) Bull. JSME. vol.19, p.298

38. Oster,D. (1980) Ph.D.Thesis, Tel-Aviv Univ.

39. Prabhu,A., and Narasimha,R. (1972) Journ. Fluid Mech., vol.54, p.39

40. Ramaprian,B.R., and Tu,S.W. (1980) Journ. Fluid Mech., vol. 100, p.513

41. Rao,K.N., Narasimha,R., and Narayanan, M.A.B. (1971) Journ. Fluid Mech., vol.48, p.339

42. Richardson,E.G. (1927) Proc. Phys. Soc., vol.40, p.206

43. Richardson,E.G., and Tyler,E. (1929) Proc. Phys. Soc., vol.42, p.1

44. Richardson,P.D. (1980) Trans ASME. Journ. Fluid. Eng., vol.102, p.244

45. Roshko,A. (1955) Journ. Aero. Sci., vol.22, p.124

46. Roshko,A. (1961) Journ. Fluid Mech., vol.10, p.345

47. Rotta,J. (1962) Prog.Aero.Sci., vol.2, p.1

48. Rubin,Y., Wygnanski,I., and Haritonidis,J.H. (1979) in Laminar-Turbulent Transition, IUTAM Symposium Stuttgart, Springer-Verlag, Berlin

49. Sarpkaya,T. (1966) Trans. ASME. Journ. Bas. Eng., vol.88, p.589

50. Schlichting,H. (1960) Boundary Layer Theory, Mc-Grow Hill, New-York

51. Schultz-Grunow,F. (1940) Forschung. vol.11, p.170 (NASA TT F-14, 881, (1973))

52. Sergeev,S.I. (1966) Fluid. Dyn., vol.1, p.121

53. Sexl,T. (1930) Zeit. fur Physik. Bd.61, S.349

54. Townsend,A.A. (1956) The Structure of Turbulent Shear Flow, Cambridge Univ. Press

55. Uchida,S. (1956) ZAMP. vol.7, p.403

56. Womersley,J.R. (1955) Journ. Physiol., vol.127, p.553

57. Wygnanski,I.J., and Champagne,F.H. (1973) Journ. Fluid Mech. vol.59, p.281

58. Wygnanski,I.J., and Oster,D. (1981) Submitted to Journ. Fluid Mech.

59. Yahalom (Dimant),Y. (1974) D.Sc. Thesis, Technion, Haifa

60. Yang,W.H., and Yih,C.S. (1977) Journ. Fluid Mech. vol.82, p.497

LIST OF FIGURES

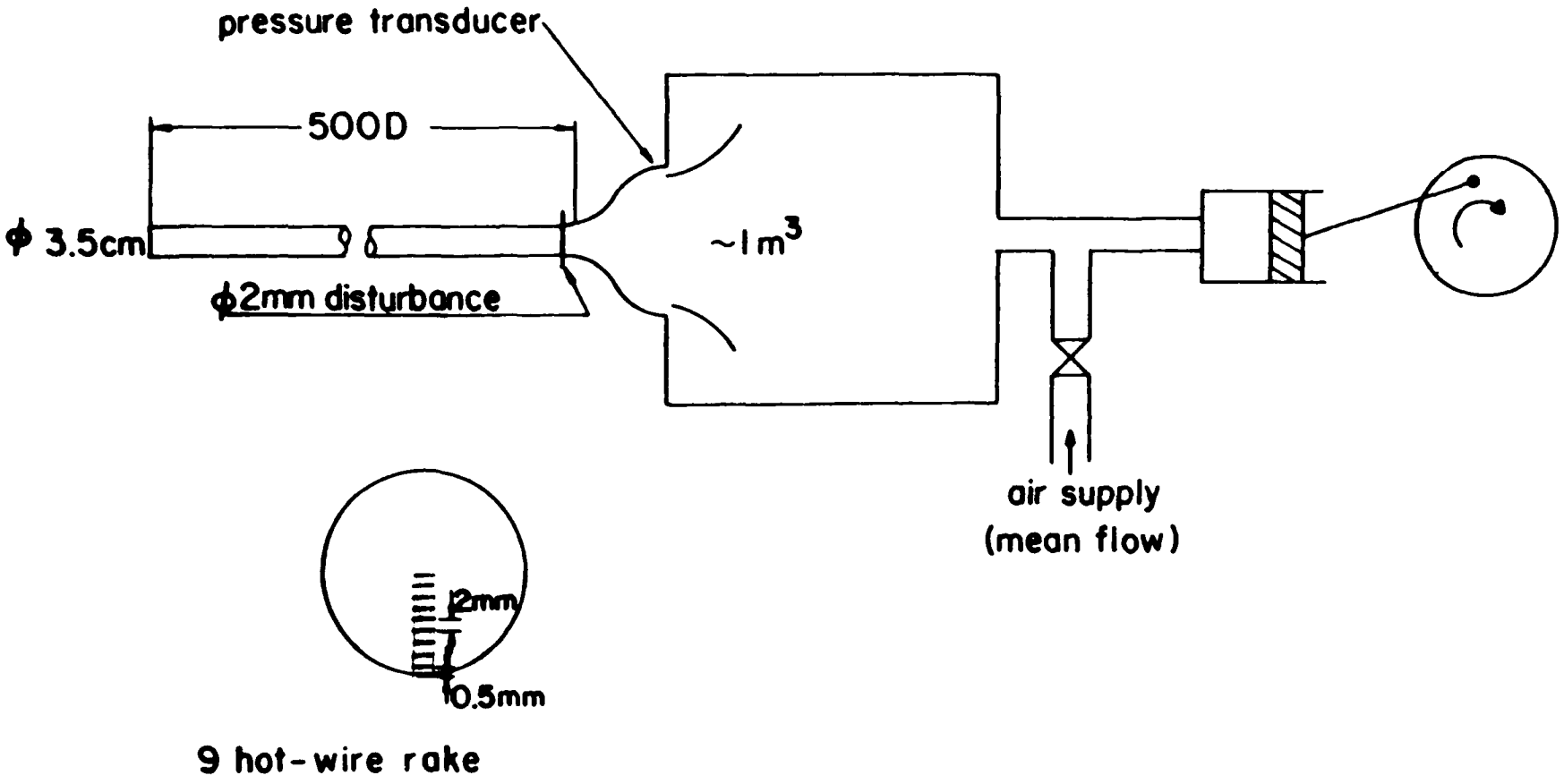
pressure transducer
500D
ϕ 3.5cm
ϕ2mm disturbance
~1 m3
air supply
(mean flow)
2mm
0.5mm
9 hot-wire rake

Fig. 2.1

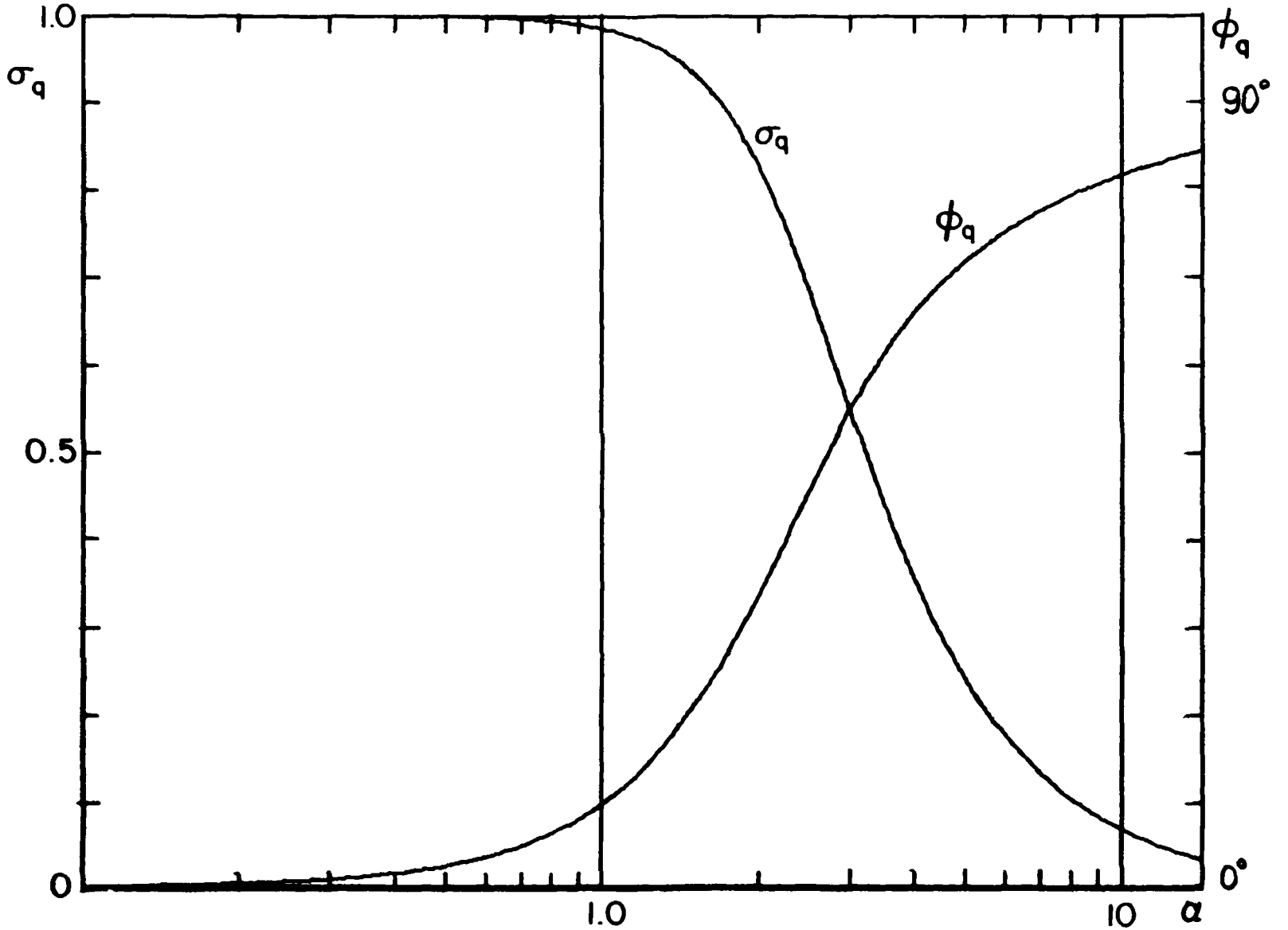

Fig 2.2

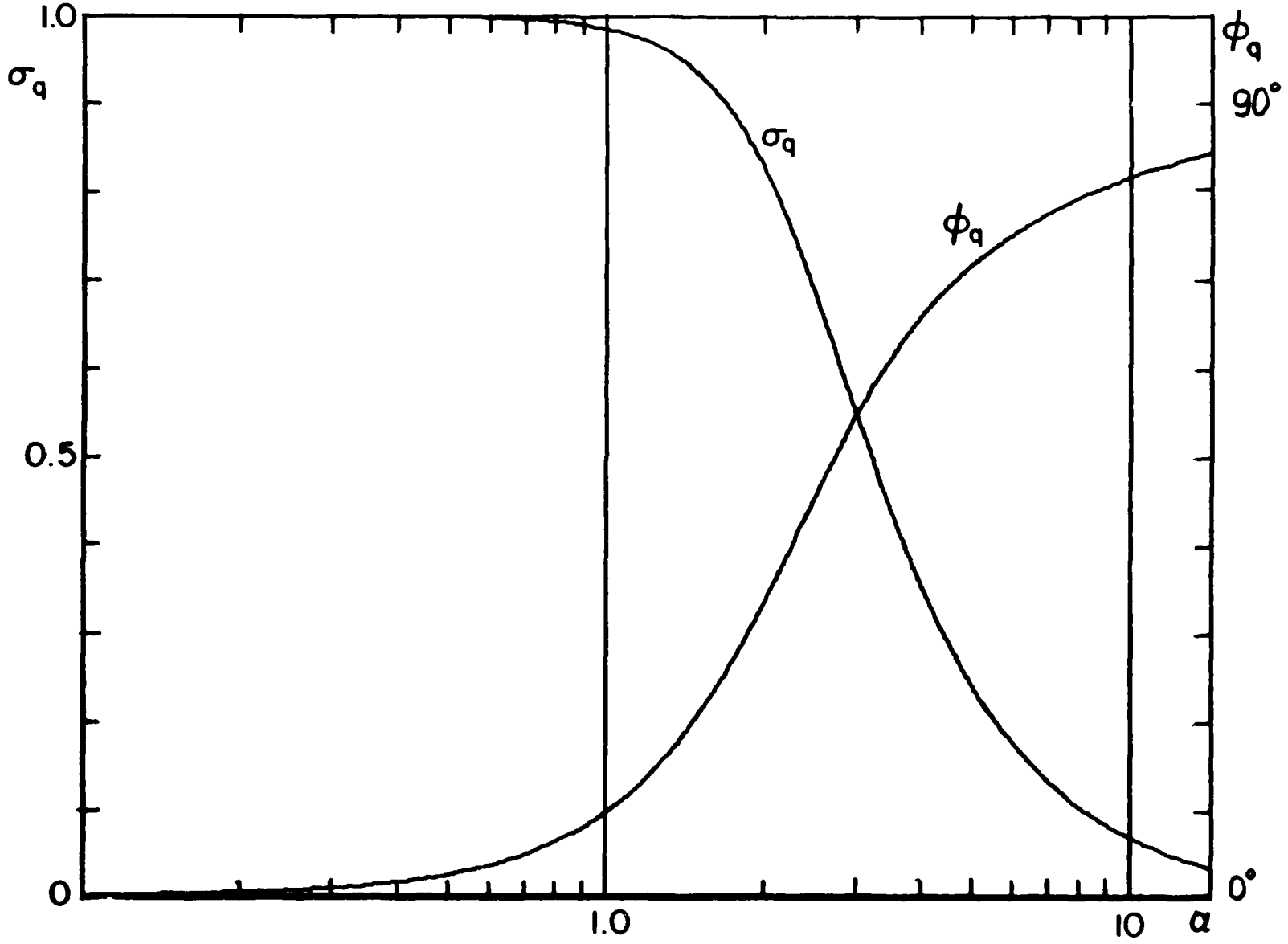

Fig 2 2

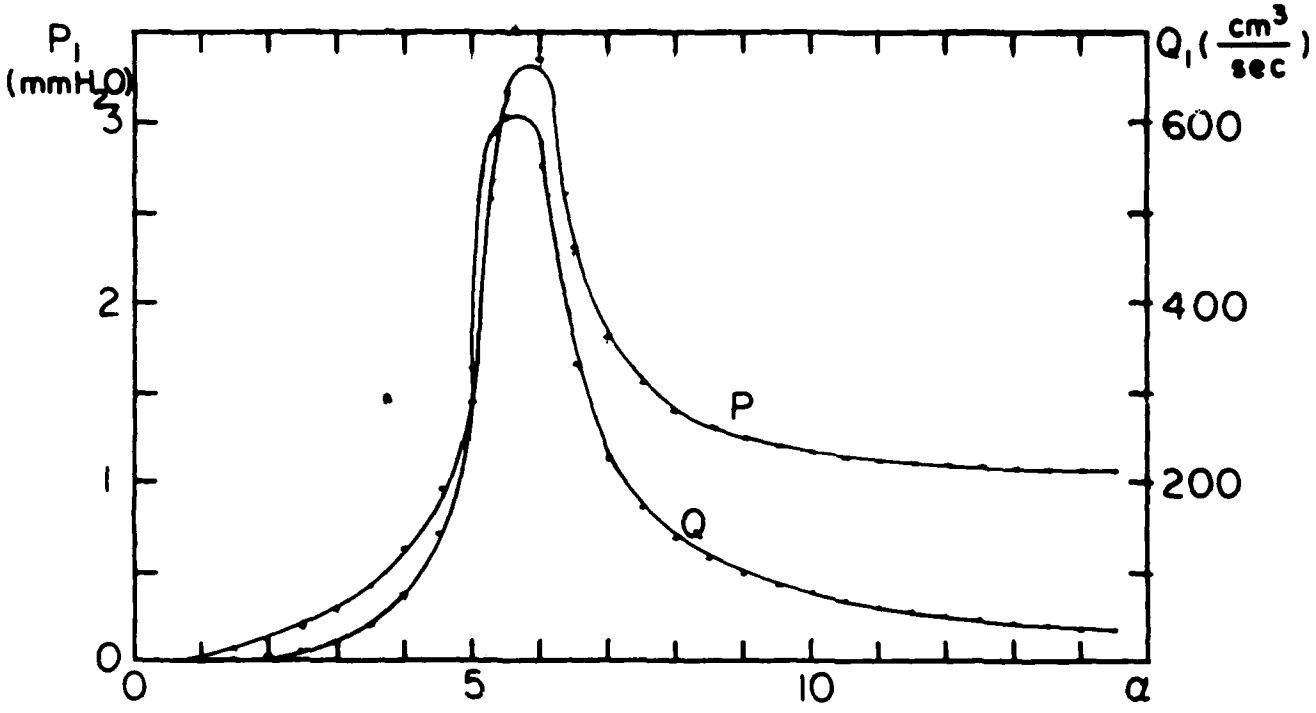

Fig. 2.3a

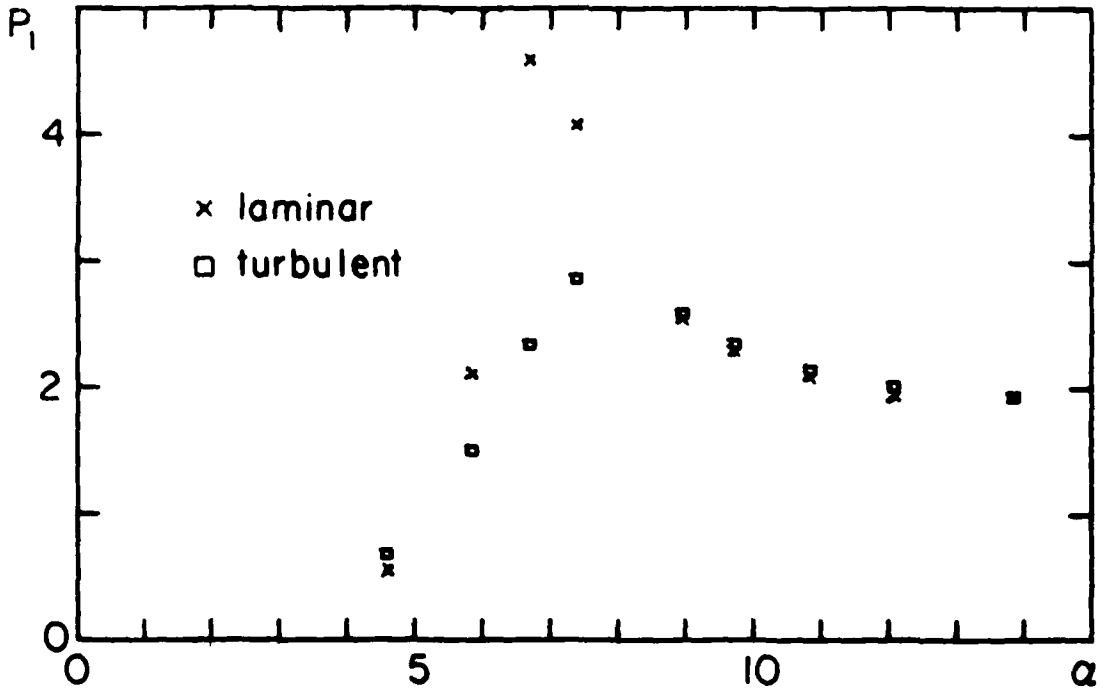

Fig. 2.3b

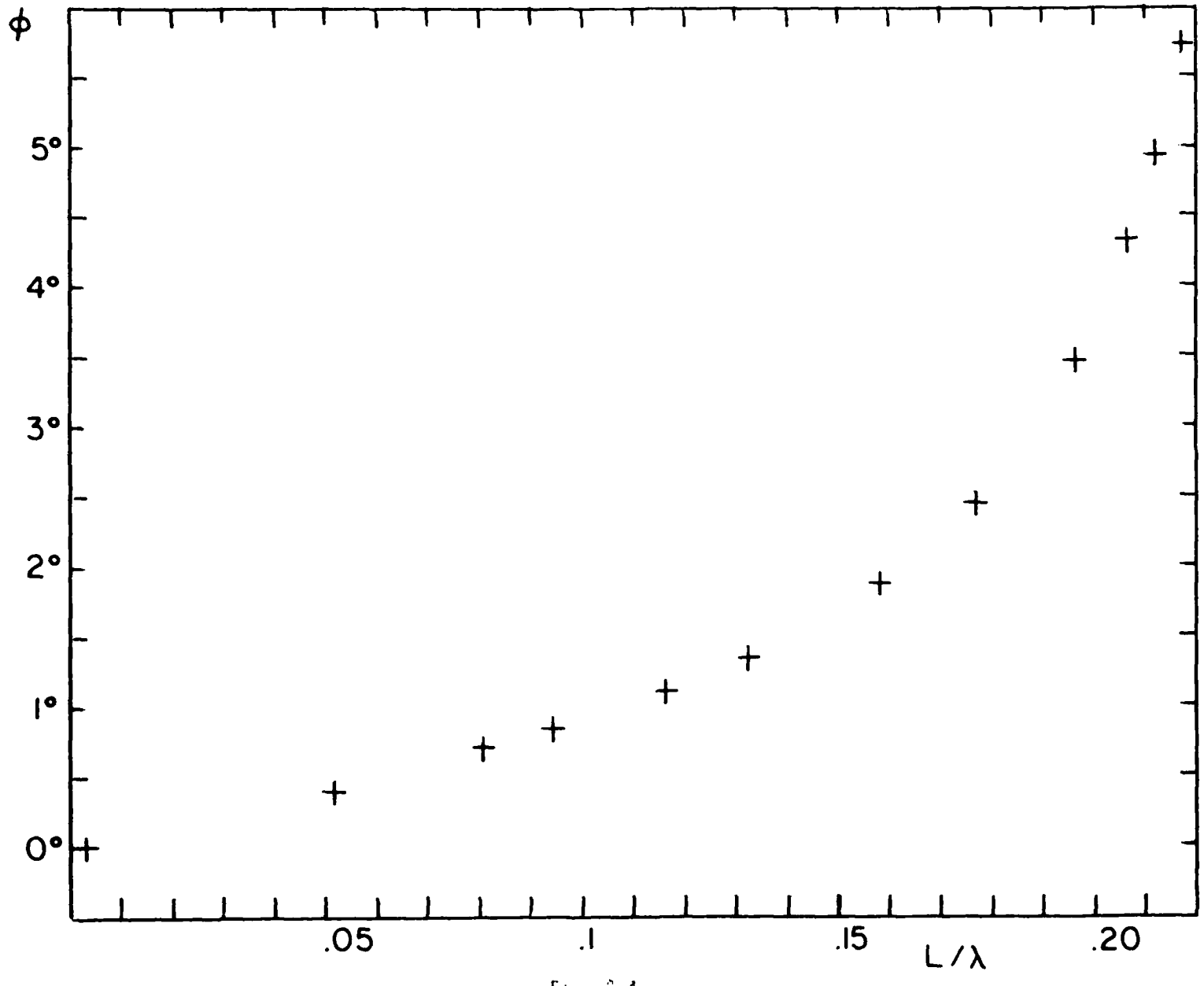

Fig. 2.4

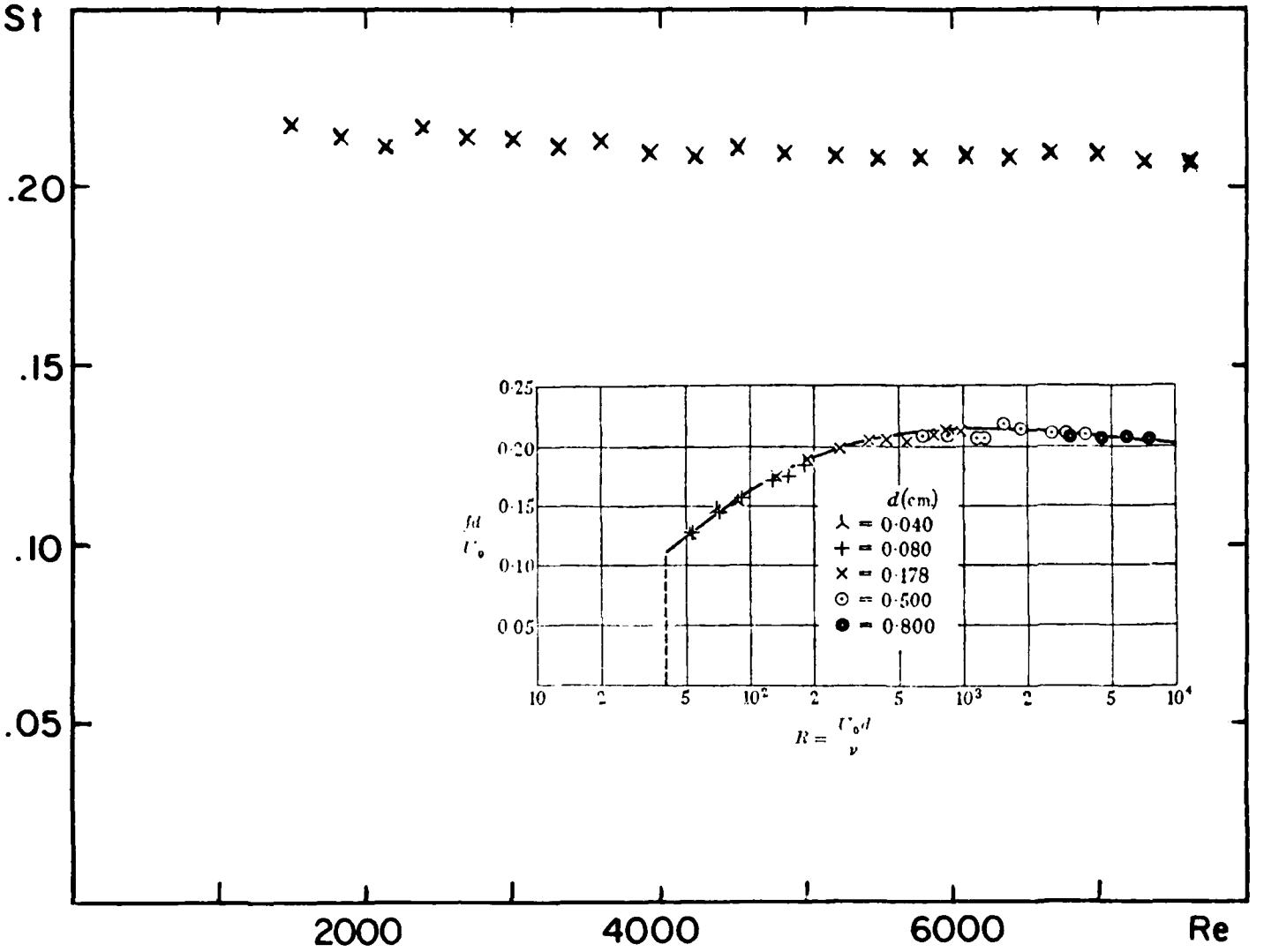
St
.20
.15
.10
.05
2000
4000
6000
Re
0·25
0·20
0·15
0·10
0·05
fd/U₀
d(cm)
= 0·040
= 0·080
= 0·178
= 0·500
= 0·800
10
2
5
10²
2
5
10³
2
5
10⁴
R = U₀d/ν

Fig. 2.5

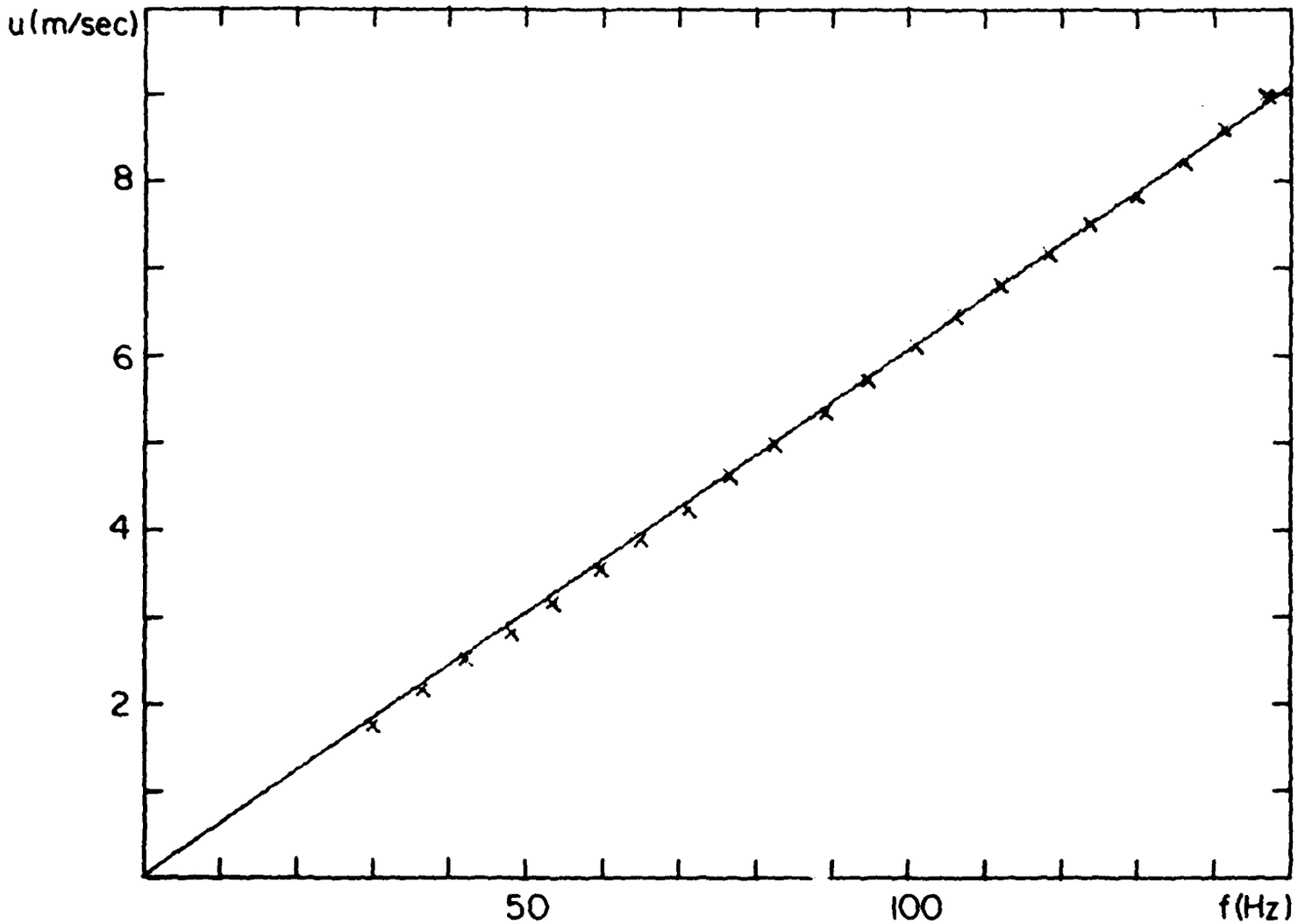

Fig. 2.6

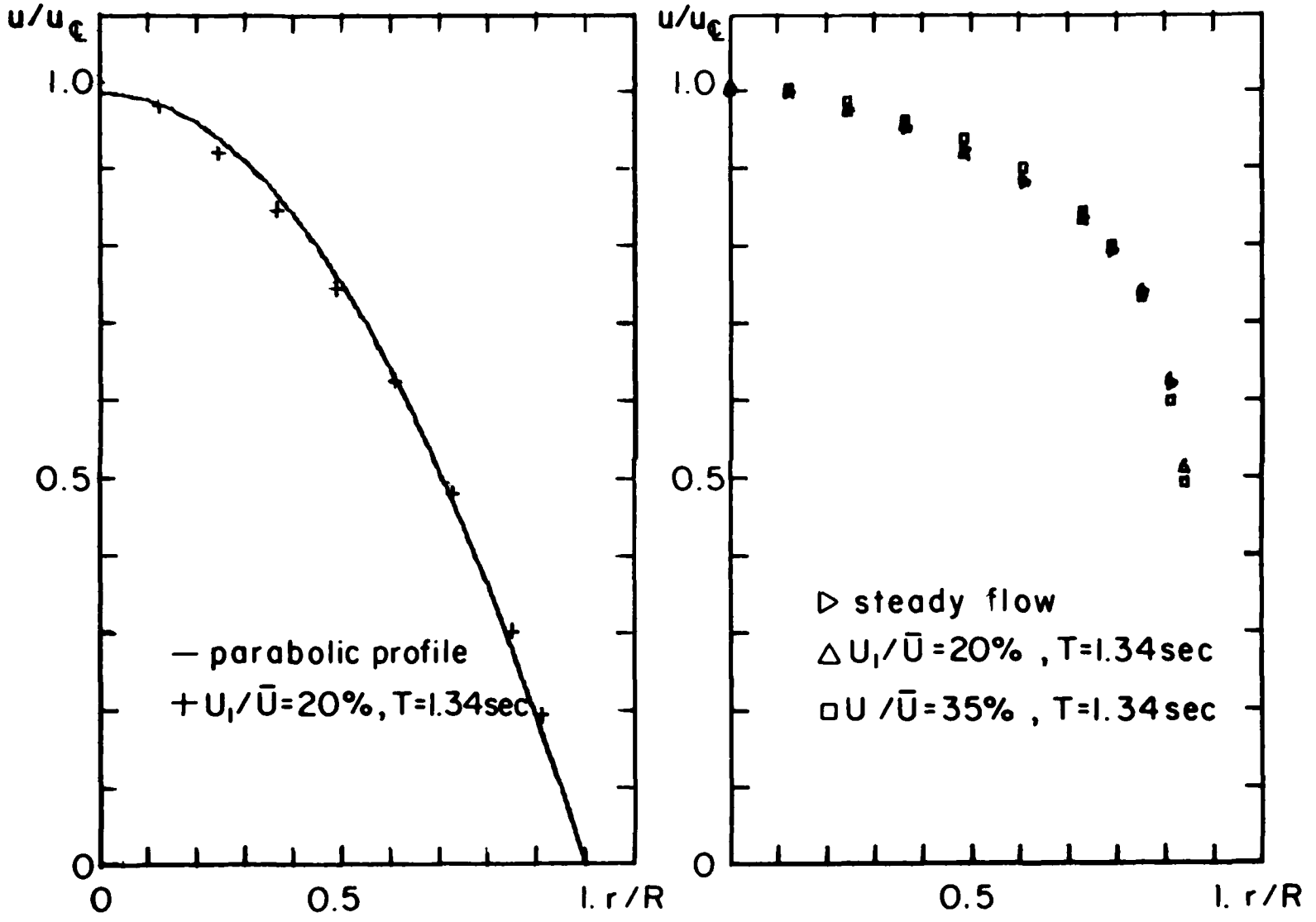
u/u_℄
1.0
0.5
0
0
0.5
1. r/R
— parabolic profile
+ U_I/Ū=20%, T=1.34sec
a
u/u_℄
1.0
0.5
0
0.5
1. r/R
▷ steady flow
△ U_I/Ū=20% , T=1.34sec
□ U /Ū=35% , T=1.34sec
b

Fig. 3.1

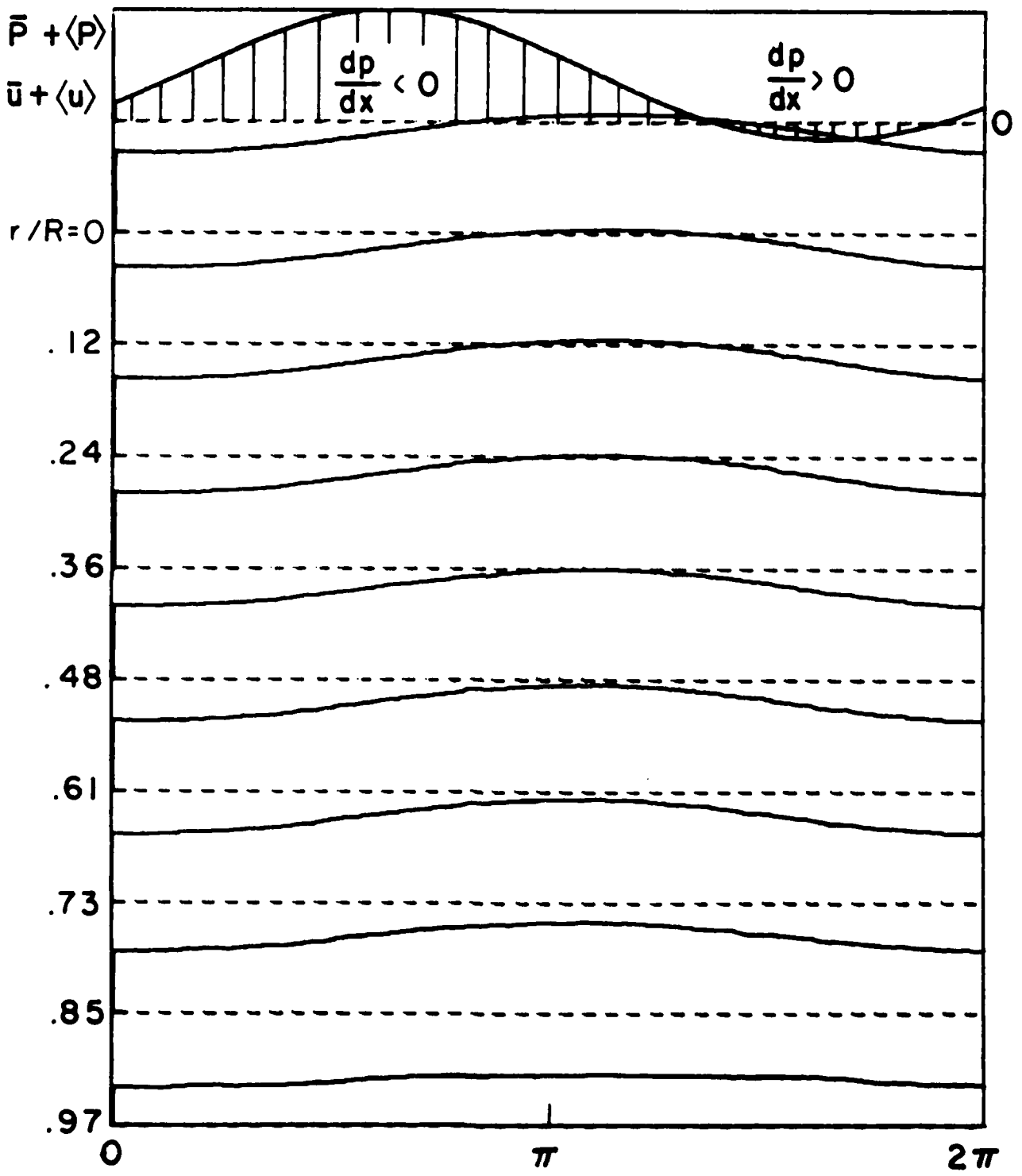
$\bar{P} + \langle P \rangle$
$\bar{u} + \langle u \rangle$
$\frac{dp}{dx} < 0$
$\frac{dp}{dx} > 0$
0
r/R=0
.12
.24
.36
.48
.61
.73
.85
.97
0
π
2π

Fig. 3.2

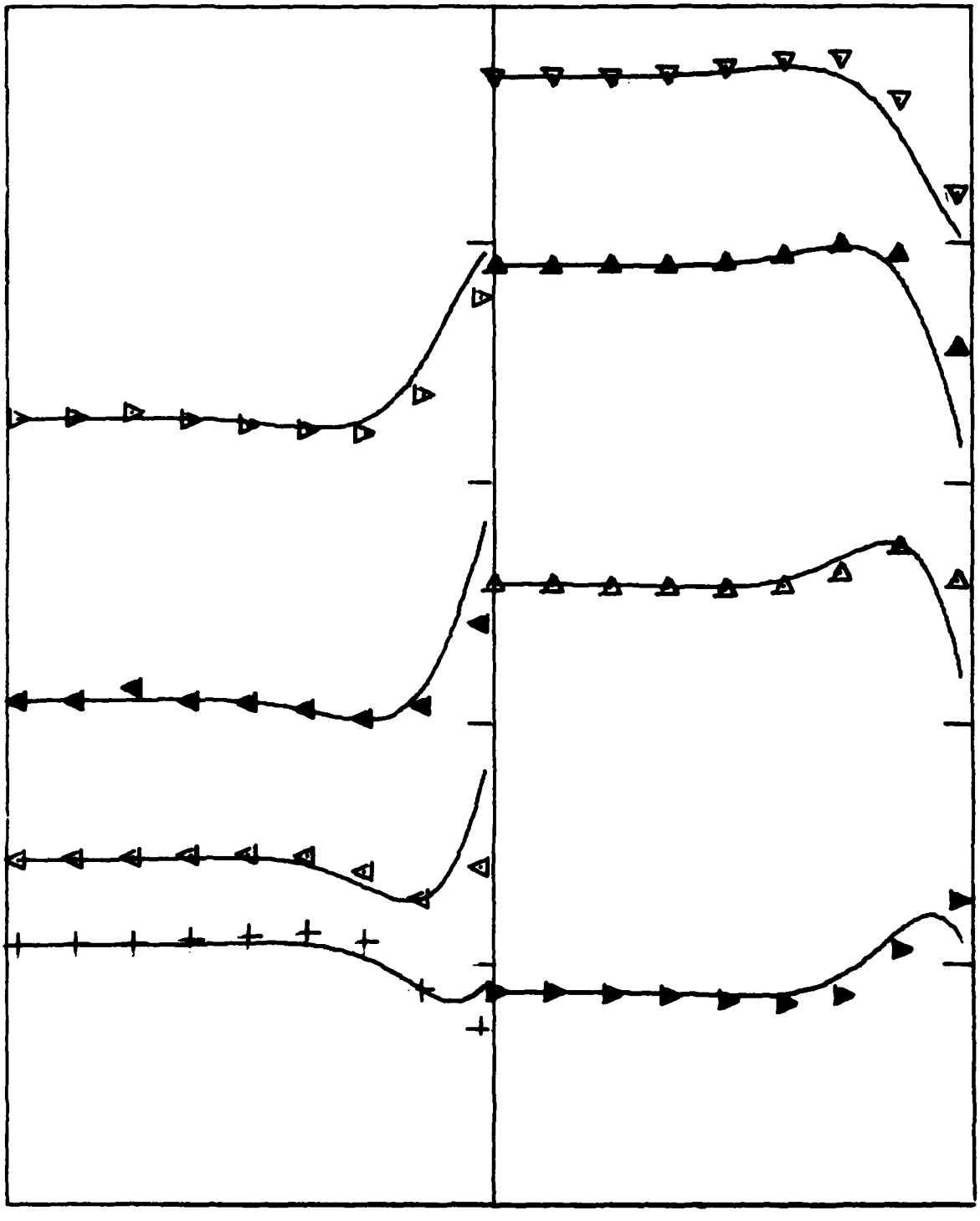

Fig. 3.3a

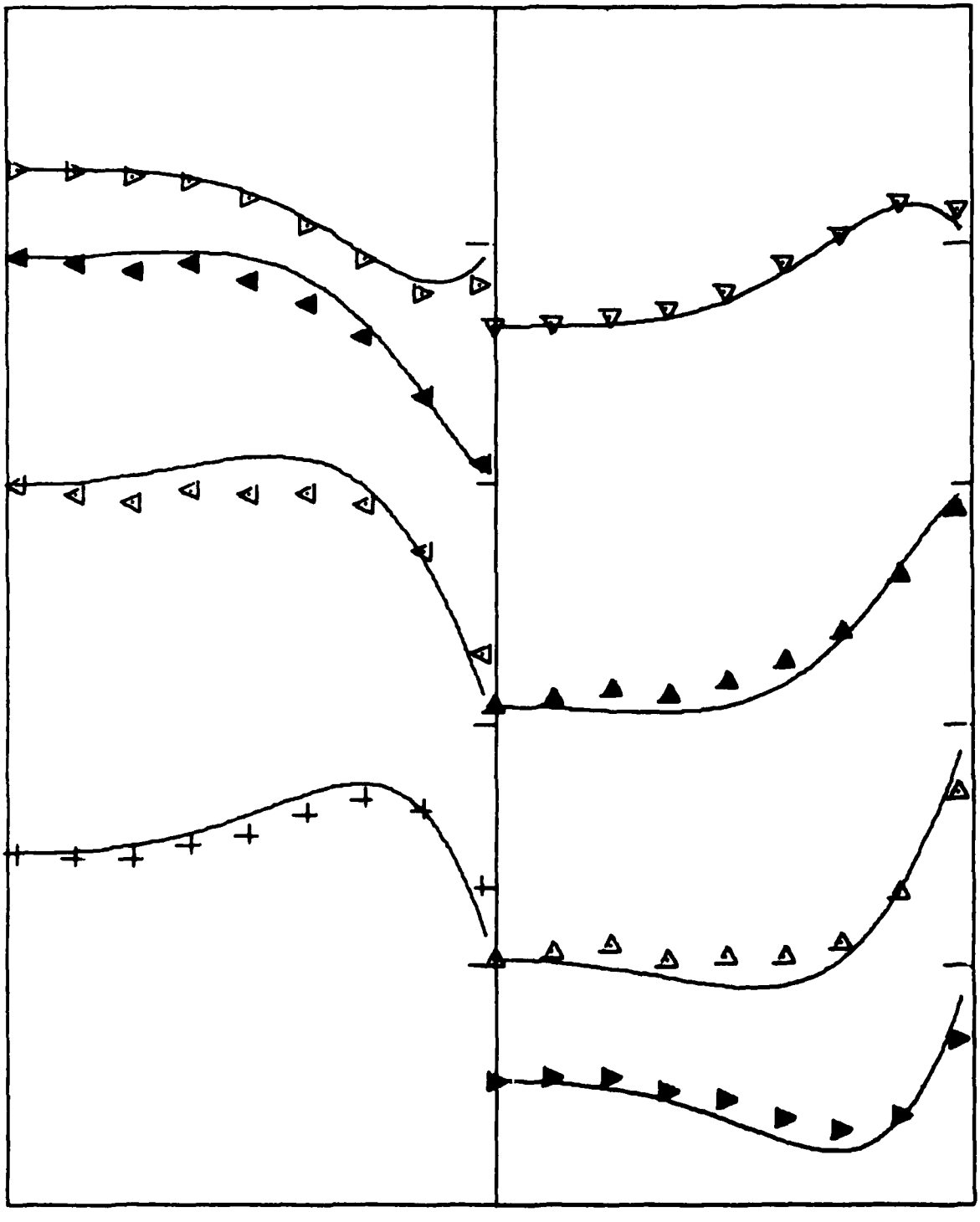

Fig. 3.3b

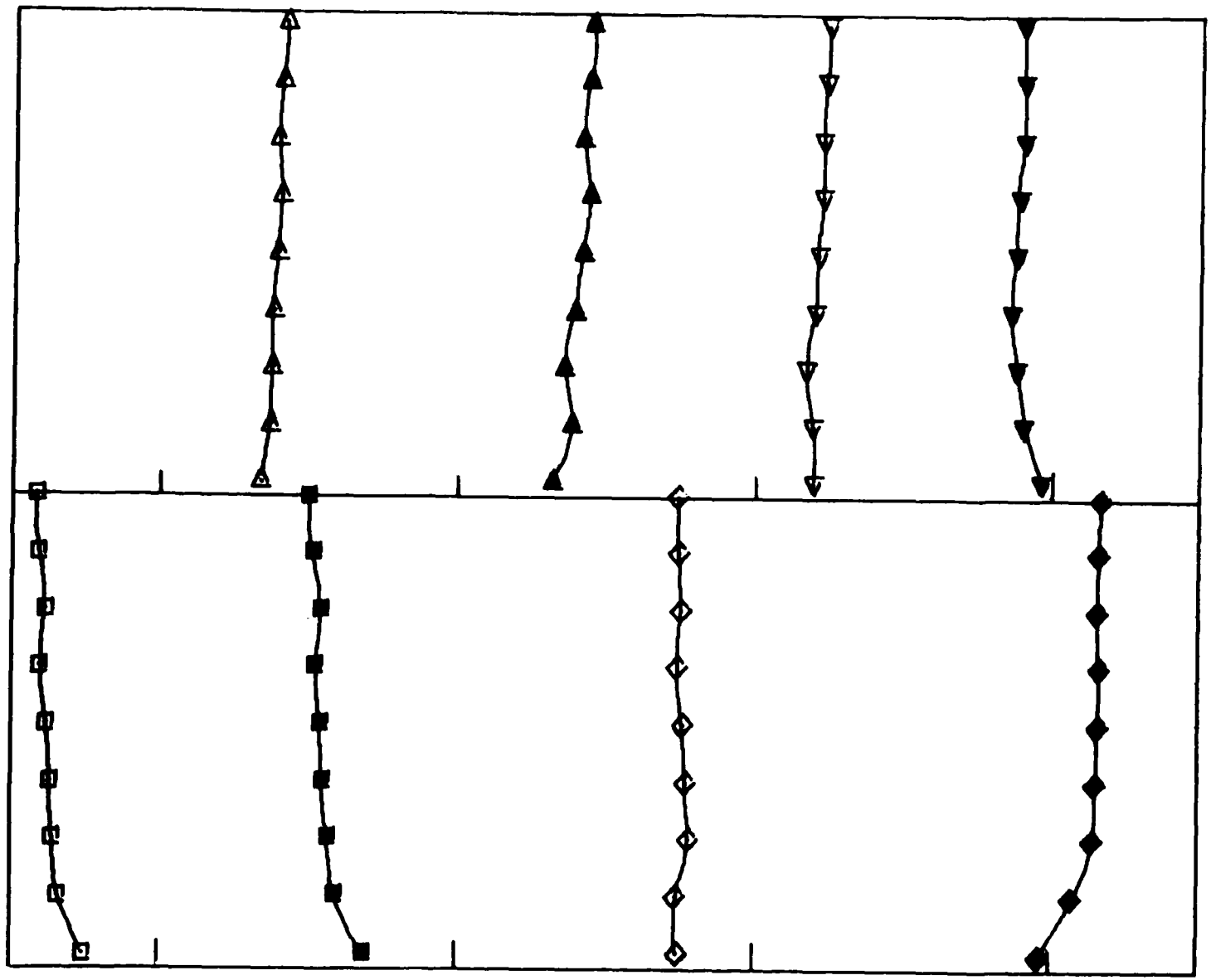

Fig. 5.4a

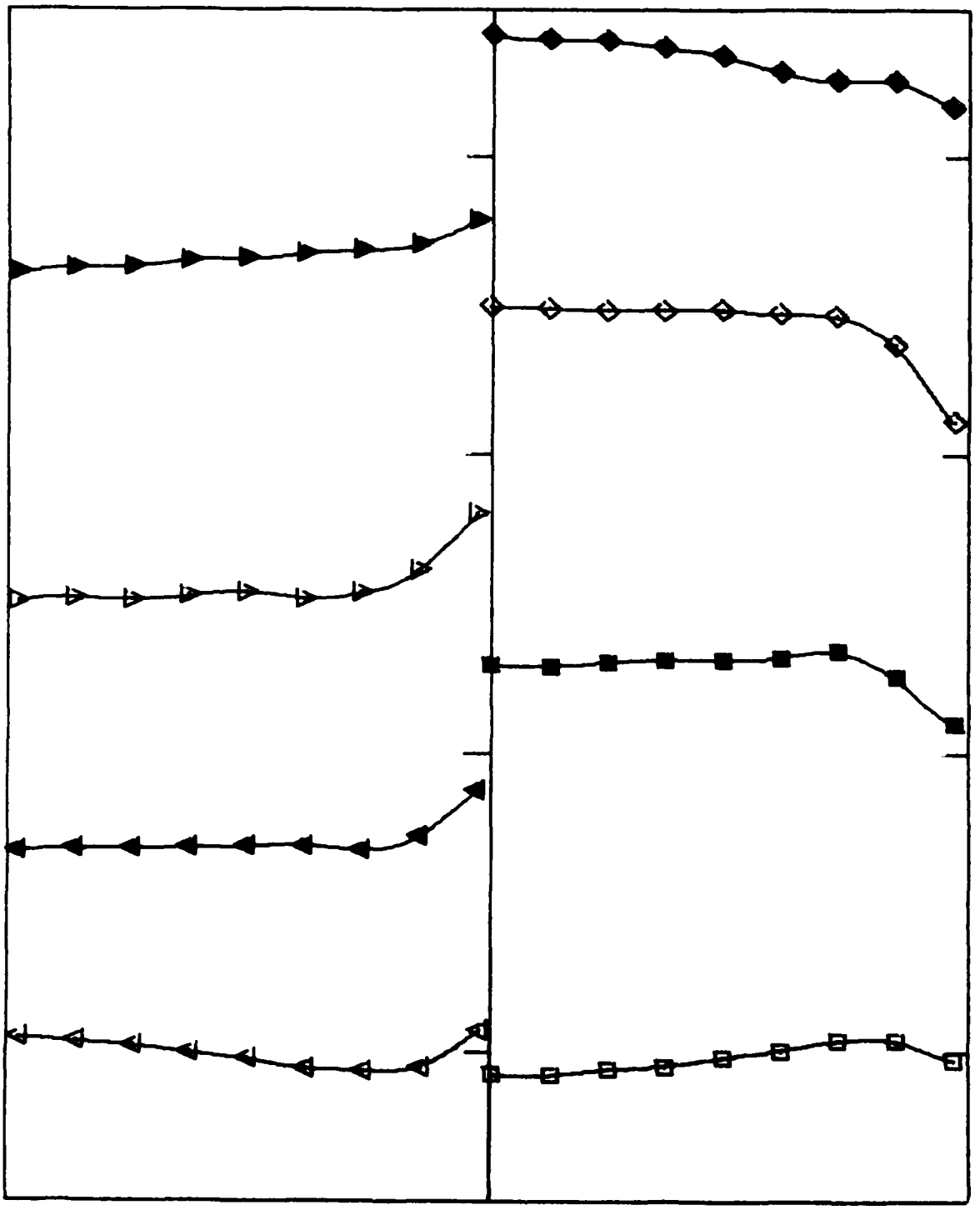

Fig. 3.4b

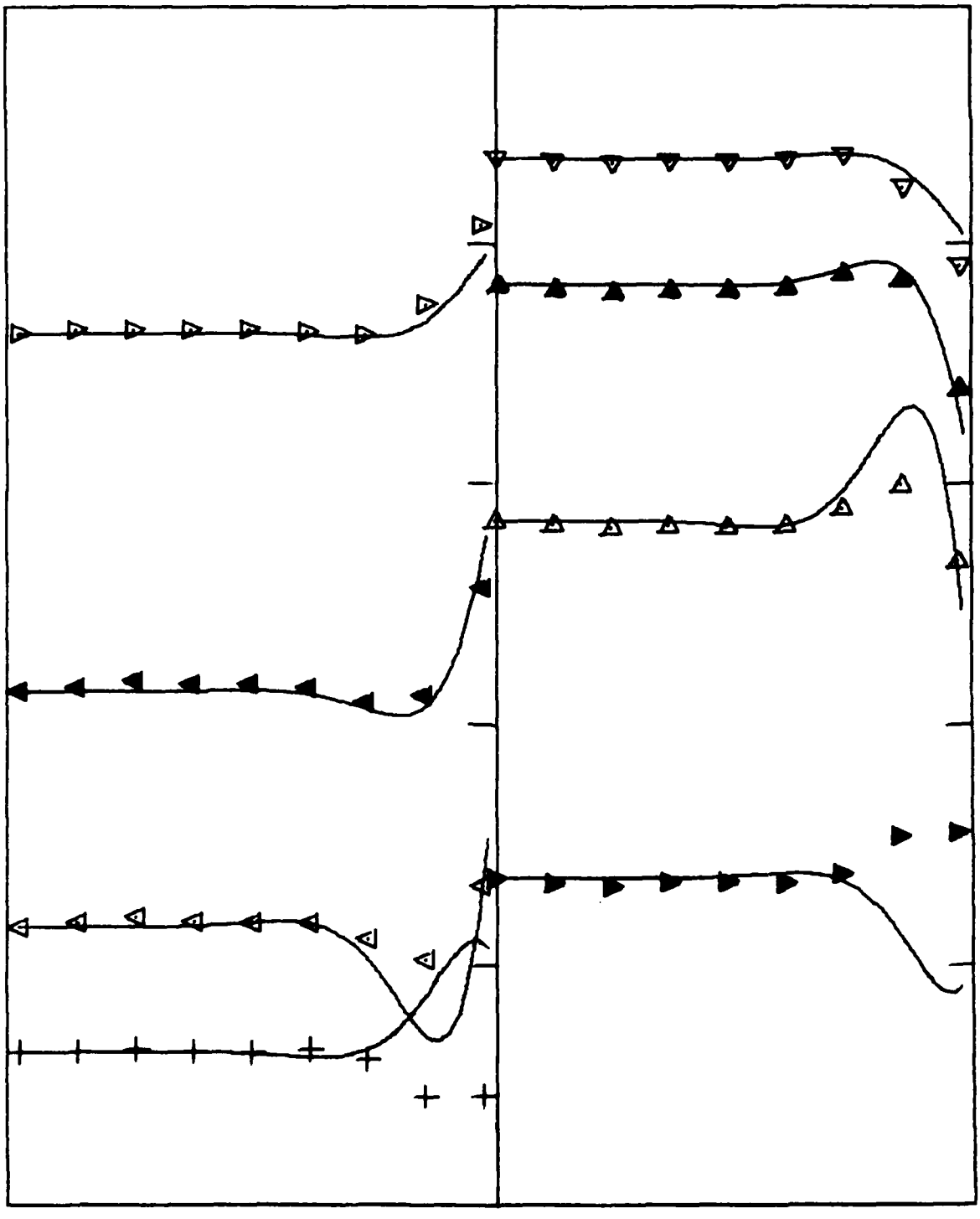

Fig. 3.4c

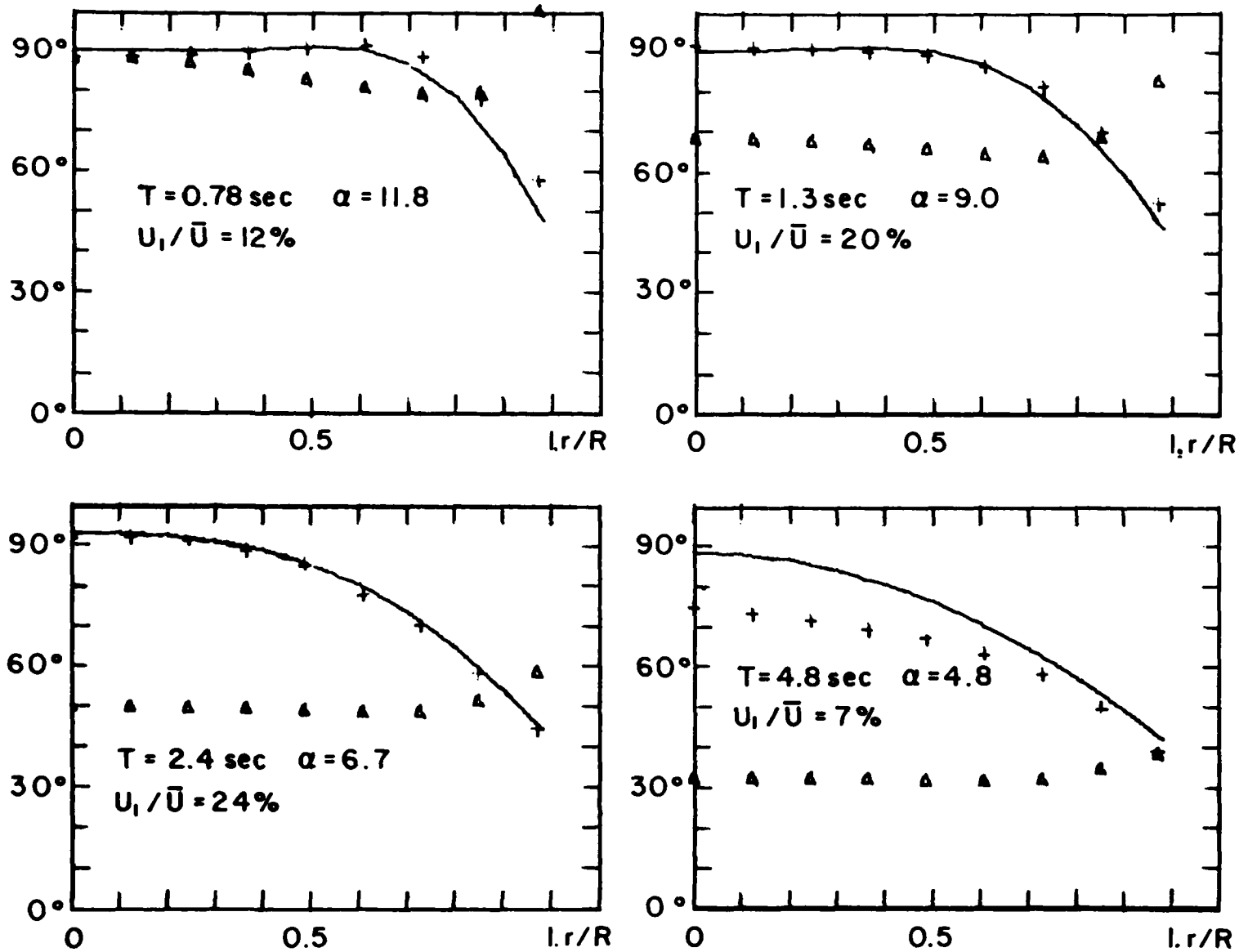
90°
60°
30°
0°
0
0.5
l.r/R
T = 0.78 sec α = 11.8
U1 / Ū = 12%
T = 1.3 sec α = 9.0
U1 / Ū = 20%
T = 2.4 sec α = 6.7
U1 / Ū = 24%
T = 4.8 sec α = 4.8
U1 / Ū = 7%

Fig. 3.5

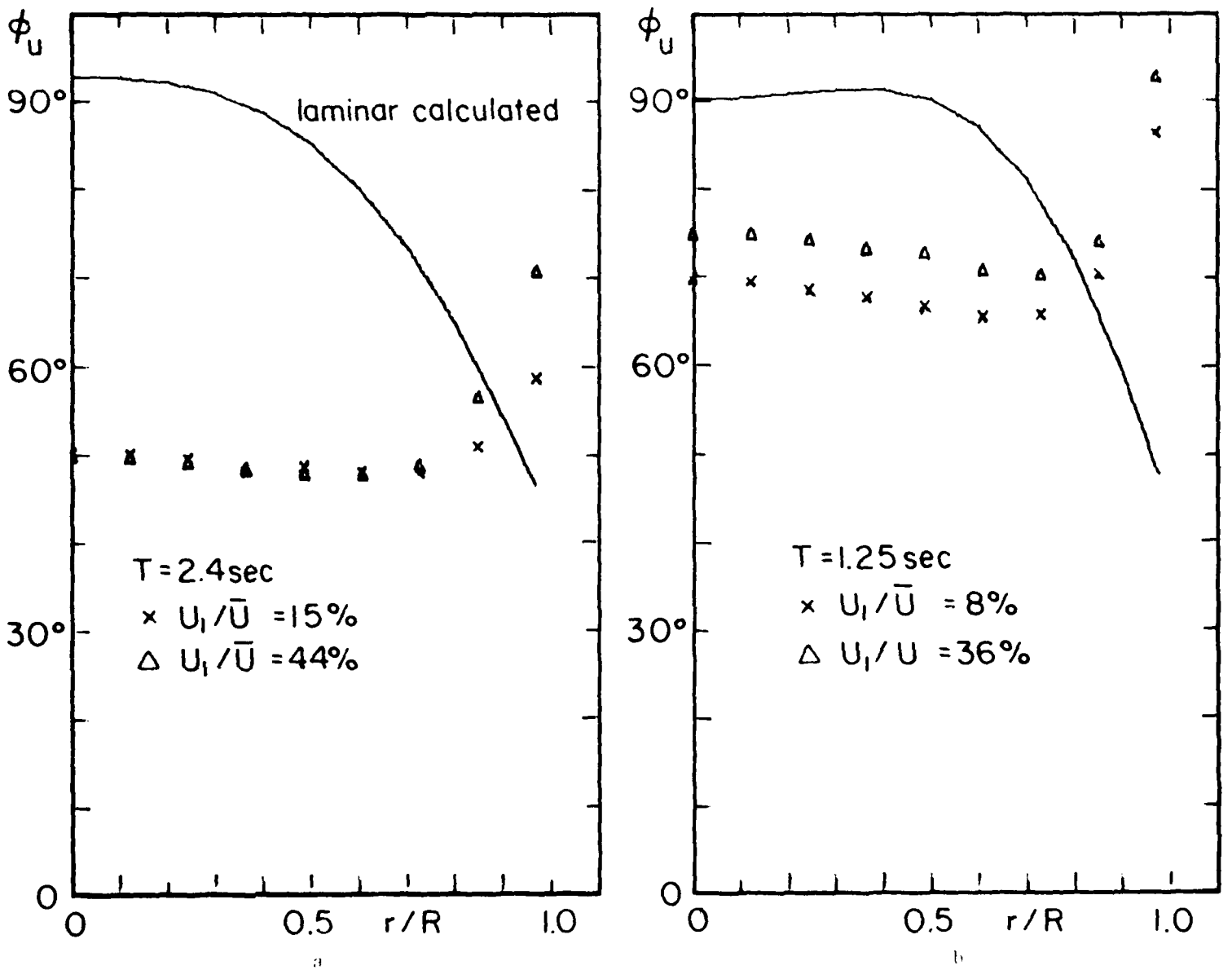
ϕ_u
90°
60°
30°
0
laminar calculated
T = 2.4 sec
× $U_1/\bar{U}$ = 15%
△ $U_1/\bar{U}$ = 44%
0
0.5
r/R
1.0
a
ϕ_u
90°
60°
30°
0
T = 1.25 sec
× $U_1/\bar{U}$ = 8%
△ U_1/U = 36%
0
0.5
r/R
1.0
b

Fig. 5.6

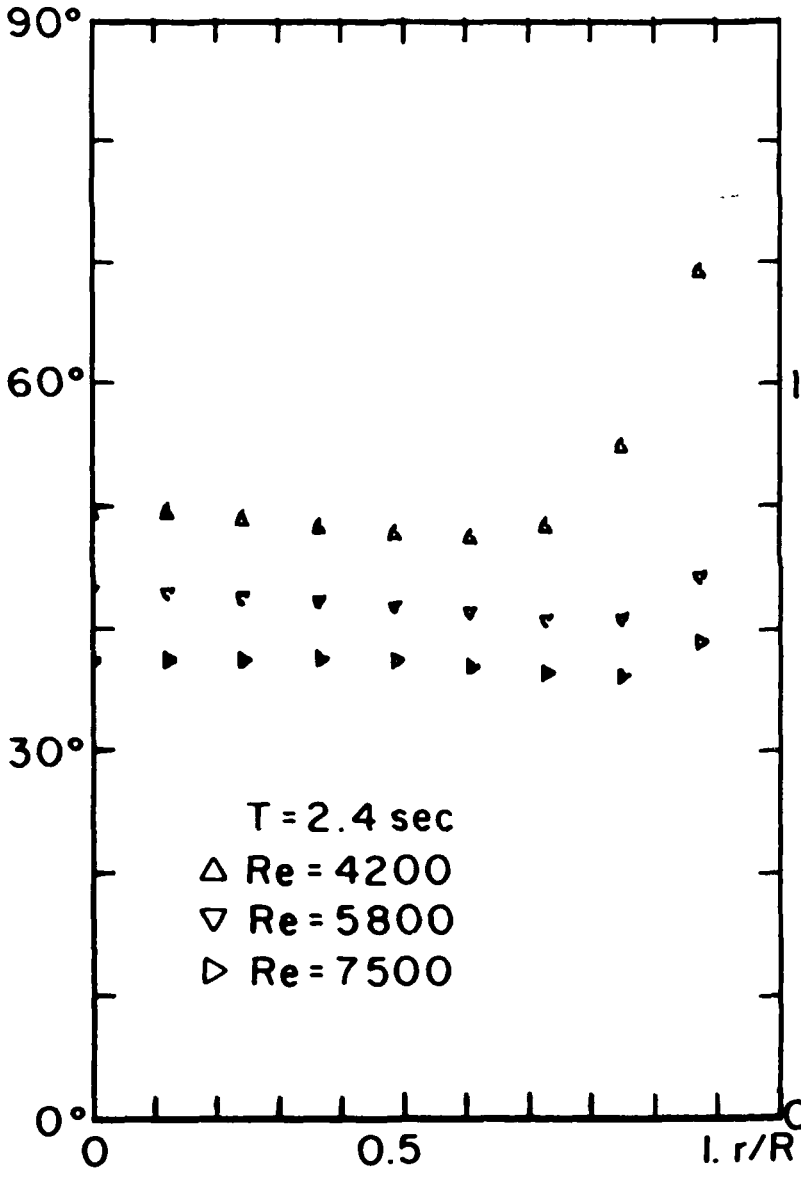
90°
60°
30°
0°
0
0.5
1. r/R
T = 2.4 sec
Δ Re = 4200
▽ Re = 5800
▷ Re = 7500

Fig. 3.7

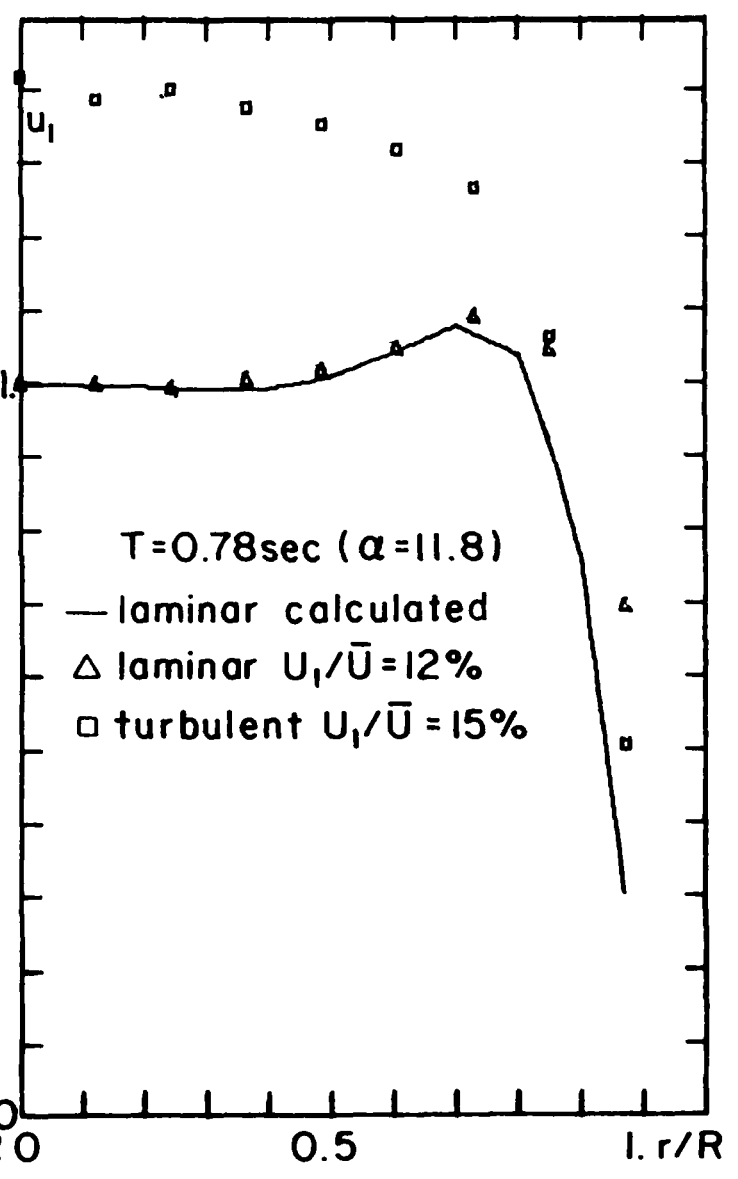
u_1
1.
0
0.5
1. r/R
T=0.78sec (α=11.8)
— laminar calculated
△ laminar $U_1/\bar{U}$=12%
□ turbulent $U_1/\bar{U}$=15%

Fig. 3.8

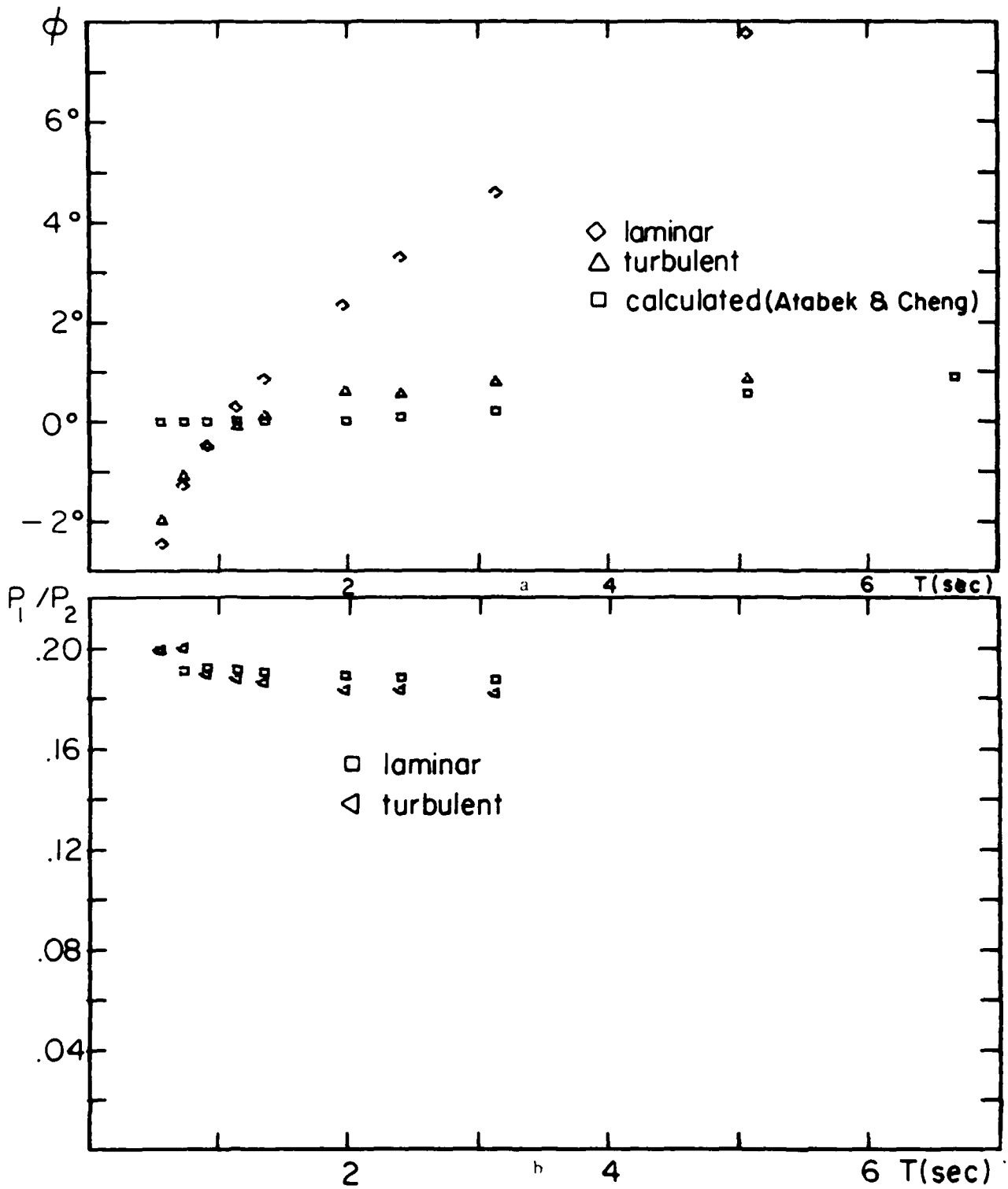
ϕ
6°
4°
2°
0°
−2°
◇ laminar
△ turbulent
□ calculated(Atabek & Cheng)
2
a
4
6
T(sec)
P1 /P2
.20
.16
.12
.08
.04
□ laminar
◁ turbulent
2
b
4
6 T(sec)

Fig. 3.9

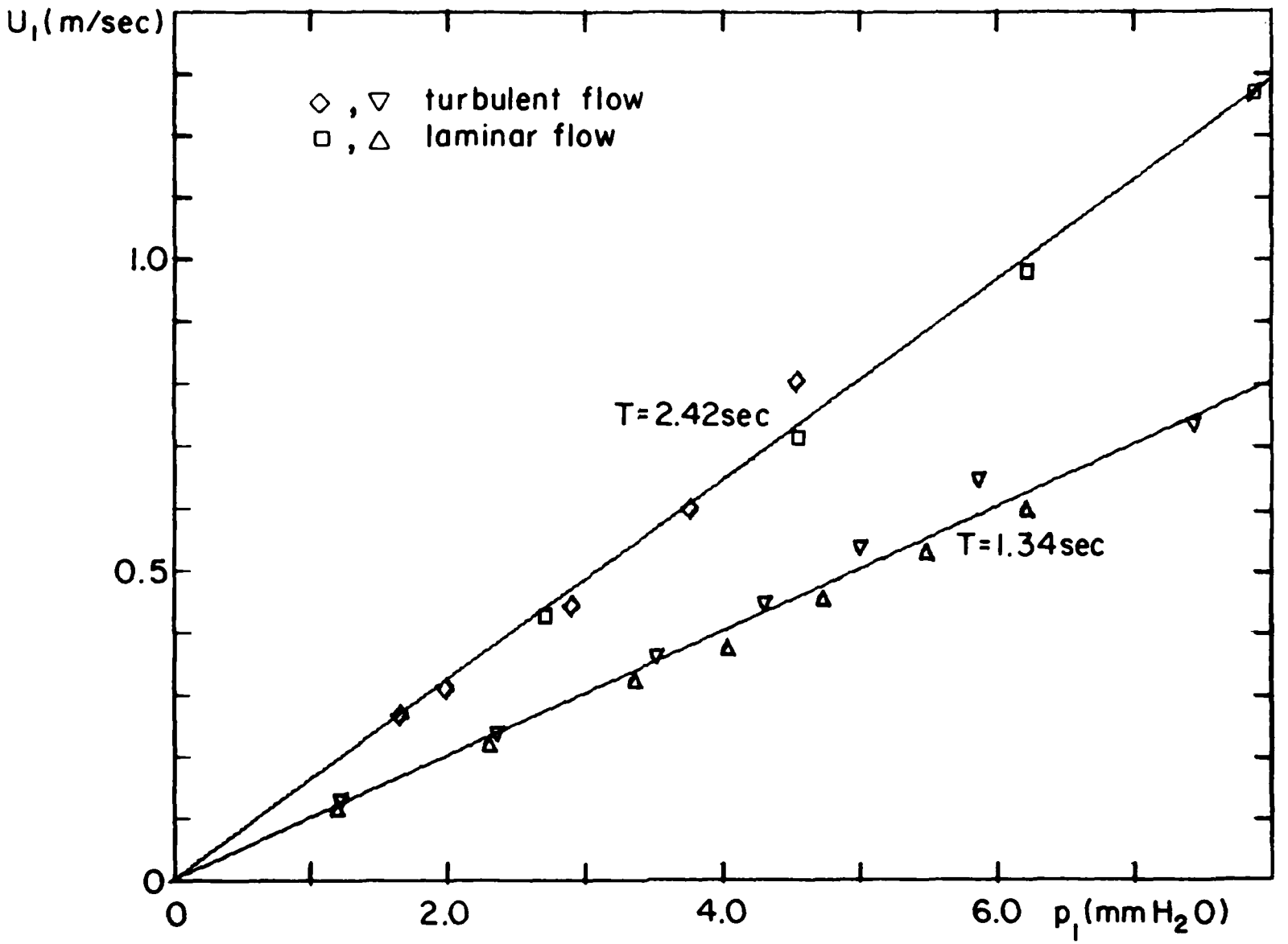
U1 (m/sec)
◇ , ▽ turbulent flow
□ , △ laminar flow
T=2.42sec
T=1.34sec
1.0
0.5
0
0
2.0
4.0
6.0
p1 (mm H2O)

Fig. 5.10

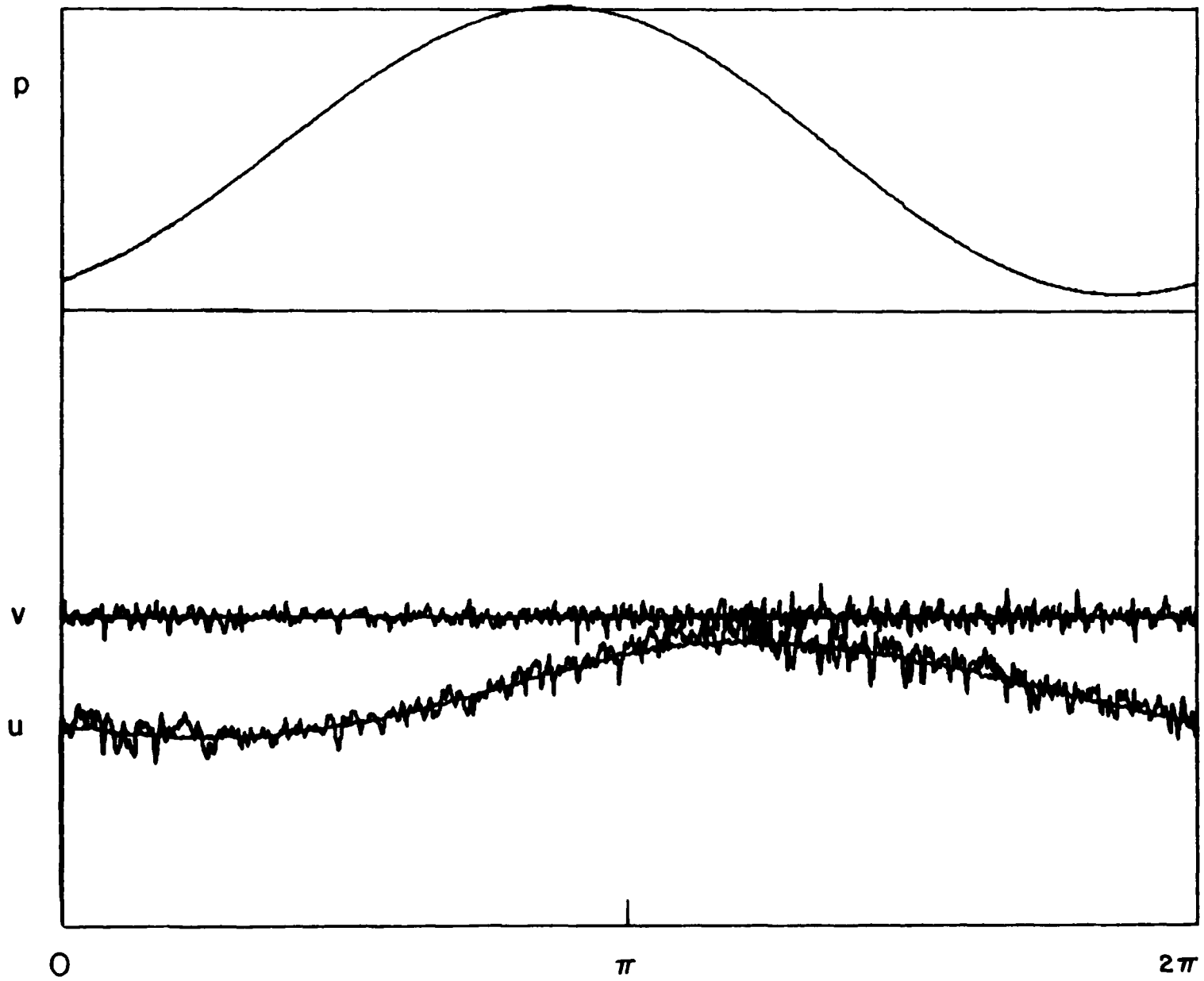
p
v
u
0
π
2π

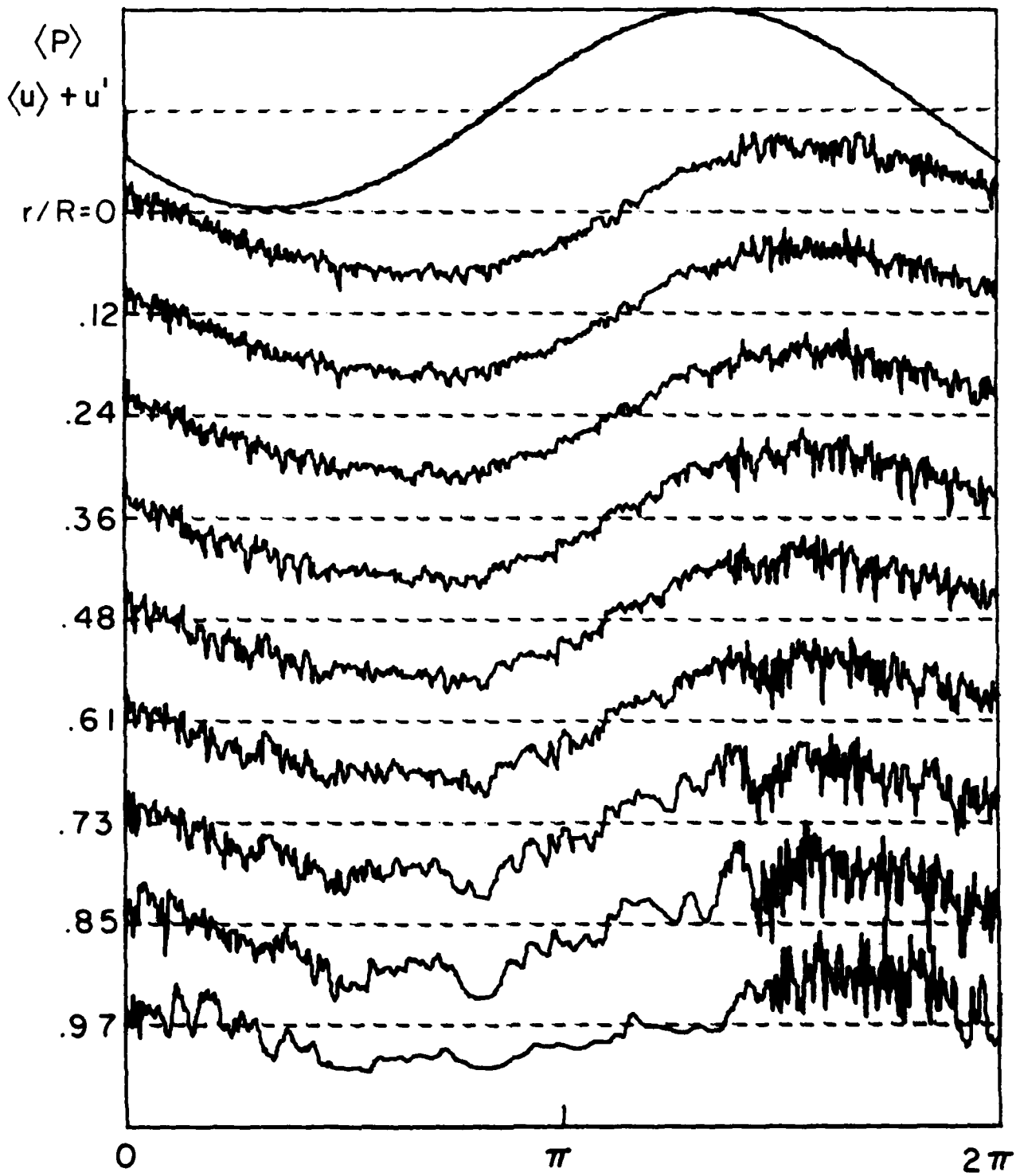

Fig. 3.12

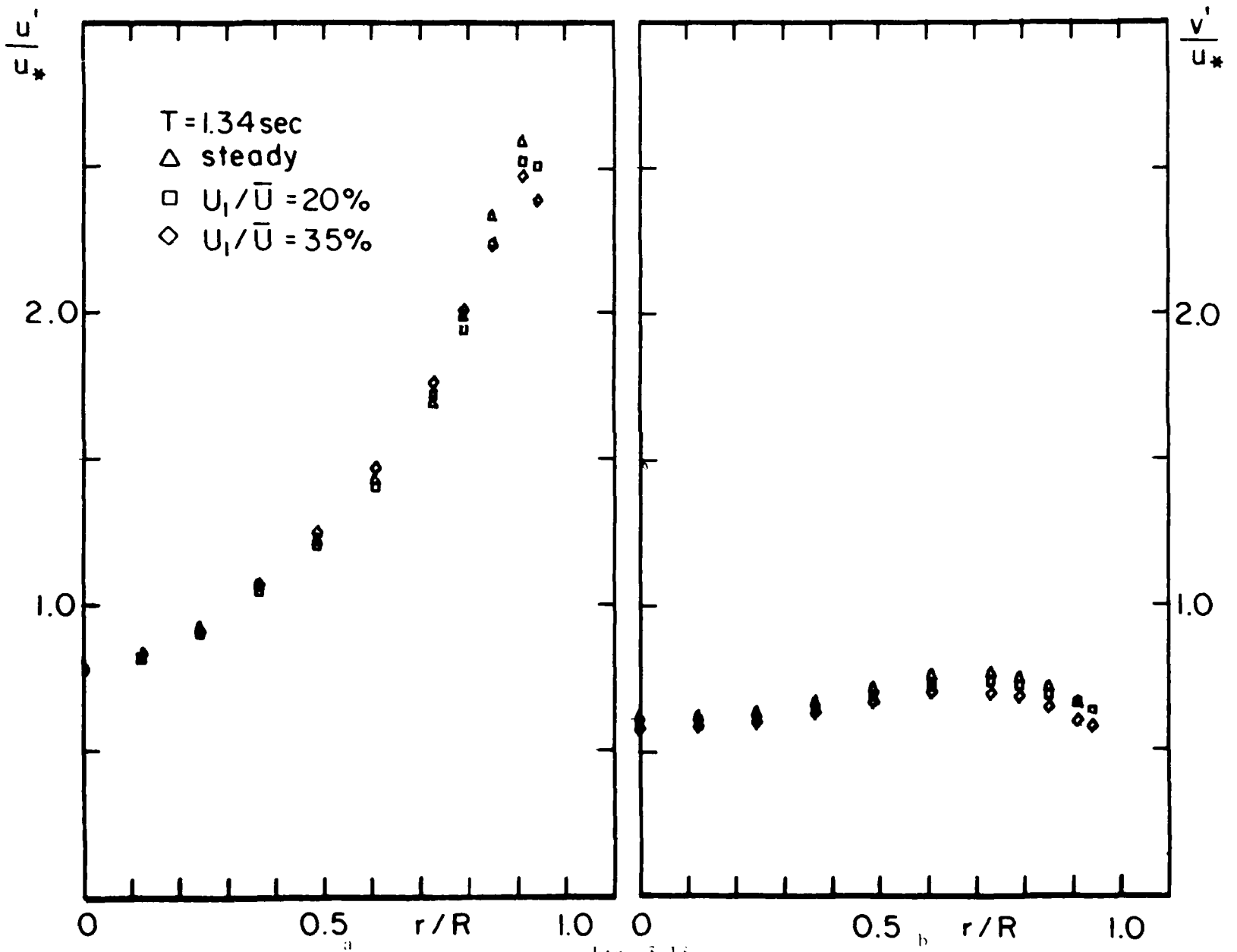
u'/u*
T = 1.34 sec
△ steady
□ U1/Ū = 20%
◇ U1/Ū = 35%
2.0
1.0
0
0.5
r/R
1.0
a
v'/u*
2.0
1.0
0
0.5
r/R
1.0
b

Fig. 3.13

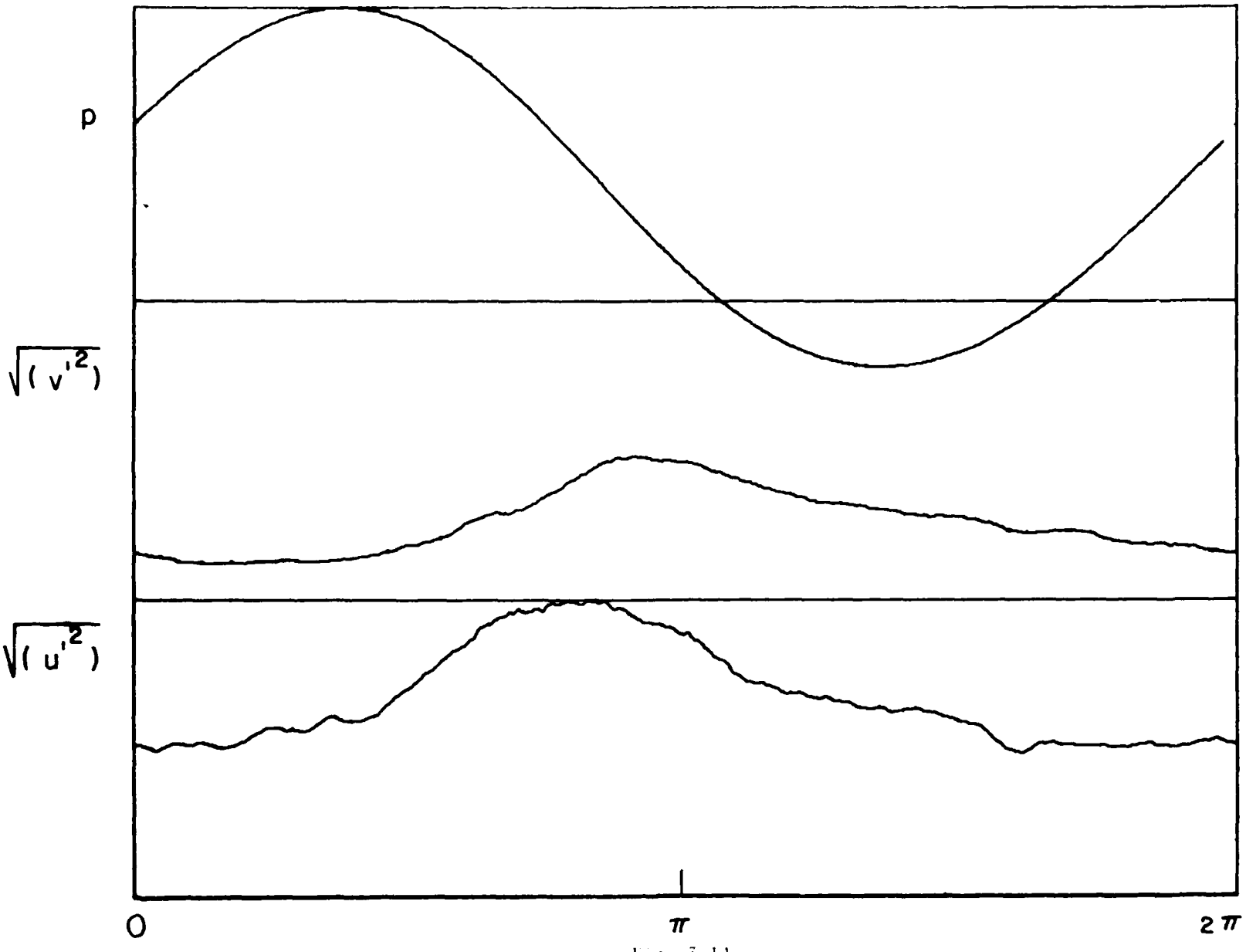

Fig. 3.11

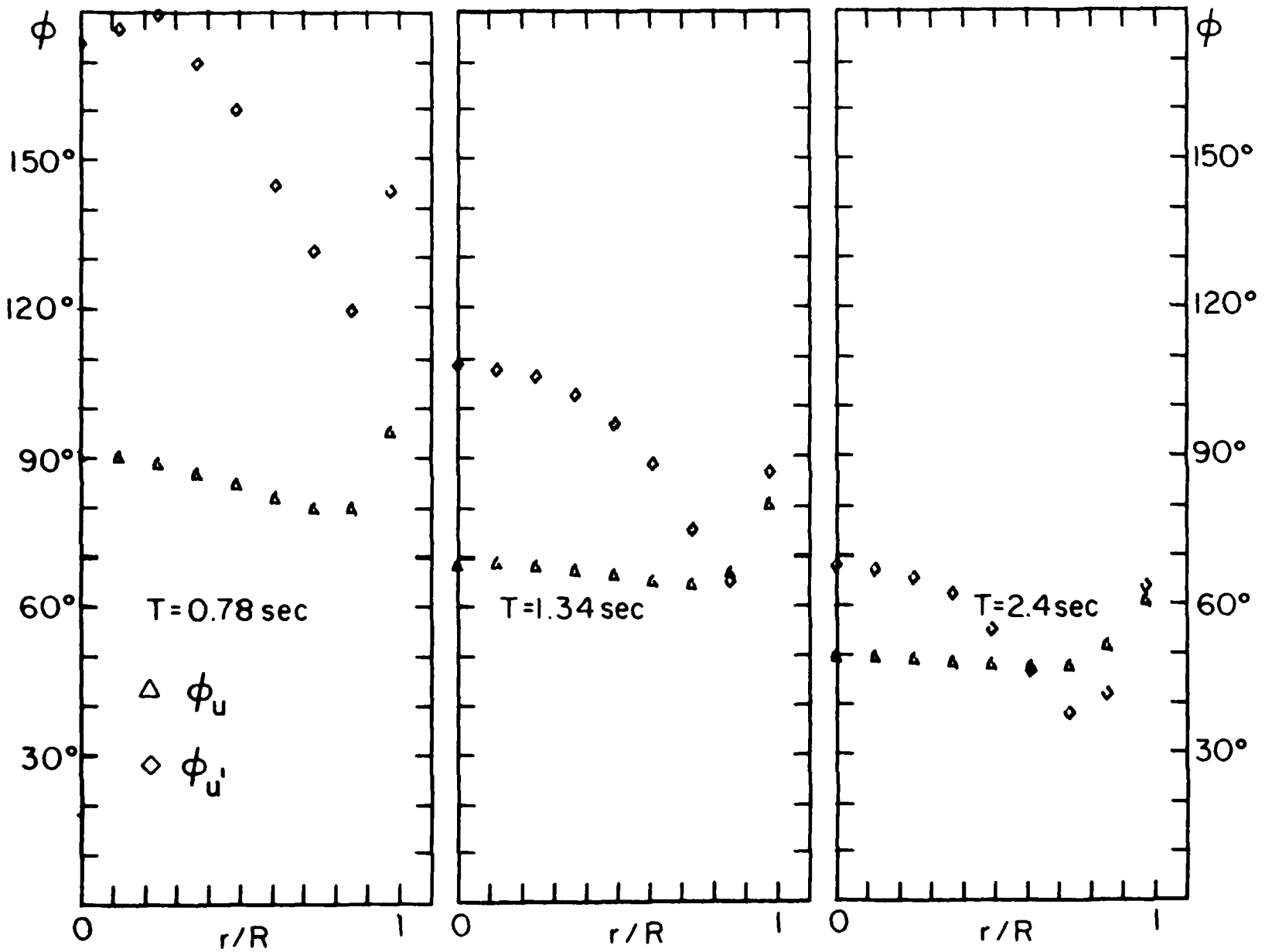

Fig. 3.15

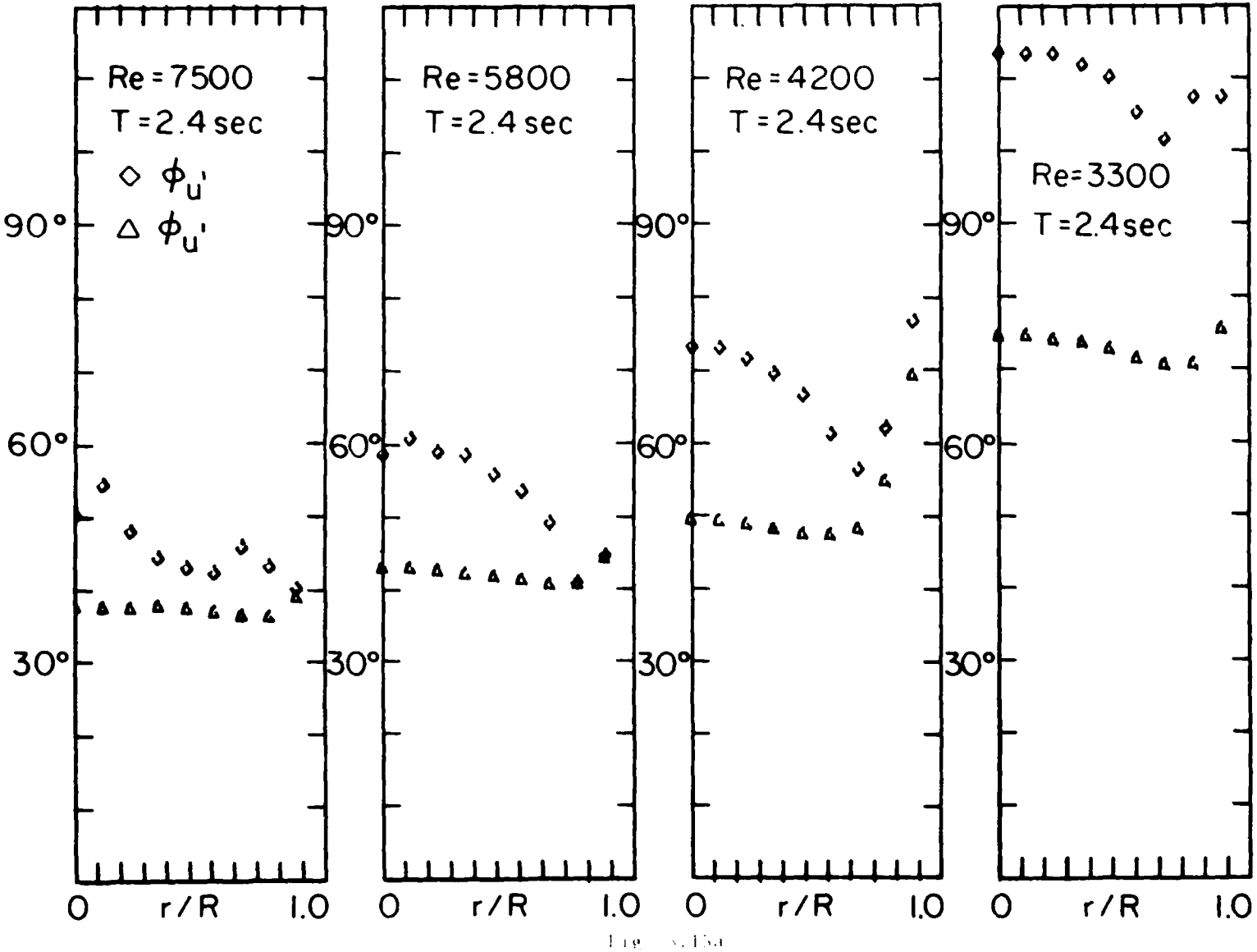
Re = 7500
T = 2.4 sec
◇ $\phi_{u'}$
△ $\phi_{u'}$
Re = 5800
T = 2.4 sec
Re = 4200
T = 2.4 sec
Re = 3300
T = 2.4 sec
90°
60°
30°
0
r/R
1.0

Fig. V.15a

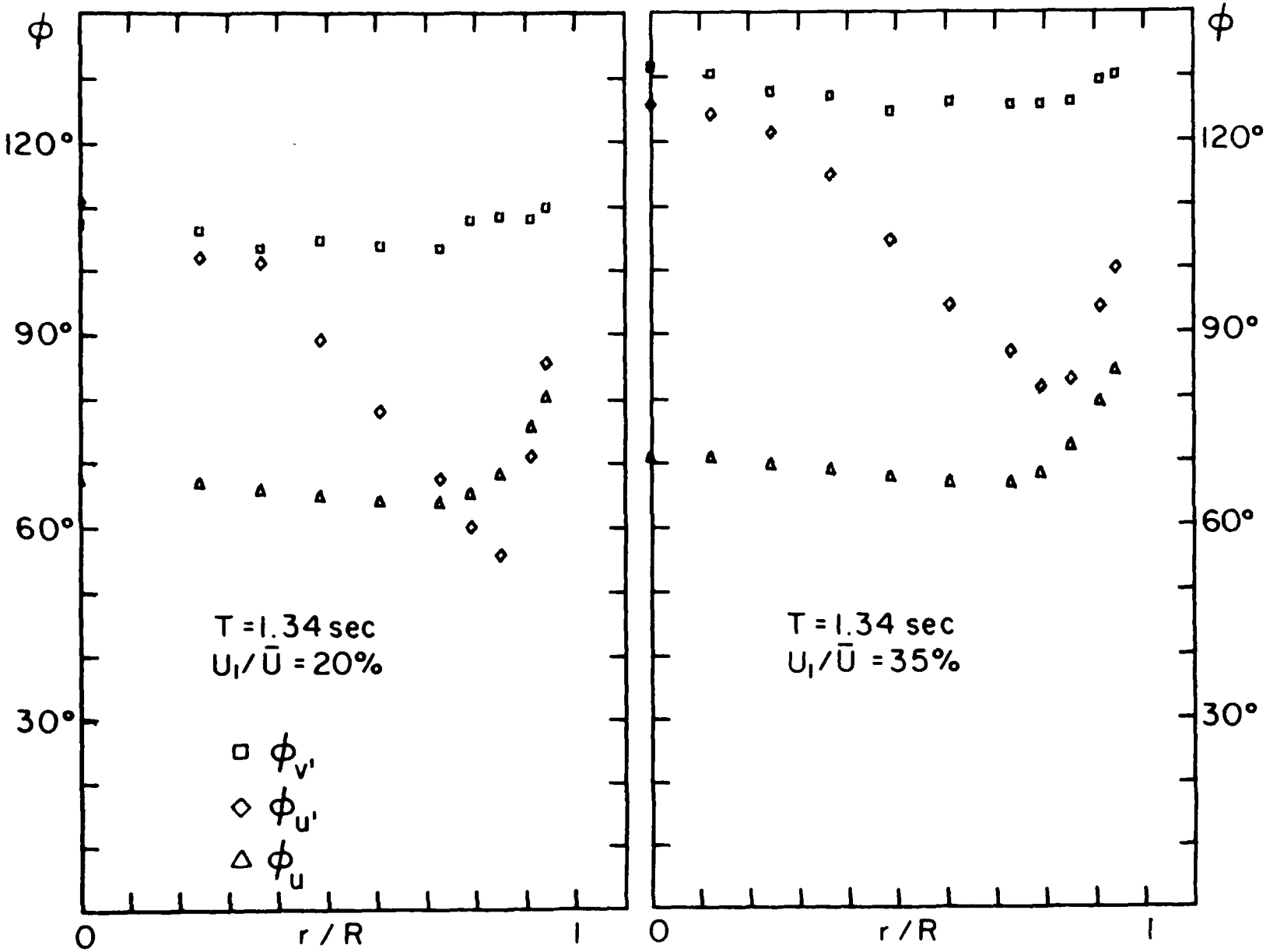
φ
120°
90°
60°
30°
T = 1.34 sec
U₁/Ū = 20%
□ φv'
◇ φu'
△ φu
0
r / R
1
φ
120°
90°
60°
30°
T = 1.34 sec
U₁/Ū = 35%
0
r / R
1

Fig. 3.16

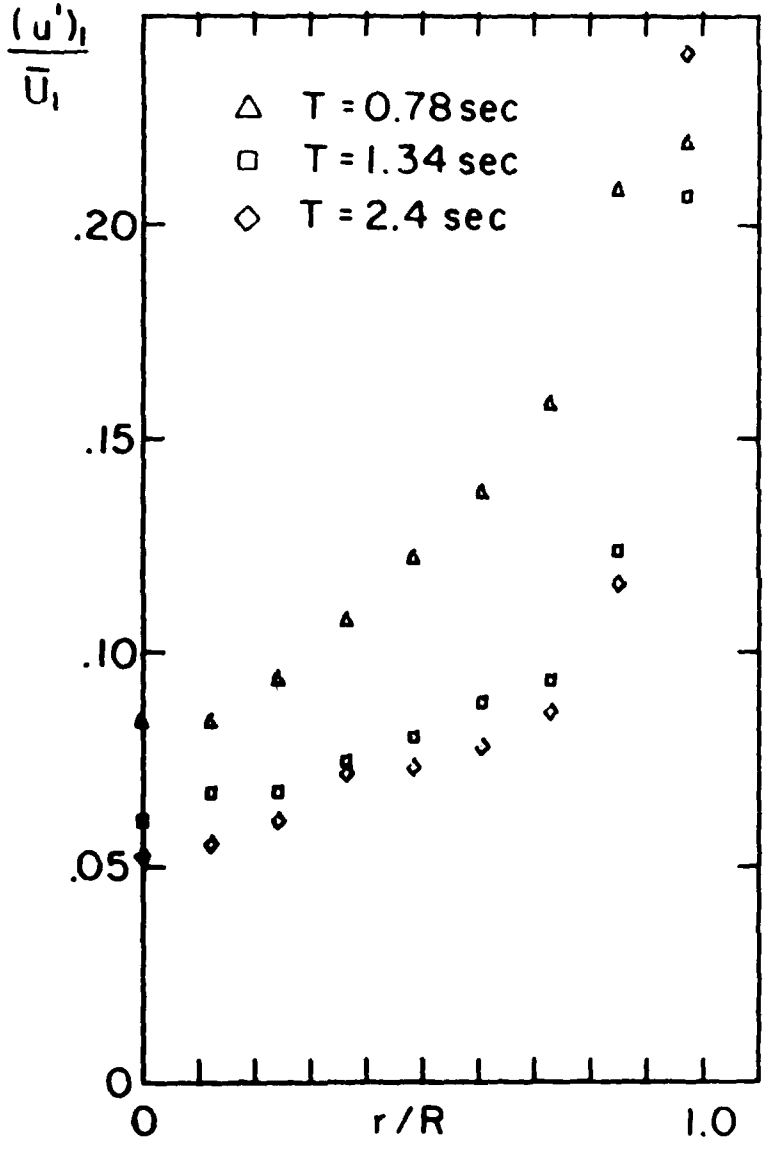
$\frac{(u')_1}{\bar{U}_1}$
△ T = 0.78 sec
□ T = 1.34 sec
◇ T = 2.4 sec
.20
.15
.10
.05
0
0
r/R
1.0

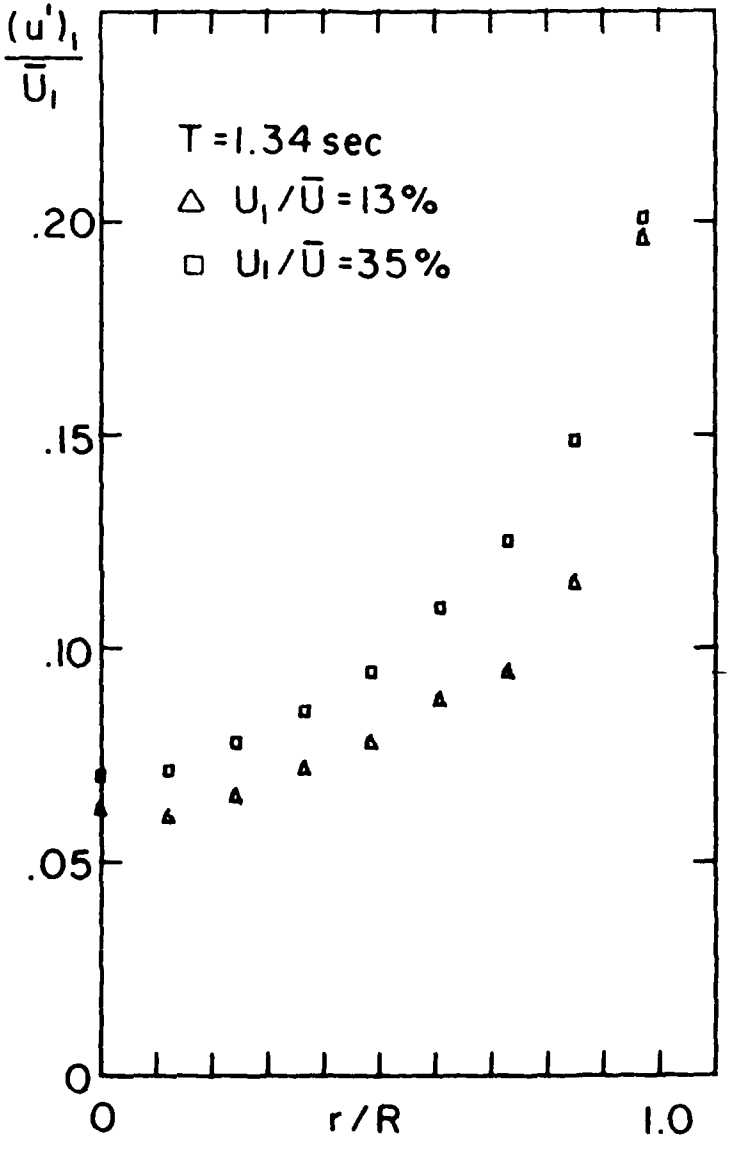
$\frac{(u')_1}{\bar{U}_1}$
T = 1.34 sec
△ $U_1/\bar{U}$ = 13%
□ $U_1/\bar{U}$ = 35%
.20
.15
.10
.05
0
0
r/R
1.0

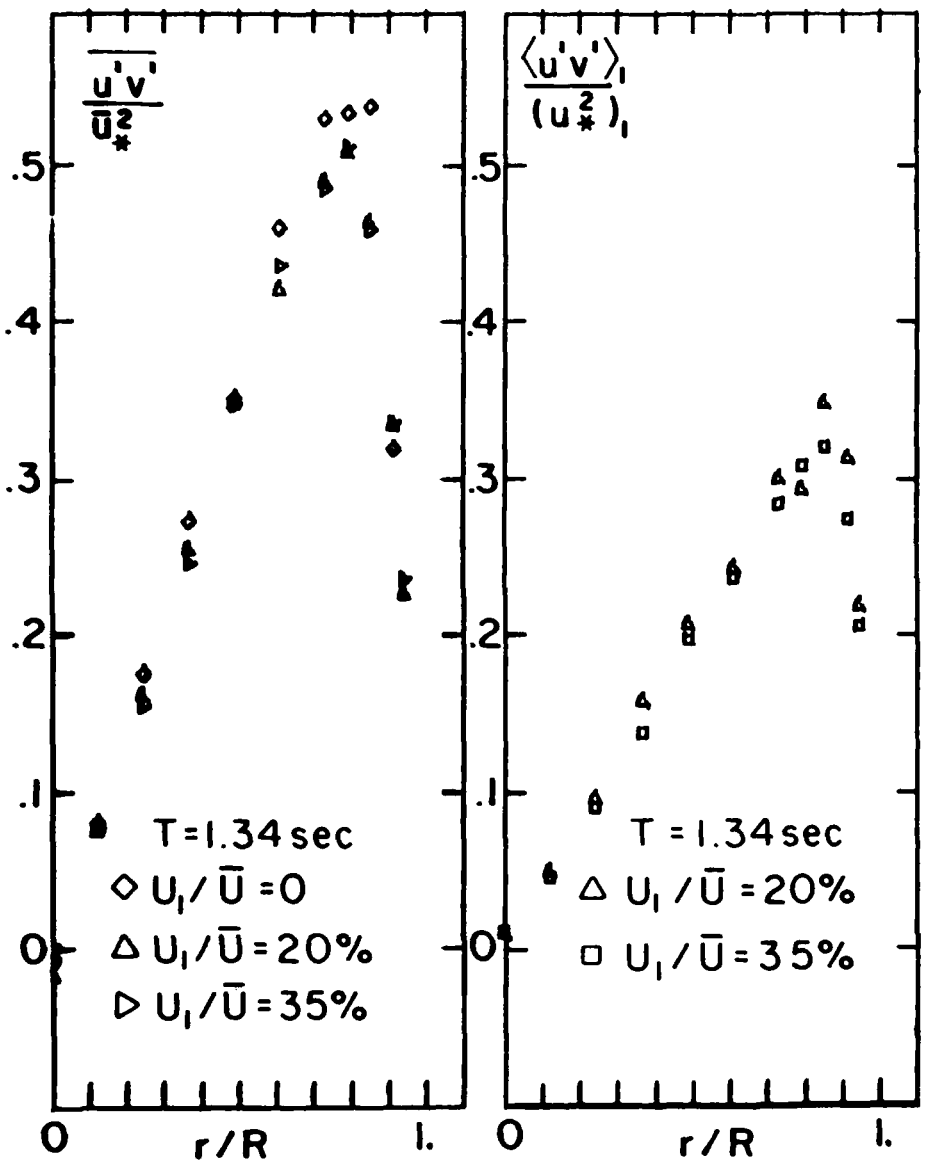

Fig. 3.19

Fig. 3.20

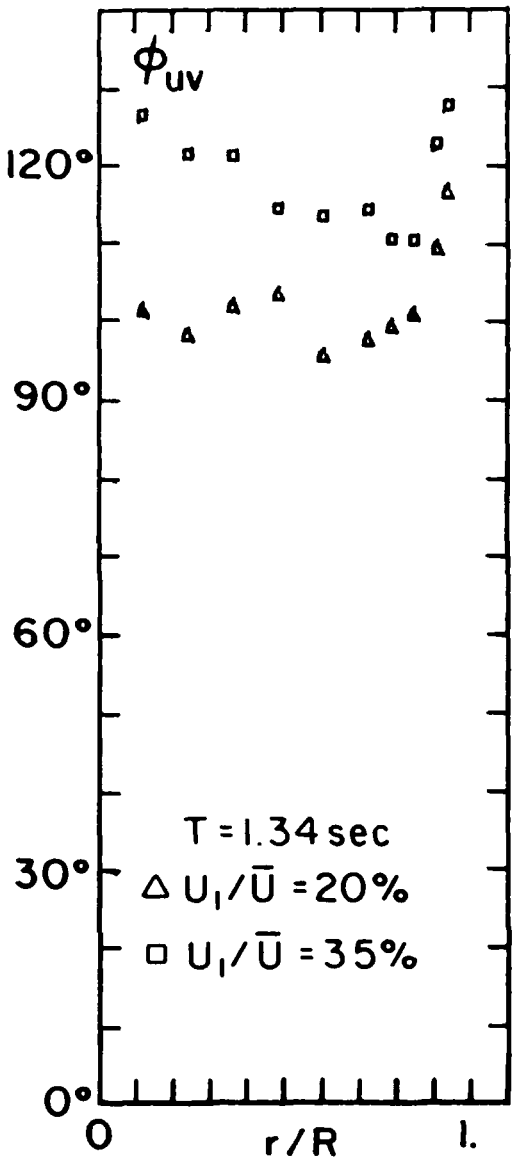

Fig. 3.21

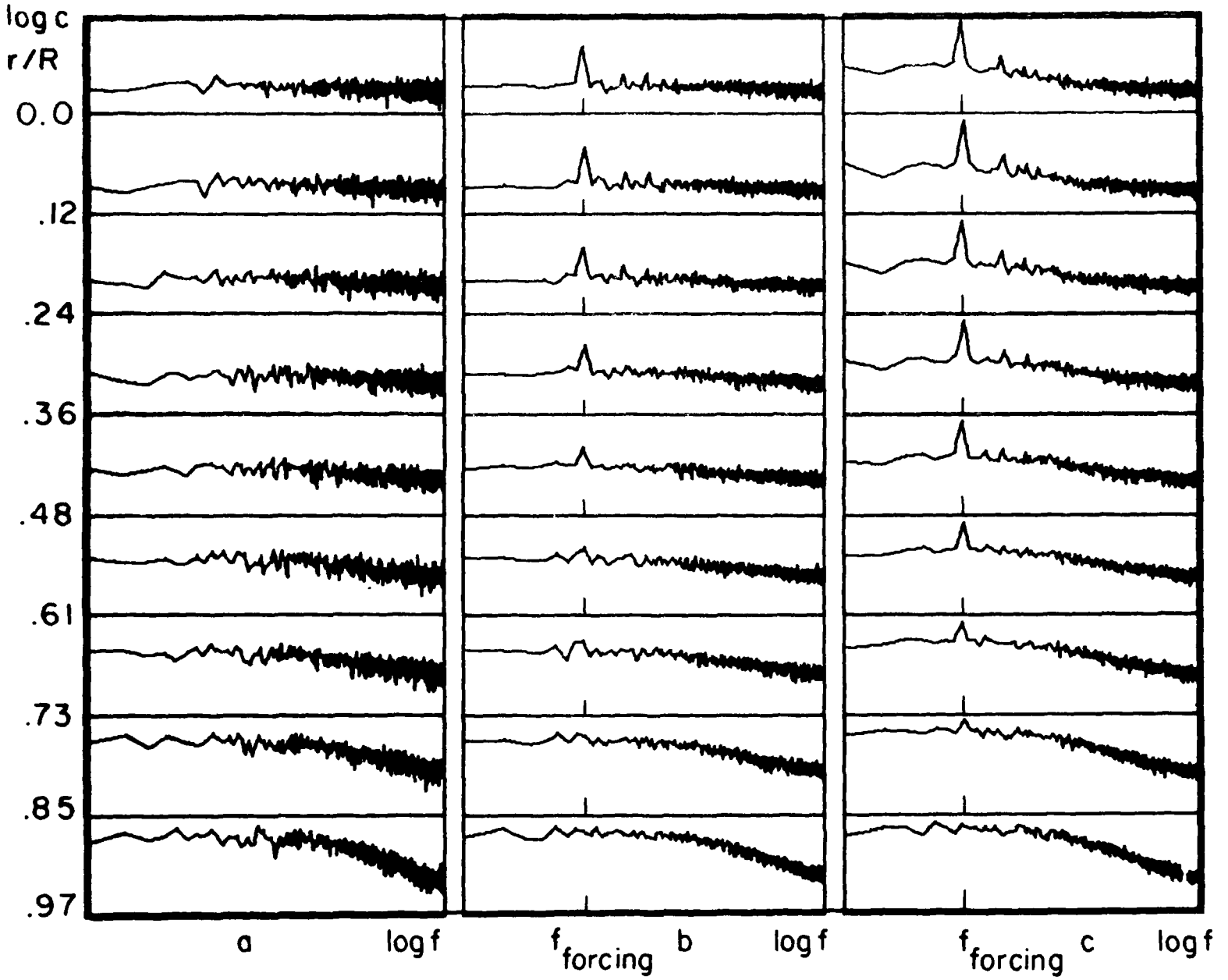
log c
r/R
0.0
.12
.24
.36
.48
.61
.73
.85
.97
a
log f
f forcing
b
log f
f forcing
c
log f

Fig. 3.22

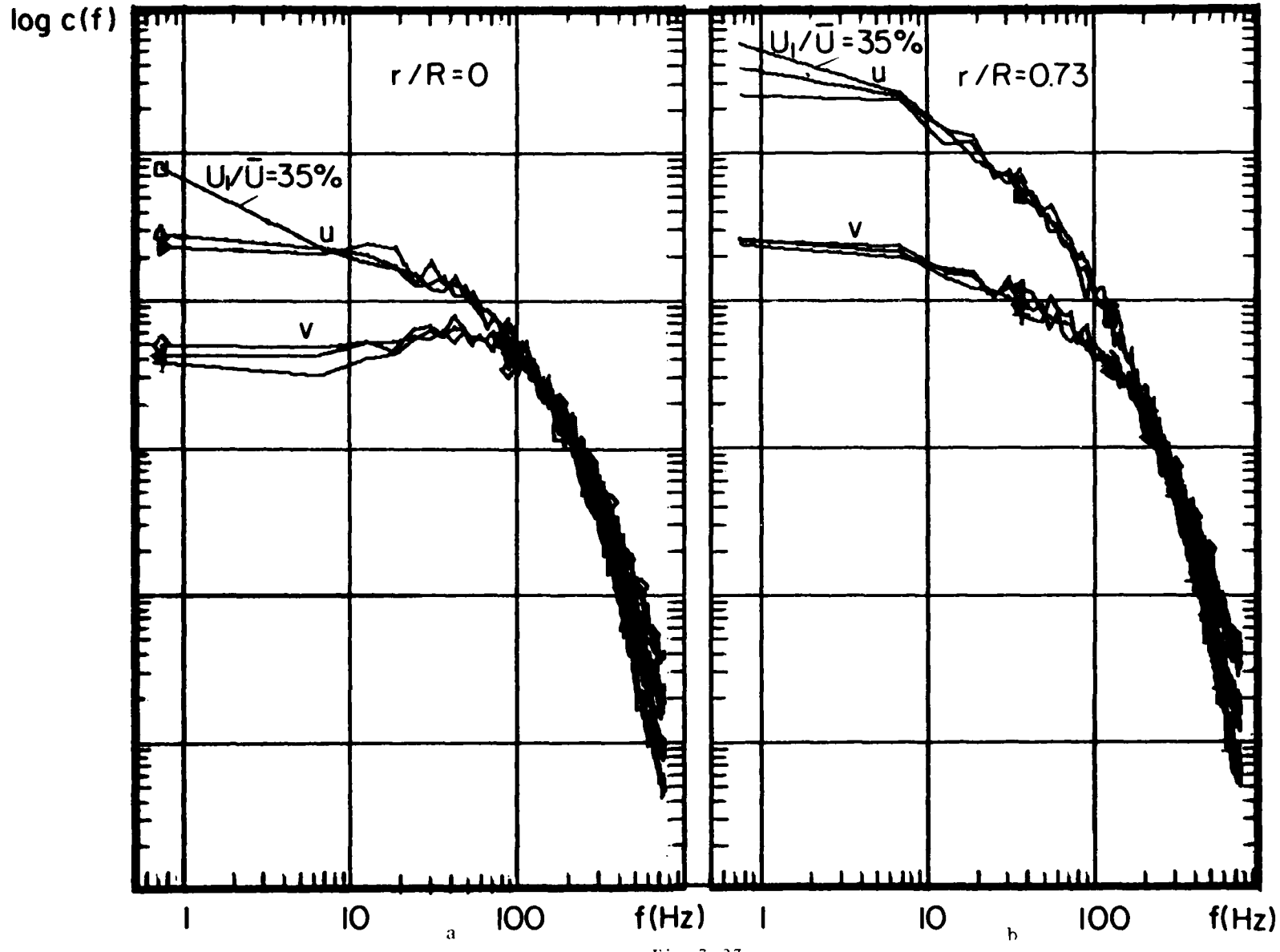
log c(f)
r/R=0
$U_1/\bar{U}$=35%
u
v
r/R=0.73
$U_1/\bar{U}$=35%
u
v
1
10
100
f(Hz)
a
1
10
100
f(Hz)
b

Fig.3.23

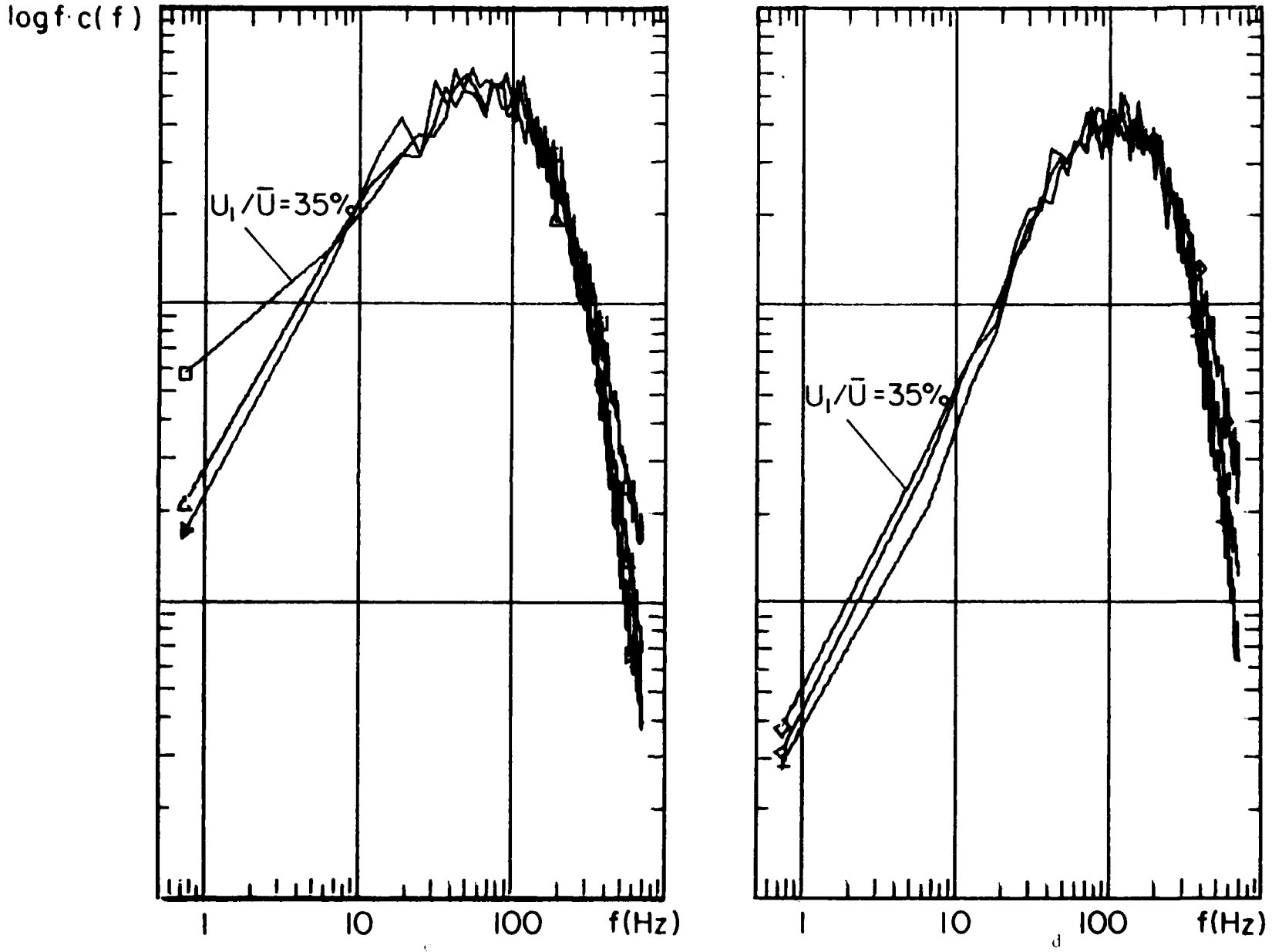

Fig. 3 . .

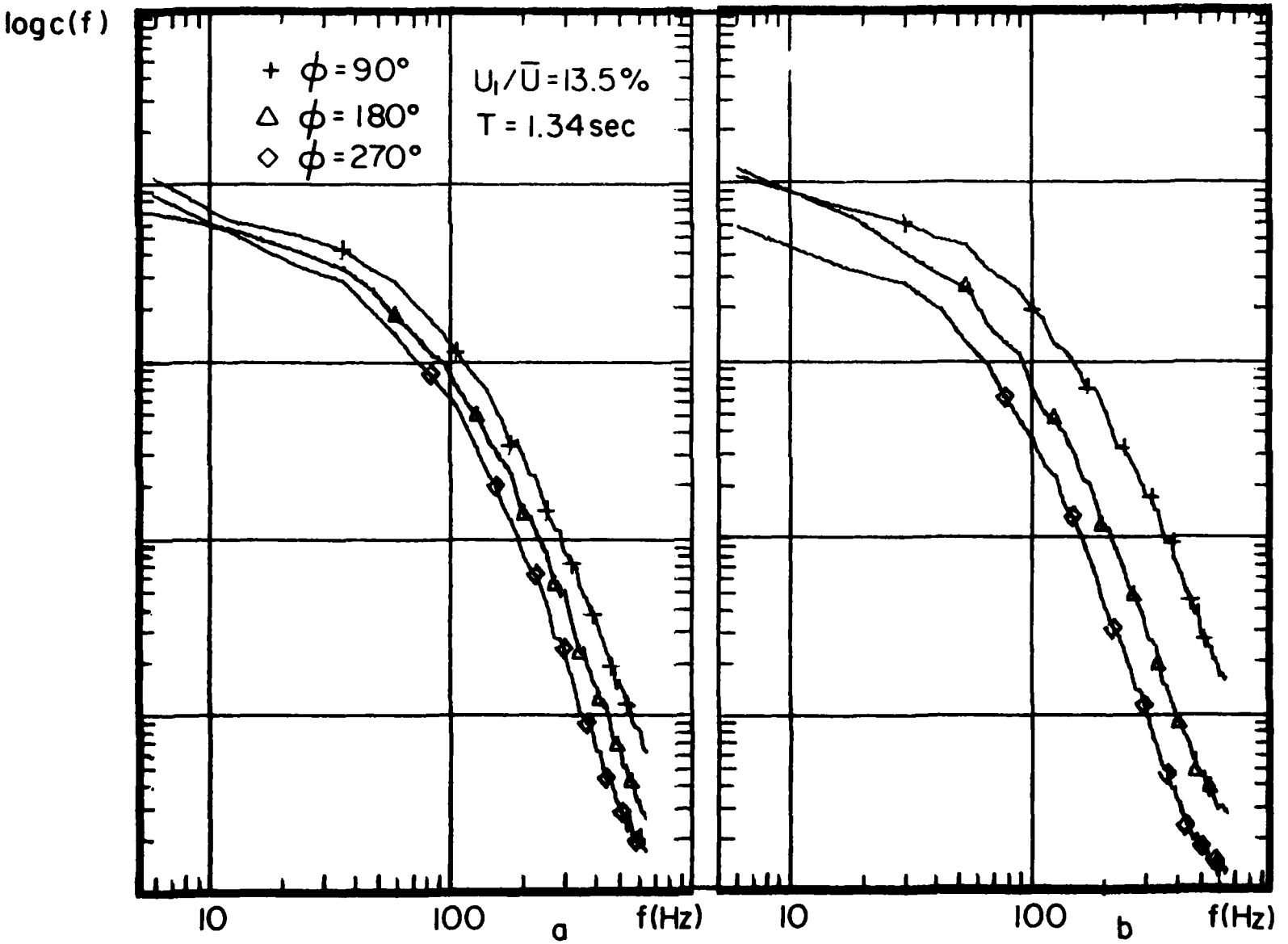

Fig. 3.24

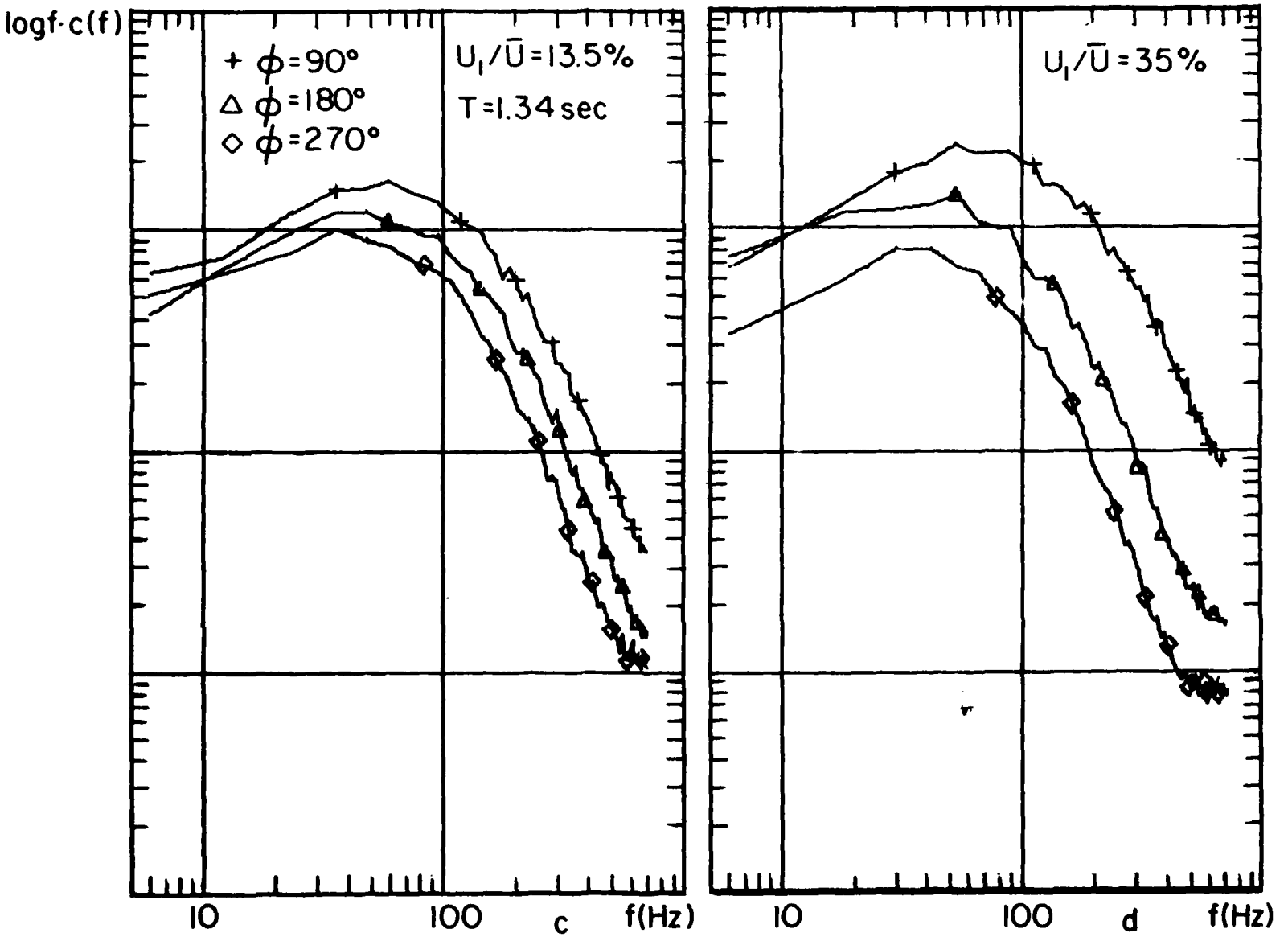
logf·c(f)
+ φ=90°
△ φ=180°
◇ φ=270°
U1/Ū=13.5%
T=1.34 sec
U1/Ū=35%
10
100
c
f(Hz)
10
100
d
f(Hz)

Fig. 3.24

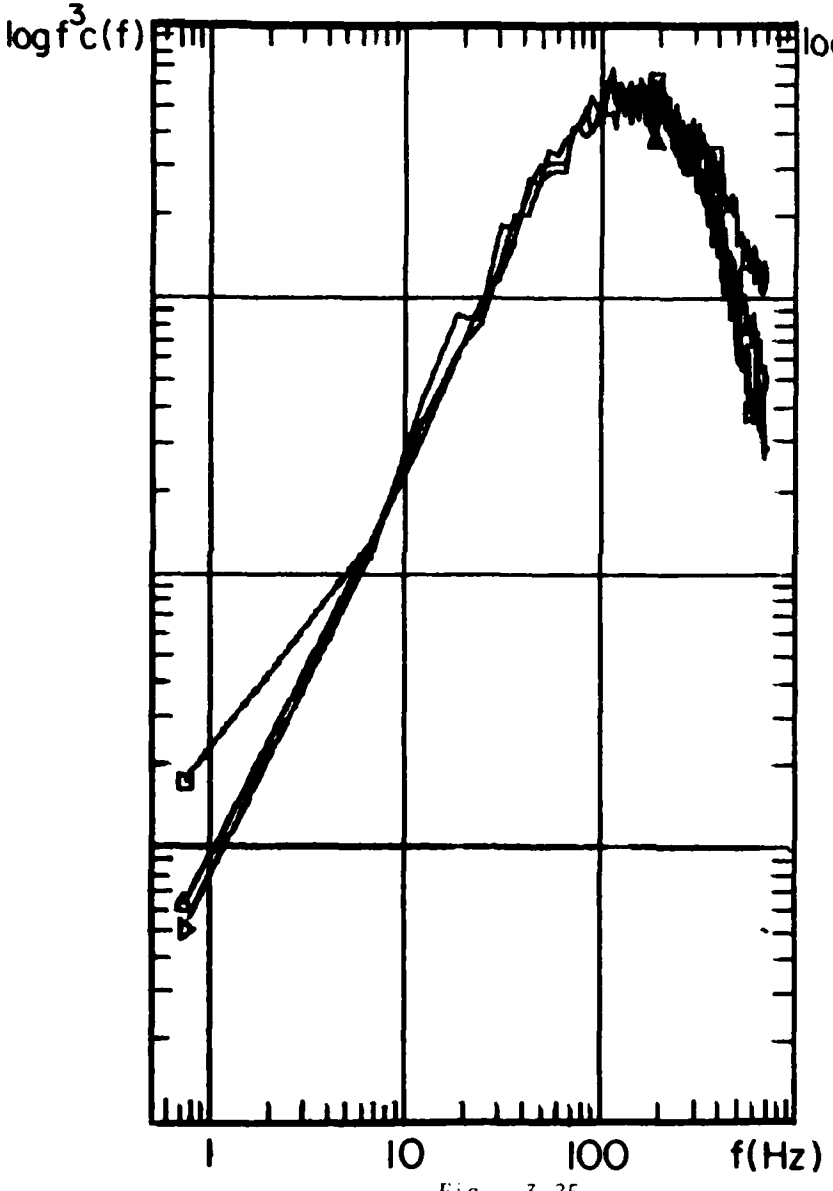

Fig. 3.25

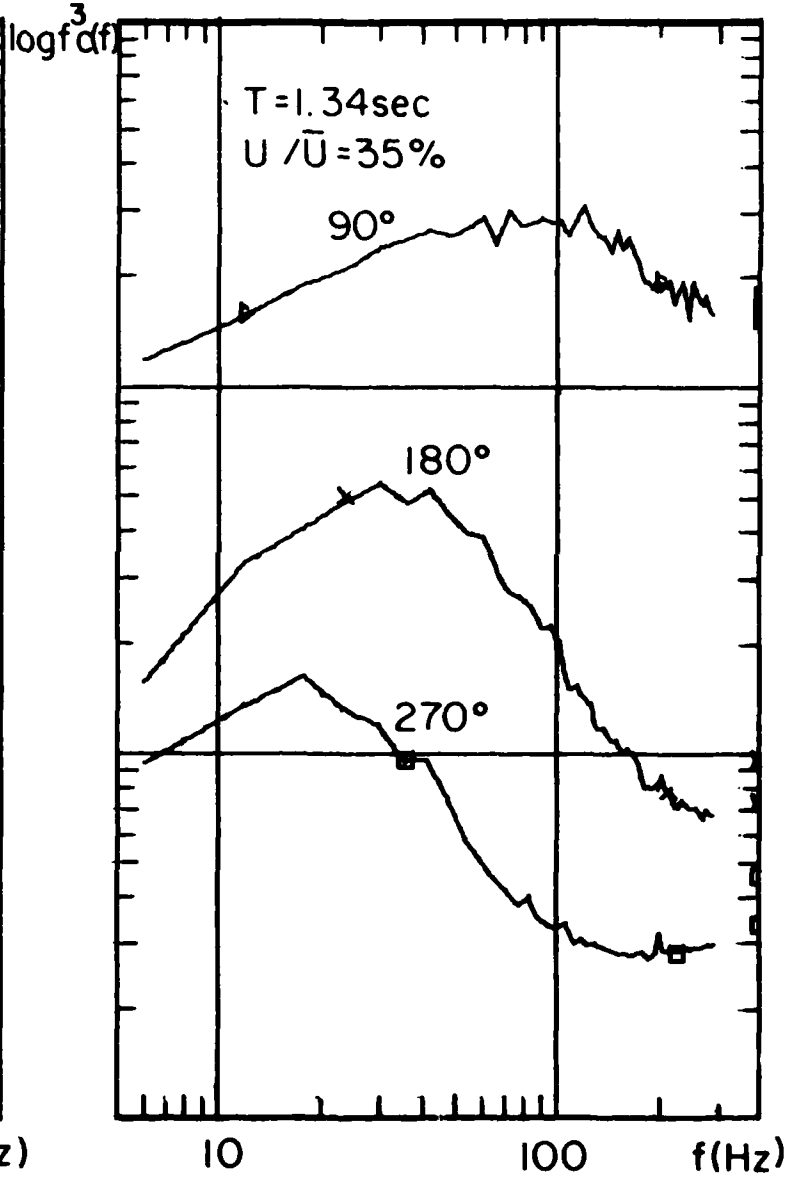

Fig. 3.26

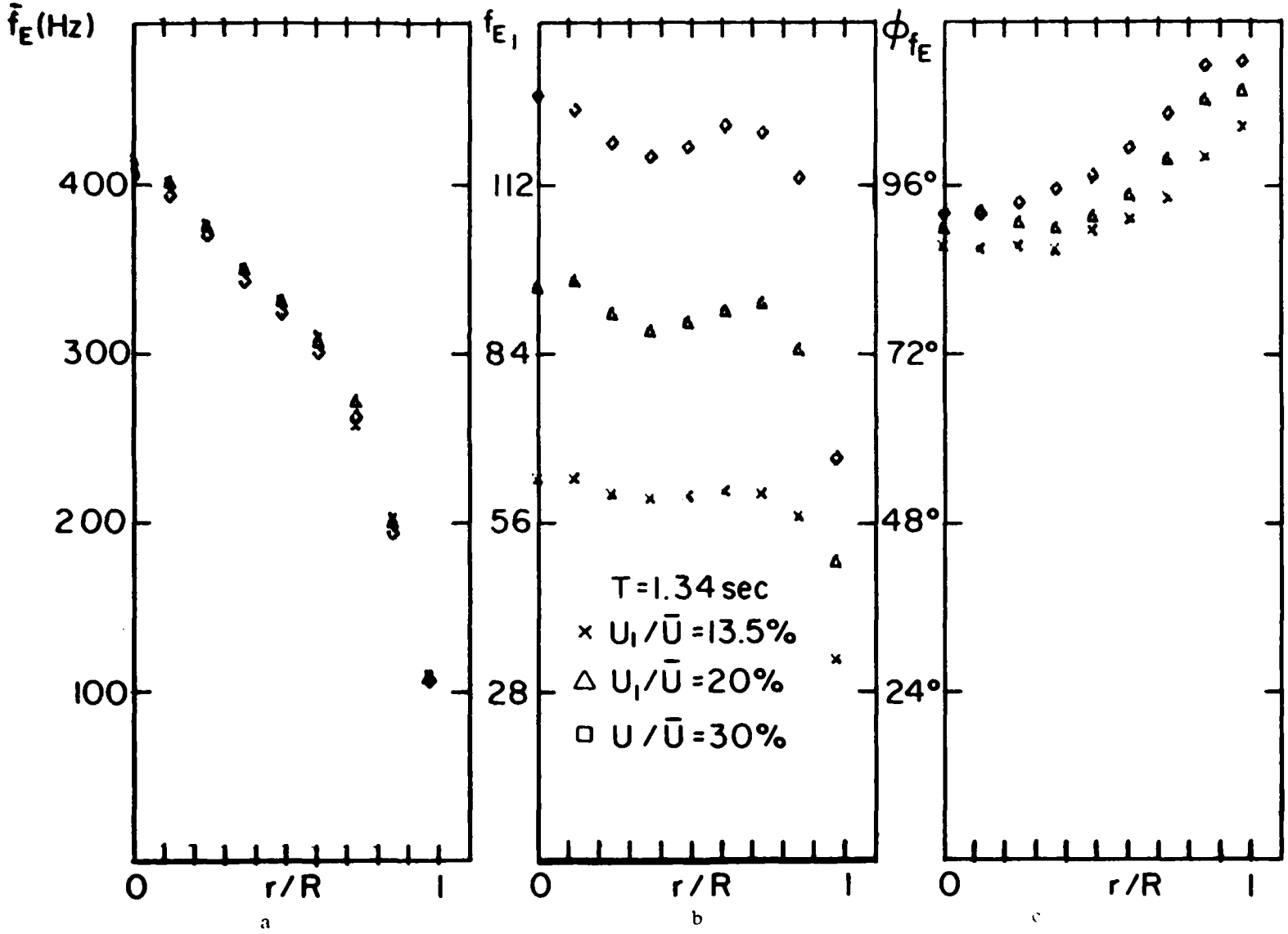
$\tilde{f}_E$(Hz)
400
300
200
100
0
r/R
1
a
f_{E_1}
112
84
56
28
0
r/R
1
b
T=1.34 sec
× $U_1/\bar{U}$ =13.5%
△ $U_1/\bar{U}$ =20%
□ $U/\bar{U}$ =30%
ϕ_{f_E}
96°
72°
48°
24°
0
r/R
1
c

Fig. 3.27

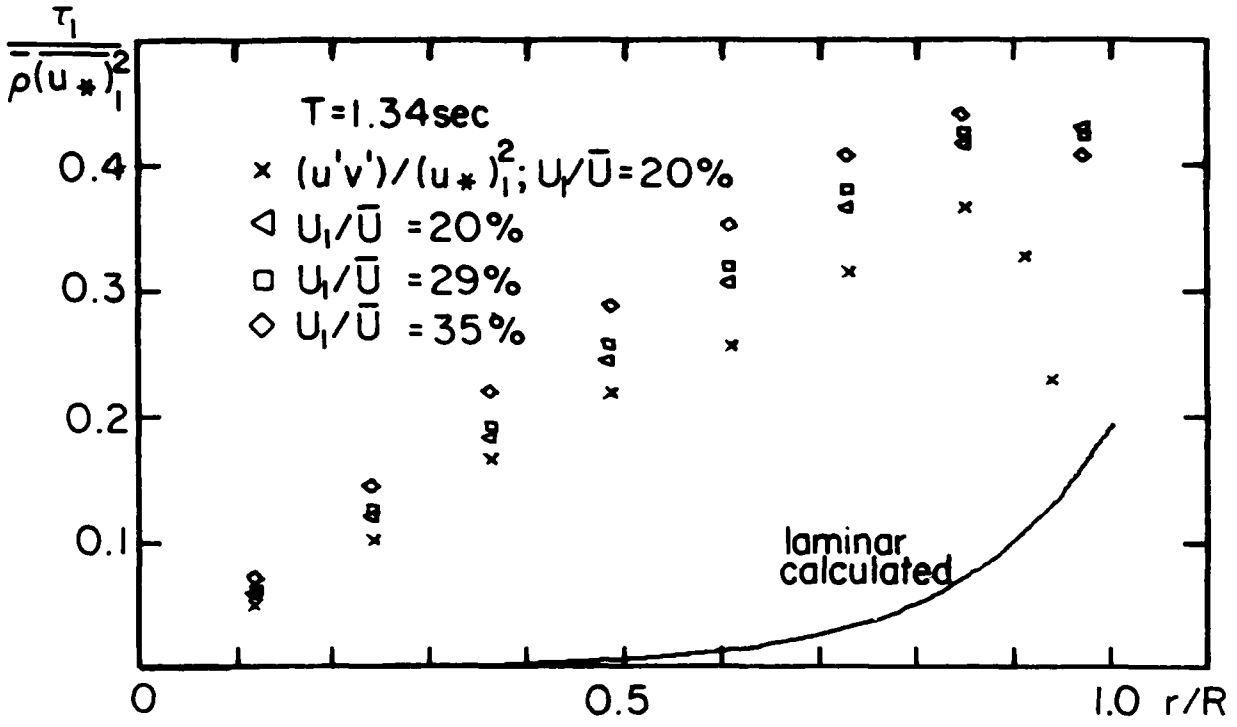
$\frac{\tau_1}{\rho(u_*)_1^2}$
T=1.34sec
× $(u'v')/(u_*)_1^2$; $U_1/\bar{U}$=20%
◁ $U_1/\bar{U}$ =20%
□ $U_1/\bar{U}$ =29%
◇ $U_1/\bar{U}$ =35%
laminar calculated
0.4
0.3
0.2
0.1
0
0.5
1.0 r/R

Fig. 4.1

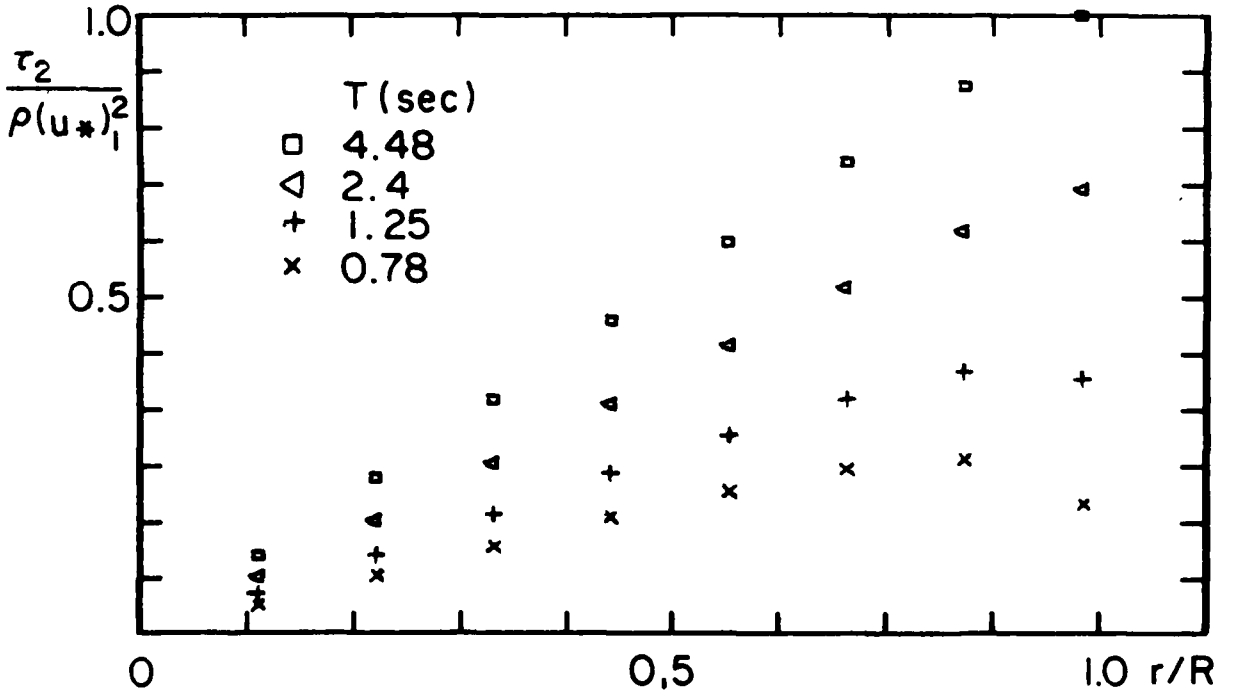
$\frac{\tau_2}{\rho(u_*)_1^2}$
T (sec)
□ 4.48
◁ 2.4
+ 1.25
× 0.78
1.0
0.5
0
0,5
1.0 r/R

Fig. 4.2

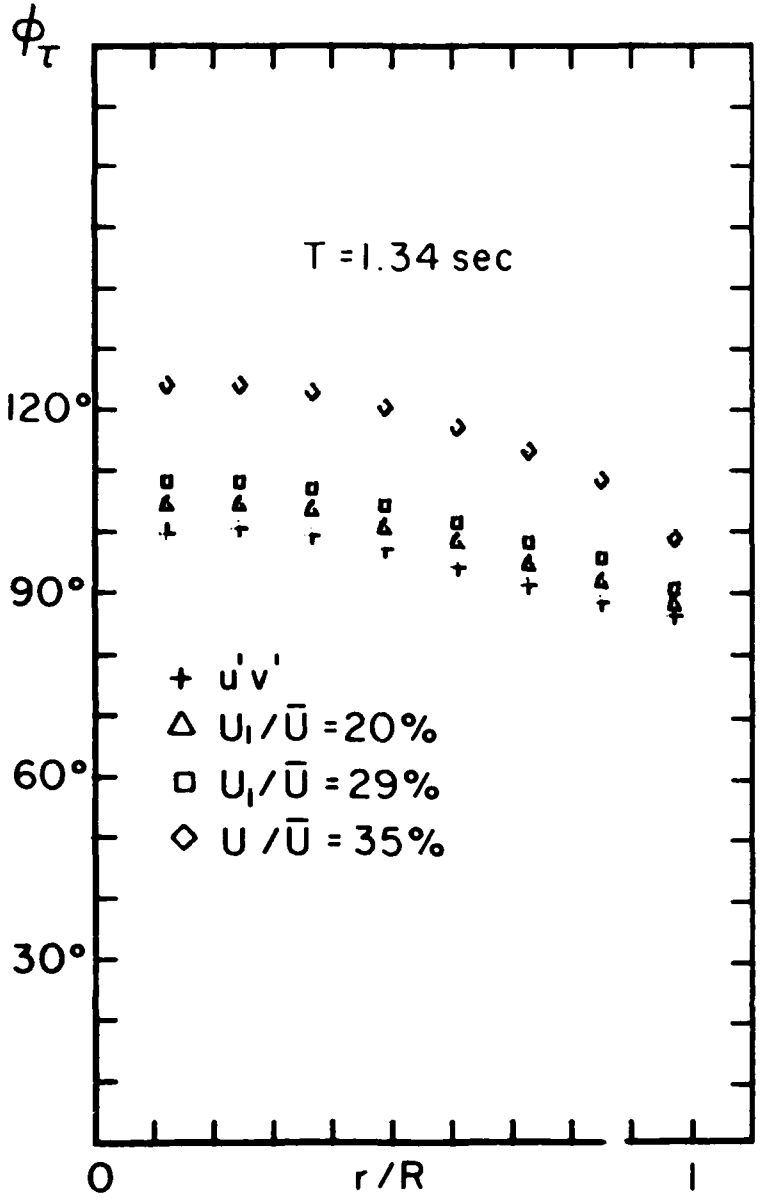
ϕ_τ
T = 1.34 sec
120°
90°
60°
30°
+ u'v'
△ $U_1/\bar{U}$ = 20%
□ $U_1/\bar{U}$ = 29%
◇ $U/\bar{U}$ = 35%
0
r/R
1

Fig. 4.3

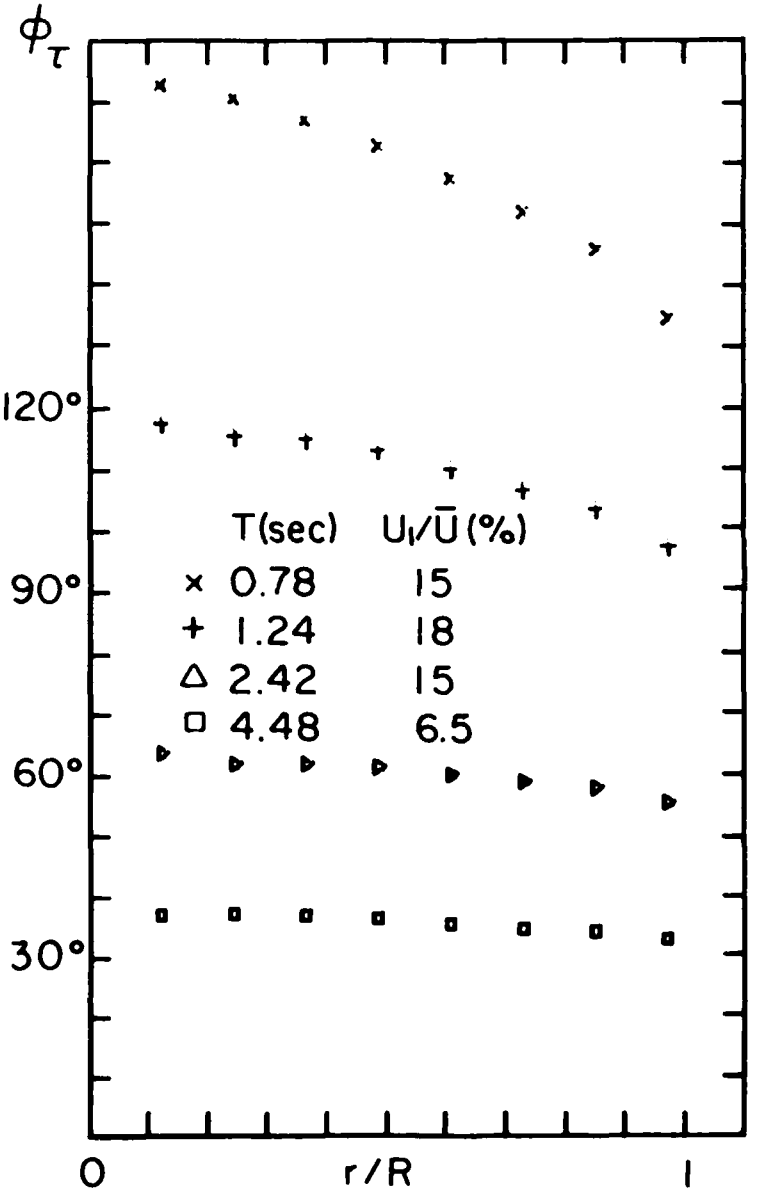
ϕ_τ
120°
90°
60°
30°
T(sec) $U_1/\bar{U}$ (%)
× 0.78 15
+ 1.24 18
△ 2.42 15
□ 4.48 6.5
0
r/R
1

Fig. 4.4

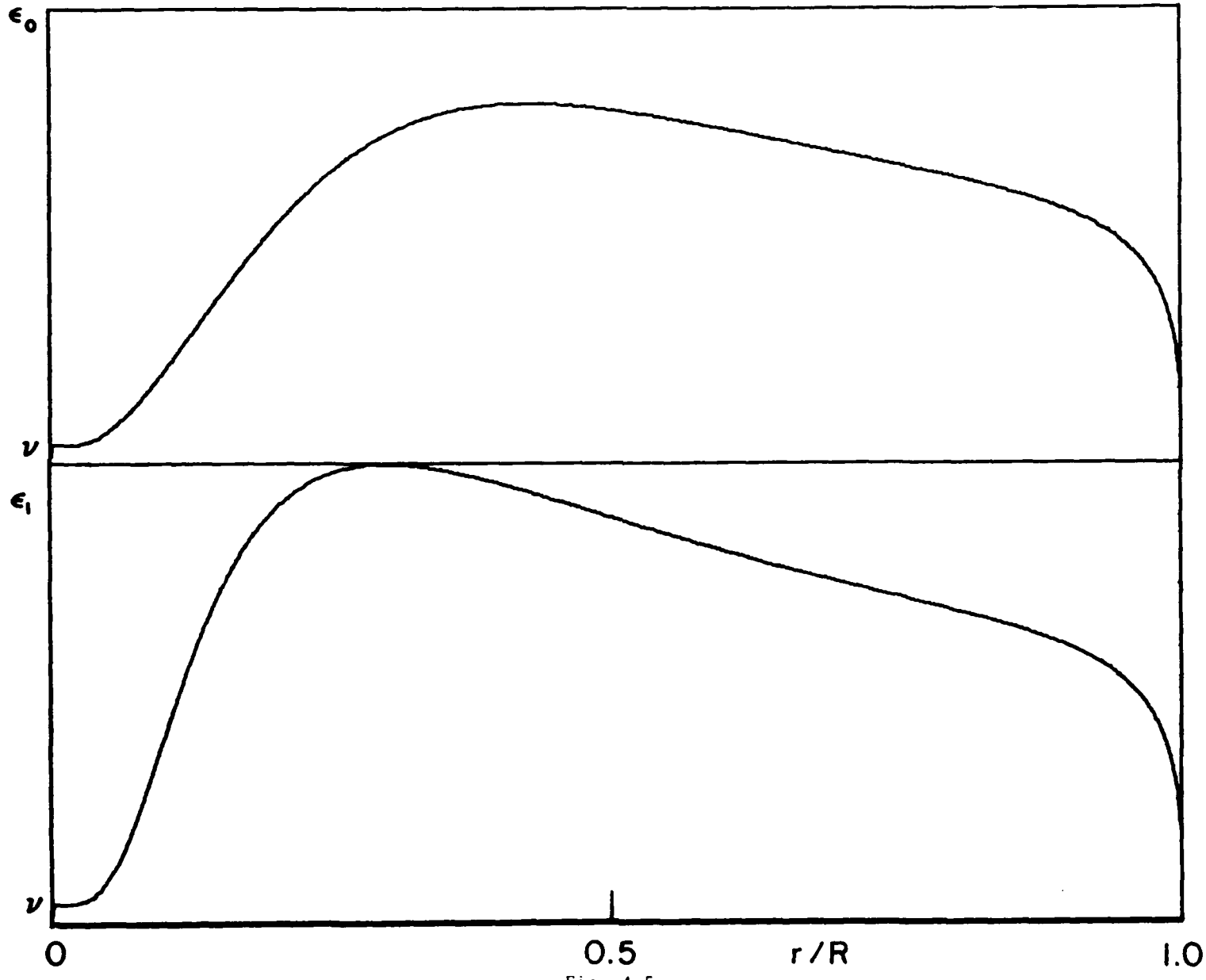

Fig. 4.5

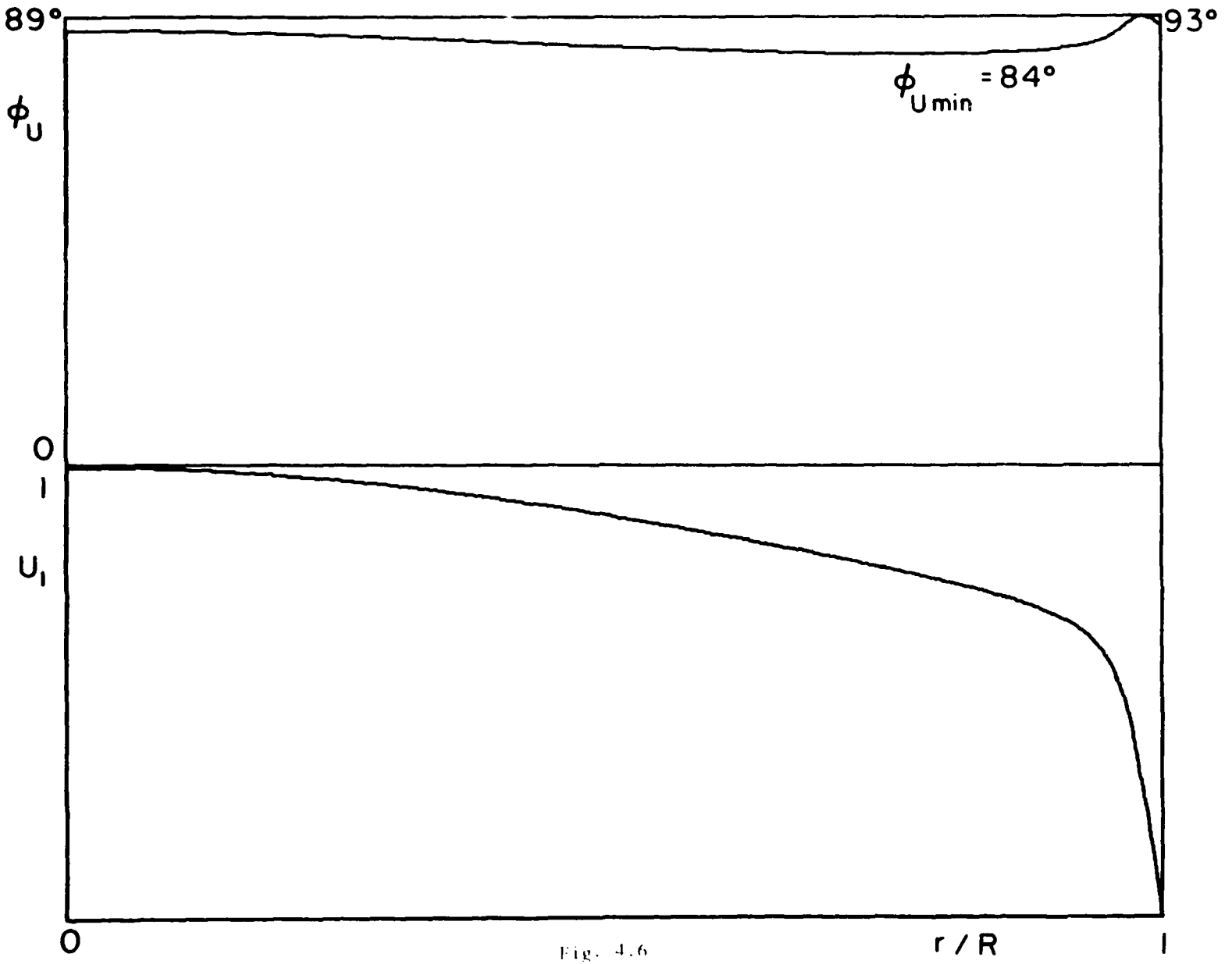

Fig. 4.6

PUBLICATION DURING CY 1980 - 81

1. A Forced, Plane, Turbulent Mixing-Layer: A Challenge for the Predictor. In Turbulent Shear Flows 2, edited by Braubury et al. Selected Papers from the Second International Symposium on Turbulent Shear Flows, Imperial College London, July 1979, Springer-Verlag Berlin 1980.

2. Further Observations on Transition in a Pipe. In Laminar-Turbulent Transition , edited by Eppler and Fasel, IUTAM Symposium Stuttgart, September 1979, Springer-Verlag Berlin 1980.

3. The Effects of Reynolds Number and Pressure Gradient on the Transitional Spot in a Laminar Boundary Layer. In The Role of Coherent Structure in Modeling Turbulence and Mixing, Lecture Notes in Physics 136, Springer-Verlag Berlin,(Proceeding, Madrid 1980).

ACCEPTED FOR PUBLICATION

1. On the Spreading of a Turbulent Spot in the Absence of Pressure Gradient , to be published in J.F.M.

2. On the Mixing between Parallel Streams, to be published in J.F.M.

END

DATE
FILMED

1-82

DTIC